UNIVERSITY OF NAPLES FEDERICO II

School of Polytechnic and Basic Sciences

Department of Chemical, Materials and Industrial Production Engineering

XXXI PhD Programme in

Industrial Products and Processes Engineering

Study of thermoplastic composite joining technology by electromagnetic induction heating

PhD COURSE COORDINATOR

Ch.mo Prof. Ing. Giuseppe Mensitieri

PhD CANDIDATE

Ing. Barbara Palmieri

PhD SUPERVISOR

Ch.mo Prof. Ing. Luigi Nele

Page intentionally left blank

Acknowledgement

I would like to thank my supervisor, Professor Luigi Nele, because without his guidance, encouragement and patience I could have never obtained these results. I wish to thank him for his help and advice during my period of research.

I would also express here my acknowledgments to Dr. Francesco Galise, researcher at Fiat Research Center, who always supported me during my PhD programme. I would like to thank him for his precious knowledge contribution and for the technical support.

Last but not least, I wish to thank all the people I met during this research period.

Table of contents

List of Figure

List of Table

Abstract

The development of light structures in the transport field is closely related to the development of manufacturing and processing technologies. The thermoplastic matrix composite materials are very interesting also for the possibility of hot forming by deformation, and their use is continually increasing. Moreover, these materials allow the possibility of performing welded joints of the parts. The automotive industry and aerospace industry seem to be the industrial sectors that have the most significant potential for application of thermoplastic composite materials.

The joining of thermoplastic composites could be carried out using hot melt adhesives or with fusion welding of the thermoplastic matrix.

The heating of a hot melt adhesive, or the thermoplastic matrix could be carried out with electromagnetic induction technology.

This PhD thesis deals with the electromagnetic induction heating of thermoplastic matrix composite materials for adhesive bonding, and also study for the first time the influence of the current frequency on the heat penetration depth.

A numerical model was developed using two different Multiphysics Software, such as Jmag and COMSOL; then the models were validated using an experimental campaign.

The main original result of the work is that in the case of thermoplastic matrix composites, the higher the current frequency the higher is the depth of the heat penetration, unlike the case of the metal alloys.

Introduction

1.1. Introduction

The development of ever lighter and with high specific mechanical properties structures, at lower costs, is a crucial factor in the transport industry, mainly as to the automotive industry.

The quickest way to improve operational efficiency is the use of structural and semi-structural lightweight materials including advanced metals (high-strength steel, aluminium alloy) and continuous fibre-reinforced composites materials.

The number of applications that require the use of thermoplastic matrix composites has increased considerably in the last years, due to their mechanical characteristic and their rapid and low-cost processing and manufacturing [1]; moreover, thermoplastic matrix composites (TPC) of more recent development have mechanical properties comparable to those of thermoset composite or even better [2].

The ideal solution would be to build a structure without joints, these being a potential source of weakness and extra weight.

However, in many practical applications, it is virtually impossible to create an entire structure in one piece, both because of the high costs, which this would imply, and both because of problems associated with the geometrical limitations. Different benefits of maintenance, accessibility, repair, transport or assembly show that the joints play an essential role in an engineering structure.

This aspect is particularly evident in the manufacture of composites, where the high viscosity of the molten resin and the constraints imposed by the presence of reinforcements limit the production components at relatively simple geometry which must then be joined together to form more complex structures [3, 4].

The joining of the various component is a critical step in the manufacturing process of TPCs products because it could introduce some irregularities in the structure that can result in weakening of the properties [5].

Traditional joining technologies, such as mechanical fastening, are not directly transferable to composites [6]; consequently, the joining techniques, alternatives

to the classic mechanical joints, are extremely interesting for these types of materials.

A composite laminate is formed by joining itself more laminae on each other, and the use of mechanical joints in the realisation of composite structures involves several problems such as:

- stress concentrations around holes; [7]
- possible delamination caused by drilling operations [8];
- temperature induced stresses caused by the different thermal expansion coefficient of composites and fasteners [9].
- the possible presence of galvanic corrosions at joints [8].

The continuous joining techniques, such as welding, and bonding are preferred over discontinuous joining techniques, or mechanical.

During the lifecycle of composite materials, a heat source is often necessary. It is generally provided by thermal transfer from the material's outer surface (heat transfer, autoclave, etc.). These processes are characterised by high cycle time since heat needs time to propagate in the volume of the material.

Additionally, the cycle time depends only on the material's physical properties and geometry and is not controllable by the heating process. These involve productivity losses.

Induction is an alternative technique to supply heat directly the composite material if the reinforce is an electrical conductor.

The main advantages of induction are the following:

- Core or surface heating, based on the generator's frequency;
- Lack of contact allowing dynamic elaboration;
- Global or localised heating;
- High transmitted power density;
- Adaptation of the inductor's shape to the charge.

1.2. Objective

Due to the complex nature of the induction heating process and processing condition a large process design, based on experimental works, is necessary.
This is expensive and time-consuming. For this reason, modelling can be a good way for a better understanding of the process characteristic and improving the process design of induction welding.
Three-dimensional models could be useful to predict the spatial temperature distribution, during the entire fusion bonding process. Additionally, coil design, that is a fundamental aspect for this kind of application can also be improved. Moreover, process optimisation and assessment of the significance of the parameters involved in the process can be achieved fast and in a very cost-efficient way.
The objectives of this study are:

1. Study the heating behaviour of high-performance carbon fibre reinforced thermoplastic composites;
2. Development a coupled electromagnetic and thermal finite element models of the induction heating process, applicable both for the adhesive bonding and for welding;
3. Analysis of the role of the process parameter for the application of the induction heating, focusing in particular on the current frequency.

1.3. Approach

In the following, the approach to the work is shown.

Chapter 2 summarises state of the art in induction heating of carbon fibre reinforced thermoplastic polymers. Selected aspects relevant to the objectives above are discussed, starting from the basics of the fusion bonding process and induction heating. Furthermore, fundamentals for modelling the process, focusing on the heating step, are presented.

Chapter 3 contains the part dedicated to the application of the electromagnetic induction heating for the adhesive bonding of thermoplastic composites. The numerical model developed, using JMag software was explained. Then materials and experimental procedures used for induction heating and bonding experiments, respectively, are illustrated. Additionally, the results of the mechanical tests performed are reported and are analysed.

In Chapter 4 the induction heating of thermoplastic composites was studied. Also, in this case, a numerical model was developed, with a different software, COMSOL Multiphysics, with the aim to assess the influence of the process parameters on heating. Moreover, the influence of the current frequency on the depth of heat penetration through the thickness was for the first time studied, keeping the power constant. The numerical model has been verified with experimental tests. The influence of current frequency was investigated using the different ultrasound energy absorption of the amorphous or semi-crystalline structure of the thermoplastic matrix: the study has highlighted that as the current frequency increases, heat penetration in the thickness of the material, at the same power supply, increases, unlike the case of metal alloys.

Chapter 5 summarises the main achievements of this work and gives suggestions for further development of the induction heating process, reporting the new results obtained changing the coil shape. Additionally, a new improved shape coil has been realized.

State of the Art

2.1. Induction Heating

Induction heating is a contactless heating process used to heat an electrically conductive or ferromagnetic material through electromagnetic induction. This technology is widely used in industry, and the underlying physics is widely described [10].

The electromagnetic induction's basic principle was described by English physicist Michael Faraday [11] in 1830 during a laboratory experiment, later Heinrich Lenz and J. Henry gave essential contributions on this research, and finally, C. Maxwell [12] evaluated the equations mathematically for electromagnetic phenomena.

When an alternating voltage is applied to an induction coil, resulting in an alternating current in the coil circuit, a time variable electromagnetic field in coil surrounding is generated. The alternating electromagnetic field generated has the same frequency as the coil current. If the adjacent material is conductive, the electromagnetic field induces eddy currents; instead, if the material is ferromagnetic, the electromagnetic field creates magnetic polarisation. In case of material characterised by a dual nature, both conductive and ferromagnetic, a combined effect may take place; heating can be obtained by Joule losses and magnetic polarisation effect respectively [13]. Conductive materials generate heat due to Joule effect and ferromagnetic materials by magnetic hysteresis loss, thanks to the friction of magnetic dipoles [14].

In conductive fibres filled composites heating occurs due to induced eddy currents flowing along conductive loops, and in each conductive loop, a drop-in voltage occurs due to the electrical impedance. This volumetric heat generation depends on intrinsic properties of the composite.

Heating of carbon fibre reinforced thermoplastic composites is a very complex phenomenon due to different mechanisms of heating generation [15].

Due to this complexity, the current distribution is non-uniform within the inductor and the workpiece, resulting in a non-uniform distribution in the workpiece [10].

2.1.1. Estimation of the generated Power

A coil connected to an alternating voltage will carry an alternating current in the coil that produces a time-variable magnetic field of the same frequency in its surrounding [10].

The power P generated during the induction heating can be evaluated only from numerical computations. The power depends on the surface power density and the workpiece surface exposed to the magnetic field, an approximation is given by the equation (1)

$$P = \frac{4\pi^2 \cdot f^2 \cdot \mu^2 \cdot H^2 \cdot A^2}{R} \tag{1}$$

Where **P** is surface power density, **H** is magnetic field intensity at the surface, **A** is the area of the surface, $\boldsymbol{\mu}$ is relative magnetic permeability at the surface, **R** is electrical resistivity, and $\boldsymbol{f}$ is frequency.

The magnetic field intensity $\boldsymbol{H}$ of a current carrying a thin conductor can be calculated with the Bio-Savart law, is given by:

$$H = \frac{i}{4\pi} \cdot \int \frac{1}{|\vec{r}|^2} \cdot \left| d\vec{l} \times \left(\frac{\vec{r}}{|\vec{r}|} \right) \right| \tag{2}$$

Where $\boldsymbol{i}$ is the coil current, $\boldsymbol{dl}$ a section of the coil length, and $\boldsymbol{r}$ is the distance between the coil and some point **p** [16].

Then, to perform iso-power analysis and experiments, it is necessary to vary the values of the current and the frequency; in particular, increasing the frequency must decrease the current and vice versa.

2.1.2. Susceptorless Induction Heating

Materials can be classified as insulator and conductors basing on their resistivity. Polymeric materials are characterised by high resistivity and act as insulators, while metals have very low resistivity, and act as conductors. Some fillers can be introduced in polymers to reduce their resistivity. The intrinsic conductivity of fillers, their aspect ratio, interactions between polymer and filler surface, their distribution and orientation are critical parameters to obtain the conductivity and their percolation threshold [17, 18].

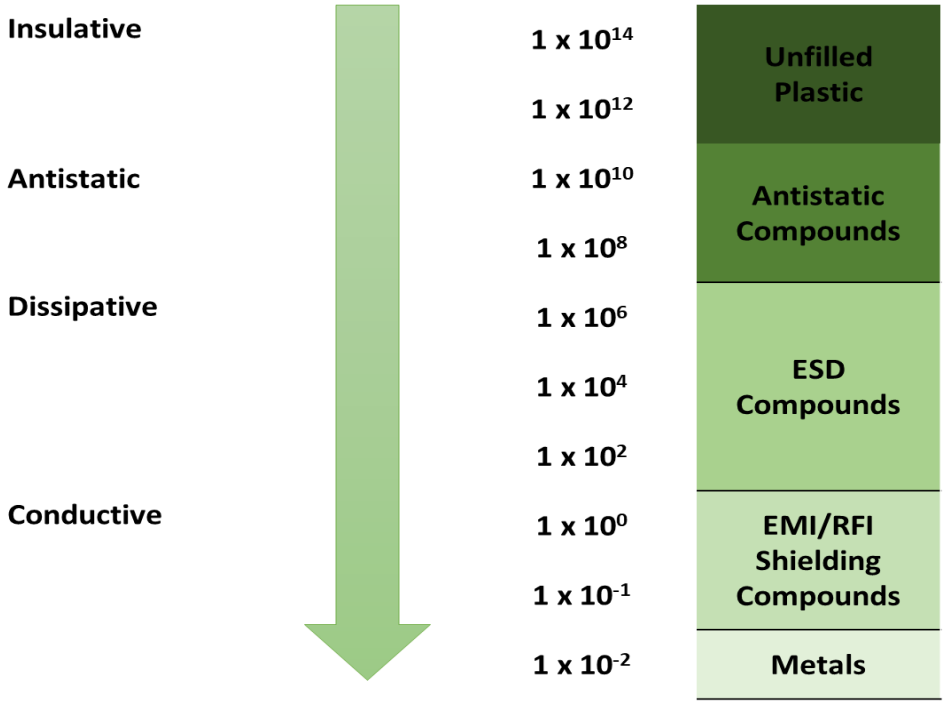

Figure 1: Volume resistivity (Ohm/cm) [19]

Figure 1 shows the volume resistivity of various materials. Unfilled polymers are insulation, and as the filler concentration increases, resistivity decreases. Electrostatic discharge (ESD), electromagnetic interference (EMI) and radiofrequency interference (RFI) shielding also need electrically conductive materials. Finally, pure metal has very low resistivity. The electrical conductivity of composites depends on the intrinsic conductivity of polymer and fillers. Polymers have very low electrical conductivities in the range of 10^{-14} to 10^{-17} S/cm, however, different fillers have higher conductivities. For example, carbon

black has a conductivity of 10^2 S/cm, graphite 10^5 S/cm and pitch-based carbon fibres have 10^3 S/cm [20, 21].

Usually, neat polymers cannot be heated by electromagnetic induction because they are neither electrically conductive nor electromagnetic. So, it is necessary to apply susceptors to convert the magnetic energy into thermal energy. Susceptor generally are in form of particles [22, 23], metallic [24, 25] or carbon fibre fabric [26, 27]. The presence of susceptors can introduce stress concentrations and lower the possible strength [28]. Ahmed et al. [29] have defined the term "susceptorless induction heating"; in this case, the workpiece already consists of a type of material, like carbon fibre fabric reinforcement, which enables induction heating to occur. Carbon fibres are electrically conductive, so they can be used as heating element [15, 16, 30–32], though this causes the heating of the whole composite [7].

In carbon fibre reinforced materials, the fundamental conditions for the generation of eddy currents are the formation of closed electrical loops as demonstrated in the works of Miller et al. [30] and then later by Fink et al. [27].

To obtain the electrical loops in the composite is primary to use fibres in woven form; electromagnetic induction cannot be applied for the heating of unidirectional laminates.

Additionally, Miller et al. [30] have shown that the eddy currents induced in the workpiece are a mirror image of the coil [29]. Consequently, the current produces its magnetic field which nullifies the magnetic field in the deeper regions of the material. The extension of this nullification depends on the intensity of the induced current on the surface closest to the inductor. The current can only flow through a conductive electric field, or along the conductive fibres. An image more like the coil shape has appeared in the fabrics, probably due to the high incidence of the electrical contacts within the fabric [15].

2.1.3. Heating Mechanism in Susceptorless Induction Heating

As reported by Bayerl et al. [33], three mechanisms co-occur for volumetric heating in conductive fibre fabrics: (i) heating by Joule losses along the fibres, (ii) dielectric heating at fibre junctions [27] and (ii) heating by contact resistance at junctions [15]. The first (i) occurs along the carbon fibres, the latest ones at fibre crossover junctions, as shown in Figure 2.

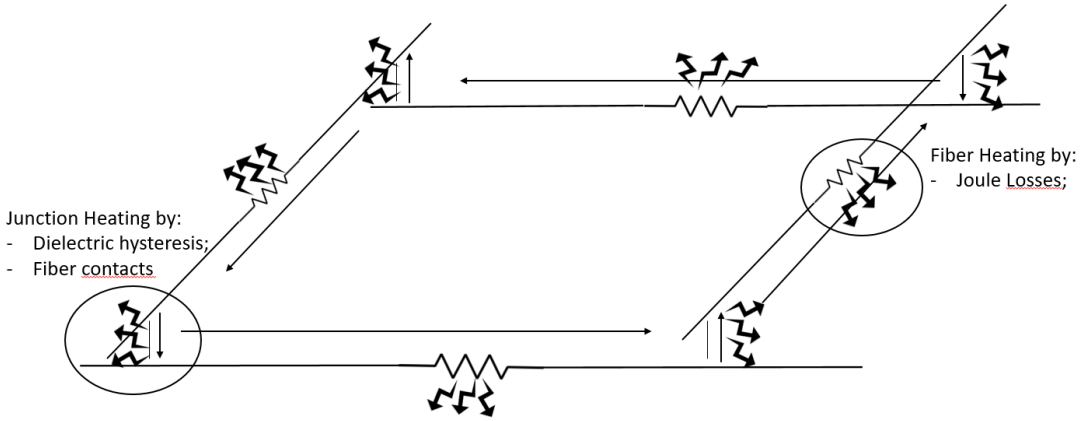

Figure 2: Heating Mechanisms of carbon fibre reinforced polymer composites

Fibre Heating

The fibres heating is the result of losses for Joule effect due to the internal resistance of the fibre.

The induction parameters and reinforcement architecture determine the amount of Joule heating in the conductive fibre; electrical resistance ($\boldsymbol{R_f}$) and heat generation ($\mathbf{P_f}$) are dependent on the cross-sectional area (A_f), fibre resistivity ($\boldsymbol{\rho_f}$), and length ($\mathbf{l_f}$), as reported by the (3) and Figure 3.

$$R_f = \rho_f \frac{l_f}{A_f} \tag{3}$$

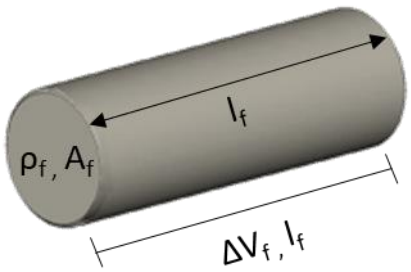

Figure 3: Fibre Heating as Intrinsic Heating

Junction heating

Junction heating occurs at the fibre junctions, and it dominates when the carbon fibres are not in good contact (contact resistance > 10^3- 10^4 [15]).

Dielectric heating at fibre junctions occurs when applying an alternating electric field, a potential difference is created between the fibres, which, being separated by a thin matrix layer, act as a capacitor [15, 27]. The dielectric heating can be modelled as a conductive circuit with a resistor (R_{hd}) and a capacitor (C_{hd}) in parallel.

The resistance between the fibres can be calculated as:

$$R_{dh} = \frac{h}{\omega e_0 k d_f^2 tan\delta} \tag{4}$$

where **h** is the distance between the fibres, $\boldsymbol{e_0}$ the permittivity of the vacuum, **k** and **δ**, respectively, the dielectric constant and the dissipation factor of the polymer, while $\mathbf{d_f}$ is the diameter of the fibre, and $\boldsymbol{\omega}$ the angular frequency.

Heat generation depends on the frequency as well as on matric dielectric properties and fibre-fibre separation distance [15].

On this basis it was concluded that to maximize the effect of the dielectric heating of the "cross-ply" or "angle-ply" laminates, the thickness of the layer above and below the interface and the volumetric fraction of the fibres must be maximized; while the diameter and thickness of the resin between the layers must be minimized, as studied by Gillespie et al. [27].

In Figure 4, the dielectric heating scheme can be seen, the presence of polymer between fibre-fibre cross-over results in the capacitive effect. The effect of dielectric properties of polymers ion heating was investigated by Fink et al. [34].

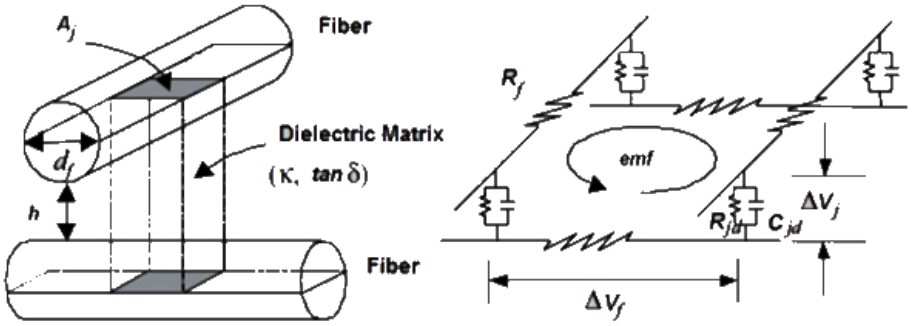

Figure 4: Junction Heating-Dielectric Heating

They have also considered that the heat generation can be written as:

$$W(x,y)_{\Delta A} = \omega \cdot tan\delta \cdot C(x,y)_{\Delta A} \cdot V(x,y)^2 \quad (5)$$

There $\boldsymbol{tan\delta}$ is the imaginary part of the complex dielectric constant for the polymer; $\boldsymbol{C}$ is the capacitance at the point (x, y) and **V** the potential difference that exists between the plates of the capacitor.

As a further demonstration of this heating mechanism, Fink et al. have observed that different polymers heat up differently and this difference depends on the dielectric properties of the matrix's polymer.

The last heating mechanism occurs when there is intimate contact between the fibres. (Figure 5)

In higher fibres volume, heating due to the contact resistance becomes predominant and depends on the value of the contact resistance of the nodes and the potential drop across these.

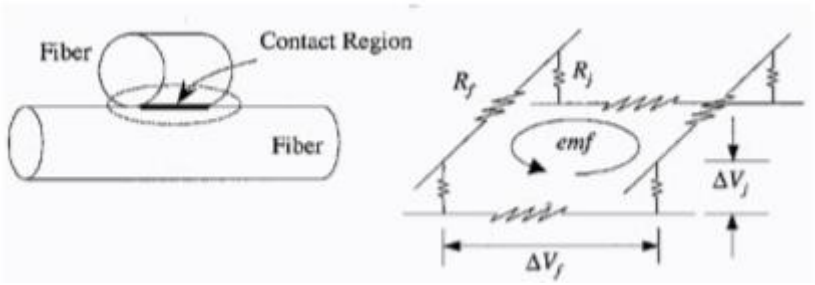

Figure 5: Fibre junction heating- contact resistance

Because of the contact, the resistance to the nodes, which generates heat, is strongly dependent on temperature and pressure. However, direct contact between the fibres is not necessary, but it is sufficient that the distance between the fibres is small enough to allow electrons to pass through this thickness.

Although many studies have been conducted to understand which heating mechanism is predominant, that depends on different parameters.
In some studies, it has been shown that fibre heating is prevalent only if the contact resistance of the fibres is very low. The type of mechanism heating depends not only on the type of fibres being heated but also on the structure of the workpiece. For the “pre-preg” and the "cross-ply", the heating at the junctions dominates because the contact resistance is very high.
For the fabrics, the heating of the fibres dominates because of a full contact area between them and therefore a low contact resistance.
Furthermore, process paraments can affect heating mechanisms. When a piece heats up, the viscosity of the matrix decreases and, applying the right pressure, the squeezing of the matrix occurs; this implies a greater contact between the fibres, and therefore the heating of the latter prevails.

2.1.4. Influence of Induction Coil Geometry

In induction heating, a fundamental aspect is the coil’s shape, that must be designed according to the component geometry [30]. Generally, the induction heating coils are developed using an empirical approach, but due to the complexity of the problem, a computer-aided approach is necessary.
The eddy currents induced in the workpiece is a mirror image of the coil, but for the carbon fibre reinforced composites, currents can only flow along electrically conductive paths, and the heating pattern may deviate from the expected shape.
For woven reinforcements, fibres in the two directions are in electrical contact, so they can provide a network of electrically conductive paths, creating a mirror image of the coil.
The coil design is one of the most critical factors affecting the heating performance.
It is possible to design the induction coil focusing the magnetic field onto the specific zone that needs to be heated.
For the final coil geometry designed it needs to be considered several design considerations, to produce the most efficient and uniform heating effect.

The coil should be as close to the workpiece, and fully over the heating area as possible, to optimise the energy transfer. [13, 30].
Moreover, it is fundamental that the rest of the coil needs to be designed to prevent magnetic field cancellation [35][36].
Generally, for heating application on composites three different shapes of the coil have been considered a pancake coil, a solenoid coil and a single turn coil.
The pancake coil can heat large flat areas; the solenoid can heat larger cylindrical areas that pass through its centre; finally, the single turn coil is characterized by a magnetic field that is concentrated around its diameter and is therefore used where the heating of circular areas area is required.

2.1.5. Skin effect

When an electric or magnetic wave flows through a conductor, a non-uniform current distribution can be observed; its amplitude value decreases according to the $e^{-\alpha z}$. The α factor is therefore called "attenuation constant", Np/m.
This phenomenon is typical for metals and is called “skin effect”, it can be obtained by Maxwell's equations, the formula of which is as follows:

$$\delta = \sqrt{\frac{1}{\pi f \mu \sigma}} \tag{6}$$

where $\boldsymbol{\sigma}$ is the electrical conductivity of the material [S], $\boldsymbol{\mu}$ is the magnetic permeability [H/m] and $\boldsymbol{f}$ is frequency [Hz].
The skin effect is dependent on the induced currents, and it is generated by electromagnetic fields. Therefore it is related to frequency, the electrical resistivity, and the magnetic permeability of the absorbing material.
Generally, based on metal behaviour, the higher the frequency, the lower is the heat penetration depth [37].
The current density along a round workpiece thickness can be estimated by the equation (7) [10]:

$$J = J_0 e^{\frac{y}{\delta}} \tag{7}$$

Where **J** is current density at the distance y from the surface, $\boldsymbol{J_0}$ is current density at the workpiece surface, **y** is the distance from the surface, and $\boldsymbol{\delta}$ is penetration depth.

2.1.6. Edge Effect

One of the main problems associated with induction welding is the effect deriving from the geometry of the welding area, called "edge effect". This effect derives from the proximity of the inductor to an edge of the workpiece. For example, if we consider a simple circular coil, the eddy currents induced in the piece also have a circular pattern. (i) shows the path of the eddy currents produced by this coil and the corresponding temperature profile through the line A-A, for a piece that is larger than the coil.

At the edges, and especially at the corners, there is a large area that allows eddy currents to flow; this results in low current densities in these regions, resulting in less heat generated, as shown by the lowest temperature profile at the edges of the workpiece [30].

If the piece size is reduced, as shown in Figure 6 (ii) and (iii) the currents can follow the coil shape; the eddy currents are therefore forced to travel along the edge of the laminate in the area closest to the coil to create closed loop paths.

In these regions, there will be a higher current density and consequently higher temperatures.

As a result, as indicated by the temperature profiles, the highest temperatures occur on the edge of the workpiece; this effect is trying to eliminate, and many efforts have been made to minimise it, or to avoid them altogether. The simplest and most common method is to use models to predict where excessive overheating of the edges occurs.

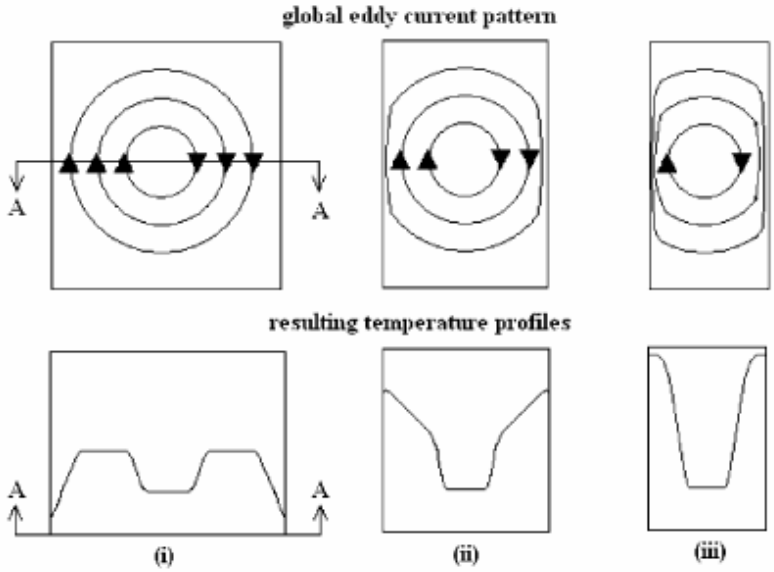

Figure 6: Edge Effect in induction heating

2.2. Fusion Bonding

The fusion bonding of thermoplastic composite is a heating joining process, able to melt (or soften) the polymer at their common interface [7, 38].

This phenomenon is defined as "fusion bonding", as the fusion of the outer layers occurs, realising the joint of the extremity layers.

The fusion bonding, or welding, is a settled technology in the thermoplastic industry where the efficiency of the welded joint can get close to most of the properties of the adhesives. Although welding can induce residual thermal stresses if carried out without adequate control, however, it eliminates the stress concentrations from the holes, generated using mechanical joints. Also, welding reduces the processing time and surface preparation. However, for the presence of carbon fibre reinforcement (CF) in TPCs, with consequent electrical and thermal conductivity, there are some difficulties such as irregular heating, delamination and laminates' distortions; these problems become more difficult when they must join large components. Also, while the volume fraction of the fibres increases, the amount of resin available at melt and reconsolidation in a molten joint is reduced and this can affect the welding quality.

The joining techniques have been classified according to the technology used for heating, basing on it is possible to identify four categories, bulk heating (co-consolidation, hot-melt adhesives, double resin bond), frictional heating (spin welding, vibration welding and, ultrasonic welding), electromagnetic heating (induction welding, microwave heating, dielectric heating, resistance welding) and two-stage techniques (hot plate welding, hot gas welding, radiant welding).

Bulk heating techniques such as autoclave, compression molding or membrane forming are available to perform co-consolidation. Co-consolidation is an ideal bonding method since no weight is added to the final structure, none external material is introduced to the contact, essentially none surface preparation is required, and the strength of the bond is potentially equal to that of the original laminate. However, the whole part reaches the melting temperature, and this generally implies to work with complex tools to carry out the pressure on the entire part and prevent de-consolidation.

The adhesive films molten thermoplastics can be inserted into the contact to improve the filling between the parts. The insertion of an intermediate layer of amorphous polymer reduces the dispersion of resistance.

The double bond of resin, or amorphous bonding, involves modelling of an amorphous TP film with a TP matrix composite laminate semi-crystalline. During the union, the amorphous film can be melted at a temperature above its transition temperature glassy, which is lower than the melting temperature of the semi-crystalline polymer, avoiding any deterioration of the bound structure.

In two-stage techniques, the heat source must be removed from the substrate surfaces between the heating and the forming phases. This aspect implies limitations on the size of the component since the entire welding surface must be heated in a single step. Heating times usually are long given the low heat conduction of heat through the polymer. Between the heating and the forming levels, the surface temperature decreases and the region where the temperature is maximum is located below the surface of the laminate. The high pressure required to consolidate the area contact may cause a flow in the inner region of higher temperature.

Frictional heating was used extensively in the plastic industry but is less suitable for merge TPCs because the movement of the substrates relative to each other can cause deterioration of the microstructure, such as fibre breakage.
The microwave and dielectric welds are suitable for joining of thermoplastics but the fact that heating occurs volumetrically and that the multi-layered compounds are excellent screens for microwaves makes these techniques not an ideal solution for welding of TPCs when CF reinforces them.
The three most promising fusion bonding techniques are: welding an ultrasound, induction welding and resistance welding. In these techniques, only the welding interface reaches the melting temperature, minimising the effect on the rest of the structure. The welding times are very short. Large-scale welding can be made with sequential methods and online control it is possible.
There are many heating methods available for welding of composites [7]; these methods are divided by the heating mechanism [9, 38, 39], Figure 7.

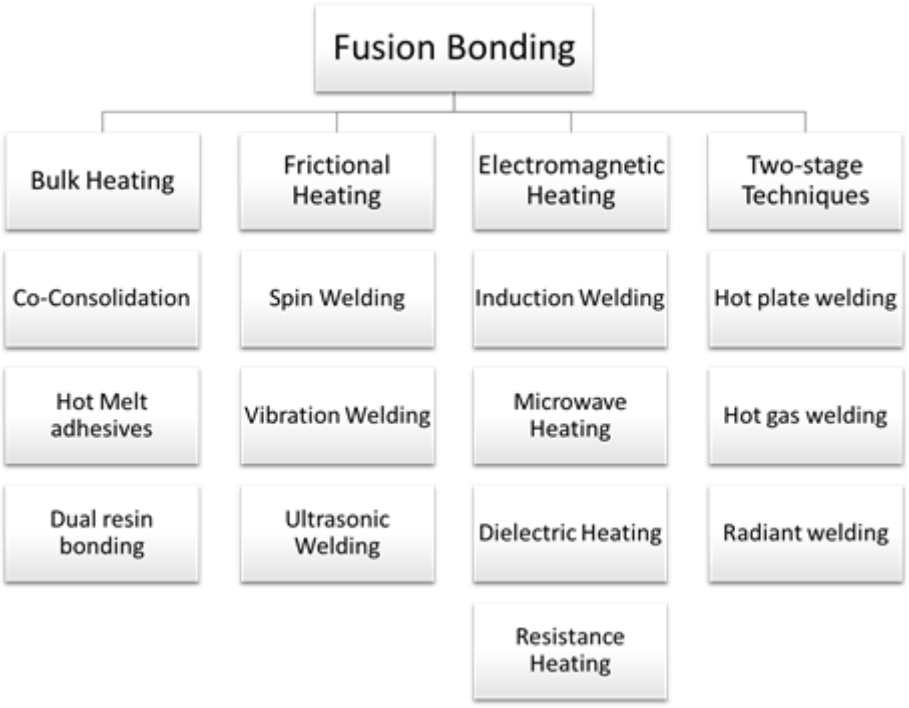

Figure 7: Categorization of fusion bonding techniques by the heating mechanism

The most interesting ones are all welding processes where only the surface near the welding interface is heated enough to melt or soften the polymer. It is more efficient to heat and melts a small area than a larger one; additionally, due to the

low thermal conductivity of polymer materials,' it is faster to melt the polymer near the joint area than to wait to melt by convection or conduction. Heating is usually considered the most critical phase in the welding process because this is not possible without the formation of a thin layer of melted or softened material on each part. This layer is necessary for the flow on the interface to reach an intimate contact and for the intermolecular diffusion and the entanglement of the chains to be possible.

As might be expected, the amount of incoming heat and the temperature required for melting and softening is different for amorphous and semi-crystalline polymers. For amorphous polymers, it is necessary to exceed the glass transition temperature to promote diffusion; but, if the polymer softening temperature is very close to the glass transition temperature, then diffusion can take a long time. To reduce the time required to perform the welding process, the recommended heating temperature of most amorphous thermoplastics is about 100 ° C above their glass transition temperature.

For semi-crystalline polymers, the melting temperature must be exceeded; this usually requires high amounts of incoming energy to overcome the latent heat of melting. For temperatures below the melting temperature but above the glass transition temperature, many molecules are still bound in crystalline regions, and therefore intermolecular diffusion is not possible. It is necessary to exceed the melting temperature of at least 50 ° C, to ensure the polymer melting along the entire interface surface. In both cases, semi-crystalline and amorphous polymers are fundamental to prevent thermal degradation of the resin during high-temperature welding successfully. The heating rate and heat transfer are critical because they affect the welding speed and the thickness of the melted or softened material. In general, internal mechanical heating methods are characterised by a high heating rate, but a shorter working time and a thinner melt or softened layers [38].

The methods of the electromagnetic heating show a moderate increase in temperature and the same apply to thickness and cycle time.

The external heating methods generally have a lower heating speed, a longer cycle time and a greater welding thickness. [38]

The process can be divided into five different steps that can be sequentially or simultaneously [38].

Surface preparation is the first step required to prepare thermoplastic composite materials for welding. This phase is particularly important when performing manual or semi-automatic processes since the level of manual handling needed in these processes increases the possibility of contamination. Typically, the preparation of the surface involves machining or cleaning. [38]. In the automatic welding process, the surface preparation is very rare, in fact, compared to thermoset adhesives the surface preparation is less critical.

After heating of the bonding line, pressure must be applied to ensure intimate contact between the parts to be welded.

This phase can be divided into two: (i) First, the surface asperities are deformed, and the intimate contact between the parts is reached. (ii) Secondly, a layer of molten material is squeezed out, and any entrapped gas and contaminated polymer are removed from the joint area [38, 40].

During welding, it is preferable that the "squeeze flow" phenomenon occurs as soon as possible [38]. As the high temperature can degrade the thermoplastic material, it is necessary to maximise the contact area and minimise the viscosity when the pressure is applied.

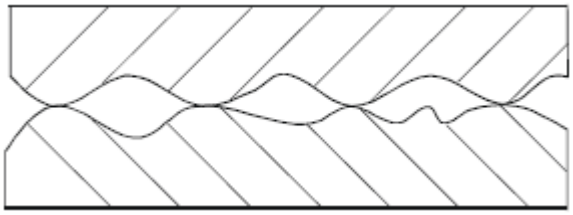

Figure 8: Scheme of two surfaces in contact [38]

This aspect is especially important when considering composite materials with high reinforcement volume contents; during the welding, a high viscosity value can affect the welded joint performance [38]. However, when the problem only concerns the surface asperities' and the molten layer, the viscosity can be reduced by a resin rich surface or a polymer film on the surface.

The presence of a resin rich allows the formation of polymer-polymer bond [40] and favouring the intimate contact between the parts.

Additionally, there are considerable differences in behaviour between semi-crystalline and amorphous thermoplastics. Semi-crystalline materials flow more smoothly, considering that the temperature is higher than the melting one; while the fluidity of amorphous polymers depends on being heated above the glass transition temperature.

Once the intimate contact between at the interface of the polymers is reached, the entanglement and the intermolecular diffusion it is necessary to obtain a welded joint [38]. The interface and its mechanical strength change [7]. The phenomenon that describes the intermolecular diffusion and the entanglement of the chains through the interface of the thermoplastic polymer is defined as “autohesion”. While the adhesive bonding is based on surface energies, autohesion basing on chain agglomeration and secondary bonds for polymer chains of similar materials, for ideal conditions, the intermolecular diffusion is complete when it is impossible to differentiate the interface by the single substrates.

The autohesion process can be divided into five phases [38]: (i) surface rearrangement, (ii) surface approach, (iii) wetting, (iv) diffusion, and (v) randomization. During the welding, the first three phases occur during the pressing step, while the last two (iv) and (v) during the intermolecular diffusion step.

The type of structure of thermoplastic polymer affects the intermolecular diffusion process. In fact, for semi-crystalline polymers it is necessary that the crystals be entirely fused; this is possible only when T_{melt} has been exceeded. Above the $T_{melt,}$ intermolecular diffusion is very rapid.

For amorphous thermoplastic, intermolecular diffusion is possible only at a temperature above T_g. The intermolecular diffusion of the long polymer molecules occurs due to the intimate contact of the interface surface.

The final step in the fusion bonding process is the cooling and the subsequent resolidification. During this phase, the semi-crystalline materials re-crystallise to obtain the final microstructure, while amorphous polymers retain the previously induced molecular orientation. Also, residual thermal stress and distortion remain partially frozen in the component [38]. For semi-crystalline polymers, the

cooling rate affects the crystallisation rate and the formation of spherulites near the welding zone [7].

Experiments and the theoretic determination of the residual stress level caused by welding are problematic due to the viscoelastic nature of the polymer and the complexity of residual stress measurement in general.

2.2.1. Ultrasonic Heating

Ultrasonic heating is the most common welding process used for thermoplastic with applications that include disks, medical devices, battery housings and many automotive parts. In ultrasonic heating, the parts to be joined are held together by pressure and are subjected to ultrasonic vibrations perpendicular to the contact area (Figure 9). High-frequency vibrations produce the heat in the material, and if the components are properly designed, this heat can be generated selectively at the interface as a combination of friction and hysteresis.

Ultrasonic welding, a possible application of ultrasonic heating, can be operative at various distances, from a fraction of the millimetre up to several centimetres, with the control process that is more sensitive to the greater distances.

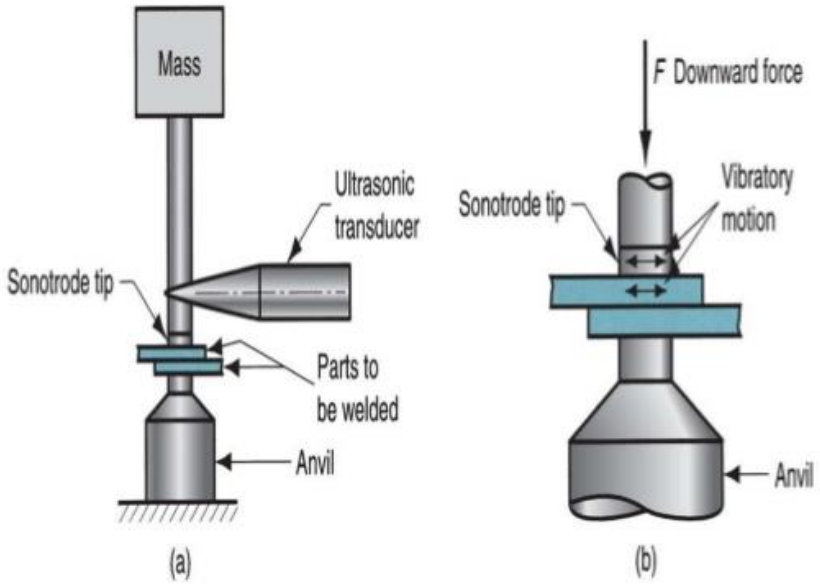

Figure 9: USW schematic for lap joint (a), zoom of the joint (b)

The application to flexible polymers is limited because they absorb energy. However this problem does not occur in their composites. In ultrasonic welding, the vibratory energy is concentrated usually around the surface bumps that

dissipate heat. Artificial asperities, called energy directors, or promoters, in shape of triangular projections, Figure 10, are modelled on the part to stimulate the fusion.

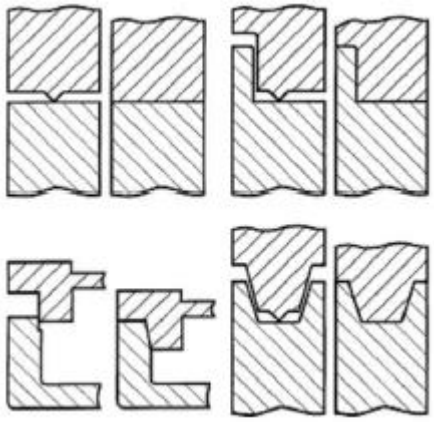

Figure 10: Energy directors

Tateishi et al.[41] proposed the use of bonding layers, avoiding the use of energy directors in ultrasonic welding. A layer of bond is an intermediate layer consisting of the substrate material which has been modified to promote preferential fusion lowering the melting temperature. Ultrasonic welding of TPCs has been studied by Benatar et al. [40]. Meanwhile, welding an APC-2 ultrasound using various configurations and various susceptors is was explored by Pires et al. [42], by Silverman et al. [43], by Hodges et al. [44], from Davies et al. [45].

Large-scale welding was made possible through sequential approaches. The absence of susceptors or the absence of the intermediate layer has made the process complicated. For continuous reinforced fibre materials, the primary limit to the use of ultrasonic welding is the difficulty of to introduce ultrasonic energy managers on the components of the layer and the consequent risk of breaking the fibre at the interface, linked to a large deformation necessary to obtain a satisfactory bonding.

Benatar et al. [40] showed that in ultrasonic welding the impedance of the composite interface was connected to the flow of the molten polymer giving the potential for online control of the welding operation.

2.2.2. Resistance Heating

The resistance heating process based on inserting a conductive mesh between the two parts to be joined. The electric current is distributed in the mesh and its temperature increases for the resistance heating.

Atkinson et al. [46] have shown how resistance heating can be used for joining biaxially oriented polyethene pipes. One disadvantage of resistance welding for TPCs is that the element resistance heater must be insulated from all conductive constituents of the composite. The introduction of resin films, as intermediate layers, not only favours the diffusion process, developing a region rich in resin as in the whole fusion bonding process but also provides thermal and electrical insulation of the laminate. Other intermediate layers, such as fibre-reinforced PEI prepreg of glass (GF) can be introduced to the contact when the insulation electric turns into a problem.

Dubè et al. [47] conducted comparative studies among the elements metal heating elements and the heating CF prepregs for the welding of APC-2. Metal mesh can improve heating efficiency, but they can also induce shear stress concentration, the added weight, the lower resistance corrosion. Also, the bond between the metal and the matrix can be reduced, and this weakens the joint.

Arias et al. [48] showed that impulse resistance welding (IRW), where heat is introduced using high electrical pulses power up to 600 kW/m^2, the main advantage is the reduced heating time, about five times less than traditional resistance welding. The reduced heating time is due to fewer problems of de-consolidation that have been attributed to heating conduction through the laminates. A similar choice to generate the current was operated by Wise et al. [49] for resistance welding of joints APC-2/aluminium. IRW simulations confirmed that the welding times had been significantly reduced.

However, a not uniform distribution of temperature at the welding interface was generated. In resistance, welding processes more suitable for long welding, with thin thickness.

Sequential resistance welding (SRW) has been proposed as an alternative method for large scale.

The SRW allowed the resistance welding of double joints length up to 1.2 m. The experiment demonstrated the feasibility of resistance welding for large-scale using SRW and identified the functions to be improved, including the alignment of the part, the pressure application using bagging with vacuum practice.
The cost and processing times were also successful be a problem in SRW, which could be overcome only by adopting a total redesign of the system.

2.2.3. Induction Heating

Induction heating occurs when the materials are subjected to an induction field produced by a coil. The induction field generates eddy currents in conductive materials (or ferromagnetic materials), and the heating happens above all for the joule loss effect Figure 11.

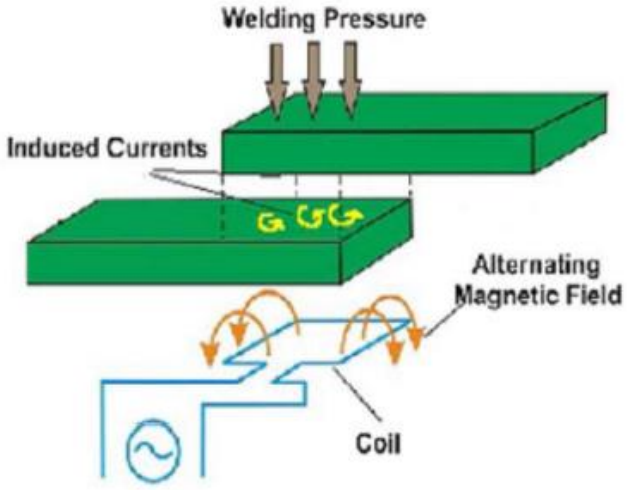

Figure 11: Schematic Induction heating

While the frequency of the induction field increases, the eddy currents are increasingly generated in the outer layer of the conductor. For polymer applications that are usually non-conductive or magnetically they have high permeability, the induction fields apply to the thermoplastic filled with iron particles, micrometric particles of iron oxide, stainless steel, ceramic, ferrite or graphite, acting as susceptors.
The magnetic field generated by a coil of induction is not uniform and generates uneven heating.

Possible Defects in Induction Heating Process

Fibre reinforced polymer composites are characterised by an anisotropic structure that affects both the mechanical behaviour and the heat transfer properties, that, often, causes temperature gradients during the heating process. Moreover, during the heating of the top laminate, can occur delamination effects, that change the way of heat transfer from conduction mode to convection one.

A heating process involves chemical and physical changes in solid polymeric materials. Although thermoplastic materials can be softened by heating without irreversible changes, it is necessary that the heat input be lower than the degradation threshold [50]. While in welding of composites the melting is an essential change, thermal degradation and thermal decomposition that occur above the degradation threshold, are undesired.

Thermal degradation, caused by elevated temperature, decreases physical, mechanical or electrical properties. Instead, thermal decomposition involves a change of chemical species, such as chain scissoring, splitting-off of substituents and oxidation. Commonly, the threshold temperature for thermal decomposition is about 370 °C for CF/PPS.

An essential factor to obtain a reasonable value of adhesion between two carbon fibre reinforced laminates is the process temperature of matrices, as demonstrated by Villegas and Rubio [51], which presented a procedure to prevent thermal degradation of the resin during high-temperature welding successfully. The laminates must be heated above the melting temperature T_m, for semi-crystalline matrices, and the glass transition temperature T_g, for amorphous one; on the other hand, the maximum temperature must be lower than the degradation temperature of the matrix.

2.3. Modelling of Induction Heating

Induction heating of fibre-reinforced composites represents a very complicated Multiphysics process, which is characterised by the electromagnetic and heat transfer physics. The prediction of the temperature evolution during induction heating is of utmost importance to optimise the process parameters and to obtain high resistance joints.

Most of the studies available, overviewed by Ahmed t al. [29], focus on the heat generation mechanism and only limited work has been published on modelling of the process on the macro-level to cover design aspects of induction welding systems such as coil design or tooling. Rudolf et al. [52] showed the adequacy of the Finite-Element-Method using a monolithic material model for the induction heating process [31, 52]. Bensaid et al. [53] modelled the inductive heating of a multi-axial CF/PPS laminate.

For analysis of electromagnetics on a macroscopic level, Maxwell's equation needs to be solved as given by Equation (6) to Equation (9),

$$\nabla \times H = J + \frac{\partial D}{\partial t} \tag{8}$$

$$\nabla \times \mathrm{E} = -\frac{\partial B}{\partial t} \tag{9}$$

$$\nabla \cdot \mathrm{D} = \rho \tag{10}$$

$$\nabla \cdot \mathrm{B} = 0 \tag{11}$$

where **H** is magnetic field intensity, **J** is current density, **D** is electric flux density, **E** is electric field intensity, **B** is magnetic flux density, and **ρ** is electric charge density.

Changes in time of currents and charges imply a change of electromagnetic field. The electromagnetic fields are delayed to the charges of the sources linked to the finite speed of propagation of electromagnetic waves. However, if the variations in time are small and the geometries are smaller than the wavelength, a quasi-static approximation is valid.

Then Equation (8) can be rewritten as:

$$\nabla \times H = J \tag{12}$$

Being fibre heating the dominated heating mechanism of composites, due to the Ohm's law:

$$J = \sigma \cdot E \tag{13}$$

where **J** is current density, **σ** is electrical conductivity, **E** is electrical field intensity. Considering an external current density $\mathbf{J_e}$, Equation (12)(12 became:

$$\nabla \times H = \sigma E + J_e \tag{14}$$

Magnetic field intensity **H** and magnetic flux density **B** can be coupled using magnetic permeability **μ**, as reported in Equation (15):

$$B = \mu H \tag{15}$$

$$\mu = \mu_0 \mu_r \tag{16}$$

where $\boldsymbol{\mu_0}$ is permeability of vacuum and $\boldsymbol{\mu_r}$ is relative magnetic permeability. Using the definition of the magnetic vector potential **A**:

$$\mathrm{B} = \nabla \times A \tag{17}$$

moreover, combining with Equation (15) and Equation (16) yields Equation (17):

$$\nabla \times (\mu^{-1} \nabla \times A) = \sigma E + J_e \tag{18}$$

After the magnetic model, a thermal model must be solved.

The heat equation is based on the first law of thermodynamics, rewritten in terms of temperature. For a solid, the resulting equation is given by:

$$\rho c_p \left(\frac{\partial T}{\partial t} + (u \nabla) T \right) = -(\nabla q) + Q \tag{19}$$

where **ρ** is density, $\mathbf{c_p}$ specific heat capacity at constant pressure, **T** is absolute temperature, **t** is time, **u** is velocity vector, **q** is heat flux vector, and **Q** is a heat source. The velocity vector u is used to model translational movement, such as a moving heat source.

The Fourier's law describes the relationship between the heat flux vector q and the temperature gradient:

$$q = -k\nabla T \tag{20}$$

where **q** is the heat flux vector, **k** is thermal conductivity, and **T** is absolute temperature. For anisotropic materials, **k** becomes a vector [86].

Heat fluxes, e. g. from convection and radiation are estimated by boundary conditions. The heat flux across a boundary can be described by:

$$n \cdot (k\nabla T) = q_0 + \mathrm{h}\left(T_{inf} - \mathrm{T}\right) + \varepsilon_e \sigma_{SB}(T_{amb}^4 - T^4) \tag{21}$$

where **n** is the vector normal to the boundary, $\mathbf{q_0}$ is heat flux entering the domain, **h** is heat transfer coefficient, $\mathbf{T_{inf}}$ is the temperature far away from the modelled domain and heat transfer coefficient, $\mathbf{T_{amb}}$ is ambient bulk temperature, $\boldsymbol{\varepsilon_e}$ is surface emissivity, $\boldsymbol{\sigma_{SB}}$ is Stefan-Boltzmann constant, and **T** is absolute temperature. The heat flux $\mathbf{q_0}$ is interpreted in the direction of the inward normal whereas convection and radiation terms are in the direction of the outward normal.

Electromagnetic Heating for Adhesive Bonding

3.1. Introduction

Adhesive bonding has allowed the development of construction of lighter structures, replacing the rivets in the joints, above all in the automotive industry; moreover, has permitted avoiding welding where temperature gradients could damage materials.

However, the mechanical properties of two surfaces joined with an adhesive depend on many parameters, such as their pre-treatment, their wetness by the liquid adhesive and adhesion forces, bonding between the substrate and the solidified adhesive, and by the cohesion, bonding forces acting the adhesive within itself.

Hot-melt adhesives are made up of adhesives based on thermoplastic polymers, elastomers, (polyurethanes) and thermoplastic terpolymers and styrene-olefins, ethylene or propylene or butadiene: these polymers liquefy for heating and solidify for subsequent cooling.

As soon as the softened hot-melt adhesive is put in contact with the surfaces to be joined, a heat transfer gradient is generated throughout the substrate's area. The high difference between the masses of the two materials, adhesive and adherends, allows to rapidly decrease the temperature to the value at which the adhesive restores its solid state by acquiring a cohesive force that holds the two adherends' surfaces firmly bonded together.

Several methods can obtain the heat required for the liquefaction of hot-melt adhesive.

In this part of the work, an alternative heating process for adhesively bonded joints, based on Induction Heating (IH) was investigated. Electromagnetic induction heating is a process that it requires no contact between the induction coil and the workpiece, and if the inductor is well designed no heating is produced

outside of the working area. This process is not an innovative technology, as is very frequently applied for heating magnetic susceptible metals [25].

Usually, thermoplastic adhesives are neither magnetic nor conductive, but it is possible to heat the adhesive heating the adherends using IH.

Moreover, recently, this technology has also been employed for heating carbon fibre-based composites; in fact, induction joining of thermoplastic carbon fibre reinforced polymer composites (CFRTP) is proving itself to be a very effective method.

Several authors investigated the principle of induction heating of carbon-fibre-reinforced thermoplastics, as reported in the previous chapter.

Recently, some authors have investigated the possibility to apply IH for the thermosetting adhesives curing process: Sanchez et al. [54] have investigated an IH curing process using CFRTP adherends and a two-component epoxy paste adhesive. In this study, they demonstrated how in this process the energy consumption is approximately 25% less than traditional curing techniques.

Additionally, Severijns et al. [28] have studied the curing and mechanical behaviour of a mix of iron particles and two component epoxy paste adhesive, demonstrating that adding iron particles to the adhesive results in a reduction of the lap-shear strength.

Induction Heating can be considered a very complicated Multiphysics process requiring understanding both the electromagnetic and the heat transfer phenomena in the laminates. The prediction of the temperature evolution during induction heating is of utmost importance to optimise the process parameters and to obtain high strength joints.

Recently, O'Shaughnessy et al. [55] have developed a three-dimensional finite element model of the induction welding of CFRTP; in their study, they have considered a stainless steel wire mesh, named heating element, located at the interface of the adherends, demonstrating that the presence of this kind of element does not affect the mechanical characteristics of the joint.

Instead, in this work, thanks to substrate's heating by electromagnetic induction, the adhesive was heated up to the liquefying temperature range, at which the adhesive is liquid and hence can wet the adherends.

In this first part of the study, a numerical model capable of predicting the temperature increase of the hot-melt adhesive and the composite adherends by induction heating was developed.

As evidenced by careful bibliographic research, there is a lack of studies concerning a numerical model predicting the heating trend during the curing process of a hot-melt thermoplastic adhesive to join carbon-fibre-reinforced thermoplastic (CFRTP).

Experimental activities were also performed to validate the developed model.

Additionally, the different parameters that affect the final performances of the induction heated adhesive bonding were optimised. Mechanical tests according to two different ASTM standard methods, single lap shear and short beam shear tests, confirmed the effectiveness of the optimised parameters. The single lap joint shear (SLS) test is one of the most used methods to measure the joint performance [56]; the principal advantages of this test method are its simplicity and low cost, but several disadvantages characterise it.

As demonstrated by Luo and Tong [57] the stress distribution is strongly non-uniform and depends on the geometry, as reported by Silva et al. [58]. De Castro and Keller [59] demonstrated how the joint strength depends on the overlap length; Reis et al. [60] investigated the effect of the rigidity of the adherends on joint strength.

The short beam shear (SBS) test has been used for evaluating composite laminates, and as demonstrated by Pahr et al. [61], the SBS test is more accurate than the SLS.

A comparative study of the two different standard methods, SLS and SBS, is finally conducted. The fracture surface and the results obtained from the SLS tests are compared with those obtained from the SBS tests.

3.2. Three-Dimensional Finite Element Model

The Software used for the simulation of the induction adhesive bonding was JMag Designer. JMag was released for the first time in 1983 as a tool to support the design of devices such as actuators and circuit components. Mathematical equations describing the electromagnetic part are based on Maxwell's equations; a quasi-static approximation was used [62].

The software divides the physical phenomenon analysis into two analyses. The first one is related to the joule loss model, where a magnetic field analysis is used to handle the phenomenon produced by the eddy current and the magnetic field in the workpiece when current flows through the coil.

This analysis aims to obtain a distribution of Joule effect losses within the specimens, which makes it a source of heat in the analysis of electromagnetic induction heating. The second one is the temperature analysis model where the thermal analysis is used for the heat transfer phenomenon that occurs within the workpiece.

The relationship between the physical phenomenon and the analysis model is shown in Figure 12.

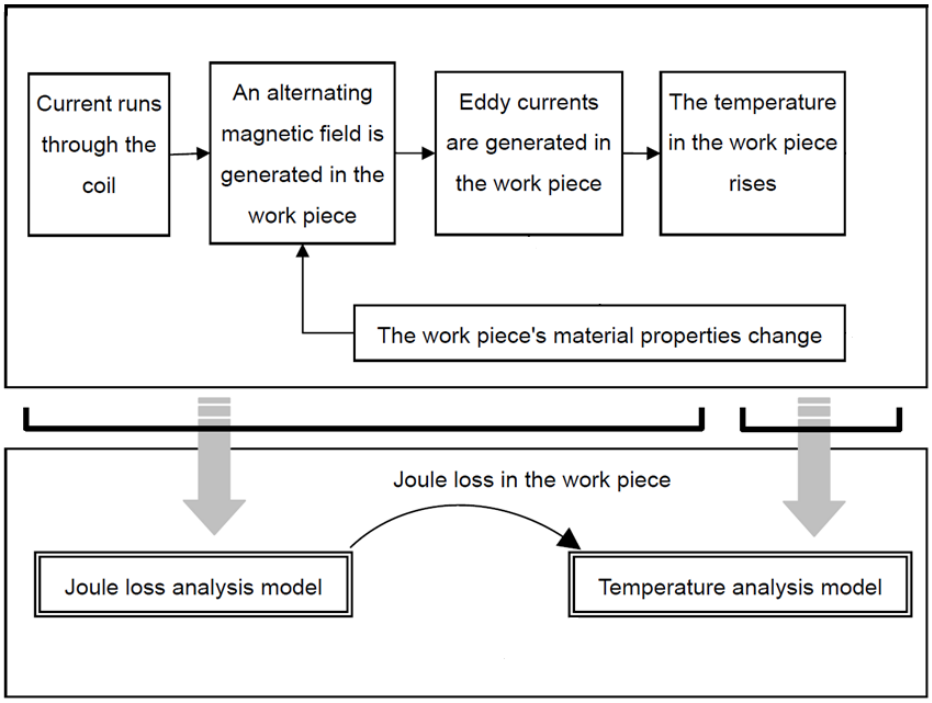

Figure 12: Relation between physical phenomenon and analysis model

Figure 13 shows the pattern of the simulation model developed. The model was developed for each analysis. In this case, two models were created, for the joule loss analysis and temperature analysis. After the models tuning, a two-way coupled analysis was completed iteratively using the results of the Joule loss analysis for the processing of the Thermal analysis and vice versa. Thermal analysis results were used to know the temperature trend during the process in the adherends and the adhesive.

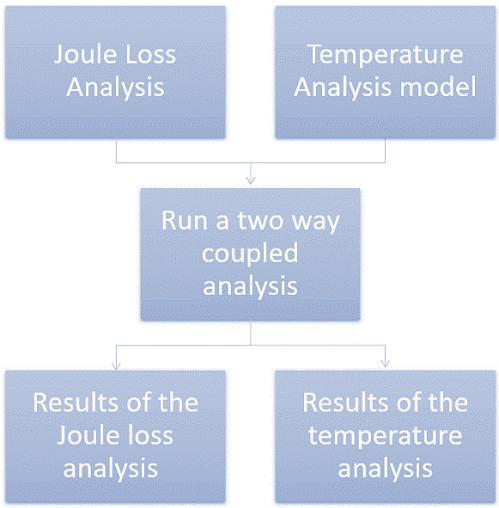

Figure 13: Pattern of the model

In the case of the Joule Loss Analysis the software allows five different types of magnetic field analysis:

- Static analysis (3D, 2D, AX);
- Transient analysis (3D, 2D, AX);
- Frequency analysis (3D, 2D, AX);
- Section analysis (3D, 2D);
- Analysis of iron loss (3D, 2D, AX).

An analysis of the frequency response is performed since the waveform of the supply current and the electromagnetic field in the circuit is sinusoidal.

The next step was to create a model of the electrical circuit (Figure 14), which simulates the induction machine generator. The circuit model was simulated by organising, and then connecting, the elements of the circuit. The analysis of the circuit is performed simultaneously with the analysis of the magnetic field.

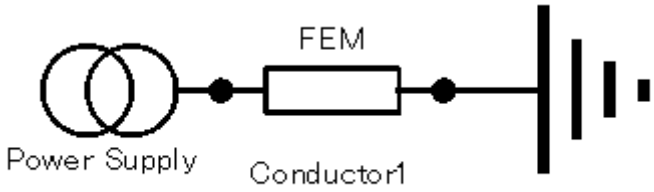

Figure 14: Electrical circuit scheme

For this analysis, the "Power Supply Current" element was used as it simulates a sinusoidal current flowing inside the inductor.

The "FEM Conductor" element is used when the distribution current must be considered in a conductor. The conductor is connected to the circuit by this element. The resistance of the FEM conductor is determined by the geometry of the model and by the electrical conductivity, so no other parameters must be set.

The third element of the circuit is represented by "grounding", that is connected to the opposite side of the FEM conductor, no parameters are necessary for grounding.

Once the electrical circuit model has been created, the boundary conditions must be set for the analysis of induction heating; these conditions are:

- Symmetry Boundary;
- FEM conductor;
- Frequency control;
- Coupling analysis;
- Circuit parameters.

The symmetry boundary condition is used to specify the distribution of the magnetic field within the coil. The magnetic field flows in parallel, and the current is perpendicular to the face in which this condition is set.

The "FEM Conductor" condition is linked to the element in the circuit. When the amplitude is positive, the current flows from the input face to the output face; when it is negative, it flows backwards.

The value of current imposed, e.g. case of 24 A, in the model has been set according to the trend shown in the graphic reported in Figure 15 to keep constant the maximum temperature during the holding time,

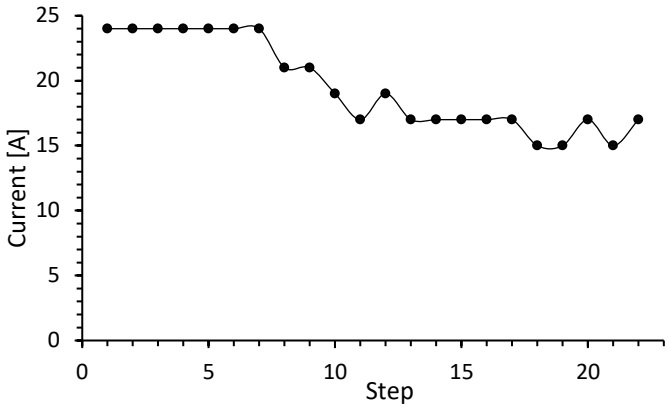

Figure 15: Current values set for the case of the current value of 24 A

Frequency control is used to specify the frequency value used in the analysis. The number of "steps" specifies the number of values used.

The frequency of the inductor, in this case, is 145 KHz and is constant, so the number of steps is equal to one. A coupling analysis was chosen , to perform both a magnetic field analysis and a thermal analysis.

Subsequently, the thermal analysis has been set. Model geometry in thermal analysis can be simplified by eliminating parts that do not affect temperature distribution, such as air and coil, in fact during the experimental part it is taken at a constant temperature by a refrigeration system. The analysis is performed efficiently even with a simplified model as the calculation time is reduced. In this analysis the heat transfer from the coil to the specimens is not considered since the heat is generated only by the eddy currents inside the specimens. Also, in this case, the software proposes different types of thermal analysis:

- Stationary analysis (3D);
- Transient analysis (3D).

The type of analysis is determined by the result to be obtained: a constant temperature (stationary analysis) or a temperature profile (transient analysis). In this case, transient thermal analysis was chosen to obtain the temperature variation inside the specimens with the time.

Once the type of analysis has been chosen, the boundary conditions must be imposed:

- Heat transfer boundary;
- Initial temperature;
- Heat source;
- Number of control steps.

The boundary conditions for heat transfer must be specified to simulate the heat distribution between the specimens; all the faces of the two specimens and adhesive were selected, in order to consider the heat transferred from specimens and adhesive, between specimen and support and also between support and surrounding air.

Furthermore, a value must also be assigned to the heat transfer coefficient, equal to 5 (W/m^2 * °C). The software requires that the initial temperature of all elements, equal to 26 ° C, is also set. The next step was to set the two specimens as a heat source. In the control panel of this condition the Coupling box must be checked, as analysis coupled with the analysis of the magnetic field was carried out. The accuracy of the analysis and the convergence of nonlinear interactions can be improved by reducing the time interval. If the interval time is too short, the number of steps increases, and the time required for analysis increases. Therefore, for the simulations carried out, a fair compromise was sought between calculation time and analysis precision.

3.2.1. Materials

The electrical and magnetic properties of the materials of all components have been set (Table 1).

Table 1: Input parameters of the FE model for CFRP, Ertalon's support and Prodas

Parameter	CFRP	Ertalon	Prodas
Heat capacity at constant pressure (C)	1000 (J/Kg*K)	1460(J/Kg*K)	1380(J/Kg*K)
Relative electrical Permittivity (ε_r)	80	1	1
Thermal Conductivity (k)	3.5 (W/m*K)	0.2 (W/m*K)	0.15 (W/m*K)
Relative magnetic permeability (μ_r)	1	1	1
Electrical conductivity (σ)	$2x10^4$ 1/(Ω*m)	$1x10^{-5}$ [1/(Ω*m]	$1x10^{-5}$ [1/(Ω*m]
Density (ρ)	1.4 (g/m³)	1.2 (g/m³)	0.98 (g/m³)

3.2.2. Geometry and Mesh

The CAD model, created in dedicated software, has been imported in JMag, both for the normative used. (Figure 16)

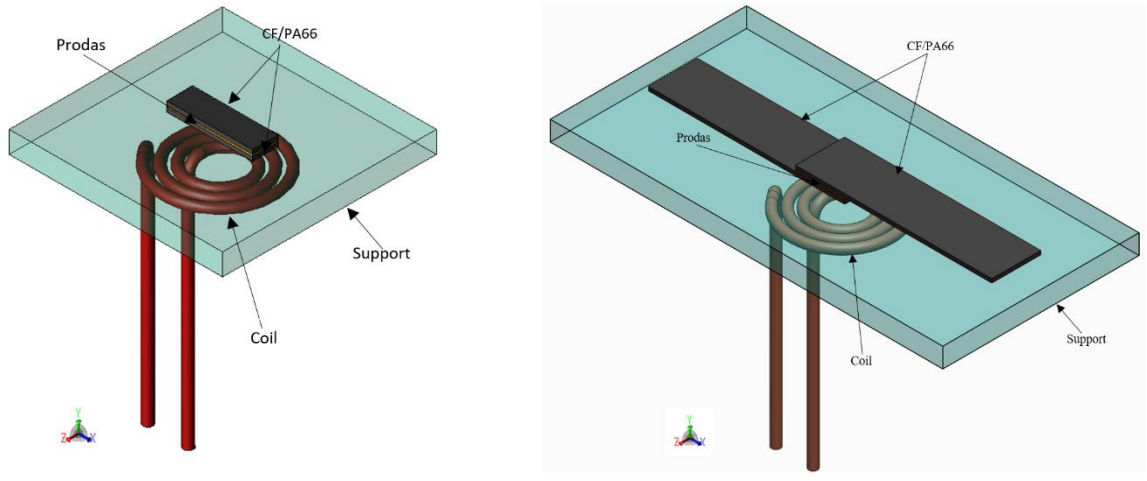

a) b)

Figure 16: a) CAD Model of ASTM standard D2344; b) CAD Model of ASTM standard D5868

Furthermore, the mesh must be generated. In a FEM analysis, the mesh must be generated in the air region with a size determined by the saturation severity. In this analysis the scale of the air region is set to 2.5 times the model's mesh to

understand better how the magnetic field is distributed in the air, starting from the boundary symmetry condition set, shown in Figure 17 ; so, it is assumed that the magnetic field is not present at the outside this area.

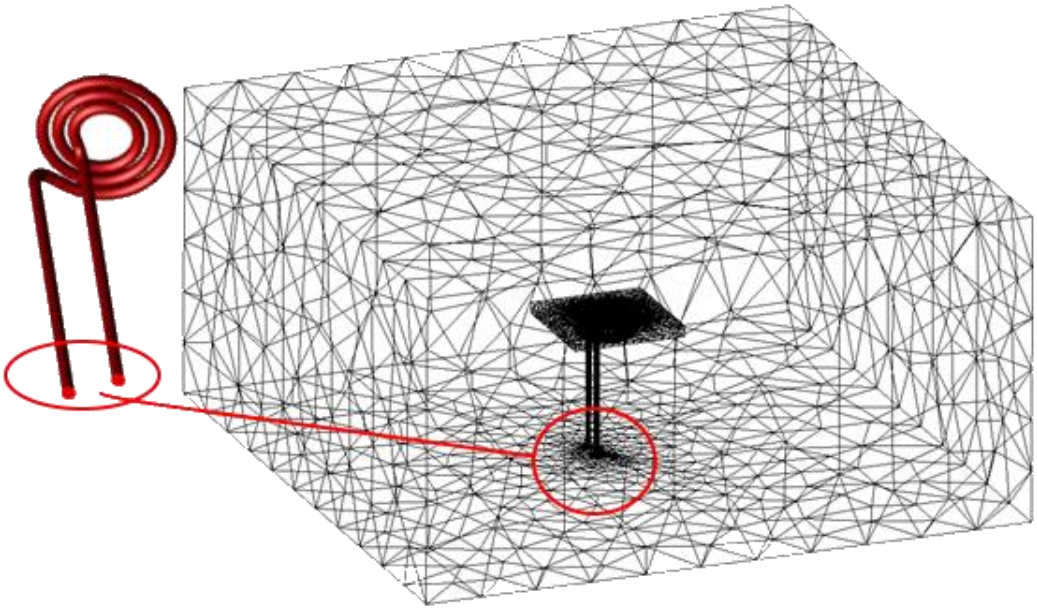

Figure 17: Symmetry boundary faces and mesh of air region

3.3. Induction Heating Bonding Experiments

3.3.1. Materials

The study on the process parameters for the induction bonding was carried out on carbon fibre reinforced polyamide (CF-PA66): Tepex® Dynalite 202-C200 (9)/50% (PA6 50% carbon fibres), produced by Tencate.

For the implementation of this project, among the different adhesives, PRODAS-1400 (Beardow Adams) was used as a thermoplastic adhesive.

The Prodas-1400 (hot-melt polyolefin) is a synthetic polymer-based adhesive allowable for assemblies where good cohesive strength and longer open time than other hot-melt adhesives (usually characterised by an open time of less than 30 s), are required.

PRODAS is a unique adhesive containing thermoplastic polymers, adhesive resins, waxes and anti-oxidants. It is indicated for assemblies which require an excellent cohesive strength. It also characterized by high resistance to high (135°) and low temperatures, it is versatile and has excellent adhesive capacity, which allow the use of plastic (polypropylene, acrylic, nylon, PVC), rubbers (natural, synthetic, neoprene), metals (aluminum, steel), fibres and porous materials (leather, textiles, ceramics, cardboard, paper, wood).

It is characterised by excellent thermal stability, excellent resistance to ageing and peel strength. One of the main advantages is that it does not contain any dangerous ingredients or impurities. As shown in its technical sheet, the temperature of the recommended application PRODAS falls in a range of temperature which varies between 175 ° C and 195 ° C.

3.3.2. Specimens

The joint mechanical performances were evaluated using short beam shear strength test and single lap joint shear test. According to ASTM's test methods, the specimens had the following dimensions:

- For ASTM D2344 [63]: 40x12 mm, and thickness of 2 mm and total overlap;
- For ASTM D5868 [64]: 100x25 mm, and thickens of 2 mm and 25x25 overlap.

The specimens were cut into single specimens, as prescribed by the ASTM's test methods, and then assembled and cured individually.

The adhesive, in the form of film, was cut with the dimension of the overlap zone, according to the ASTM's applied:

- For ASTM D2344, 40x12 mm, and thickness of 1 mm;
- For ASTM D5868, 25x25 mm, and thickness of 1 mm.

Figure 18 shows the load configurations and the dimensions of the specimens for the two different testing methods.

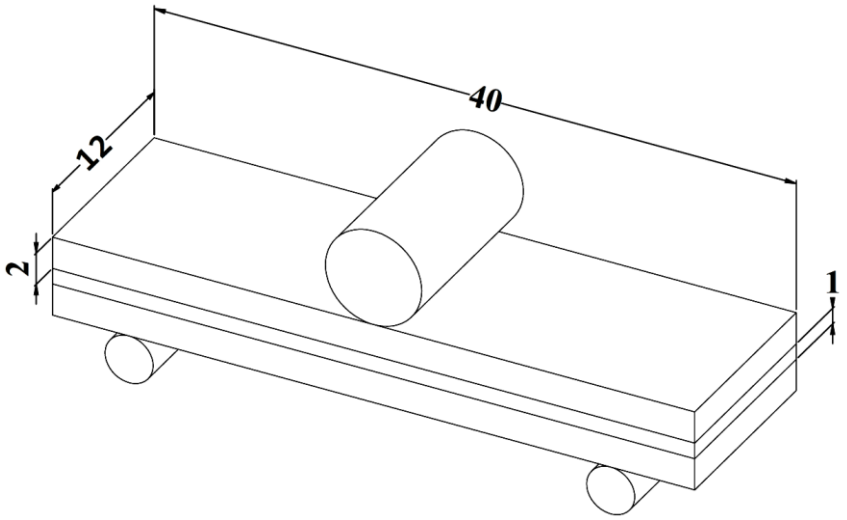

a)

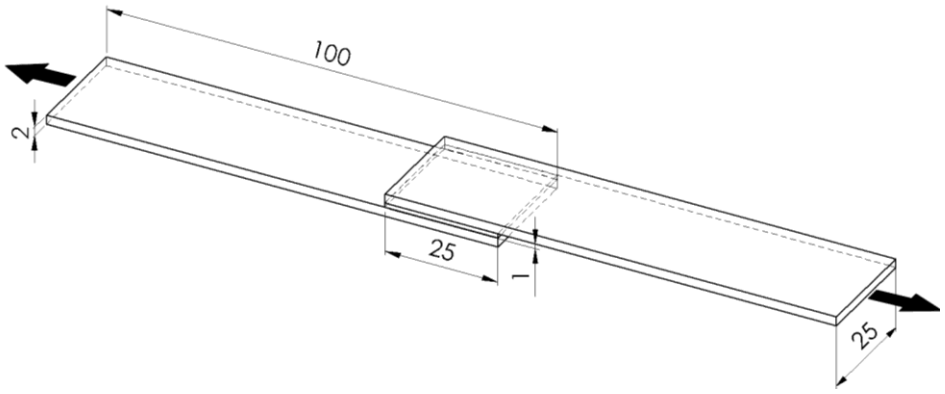

b)

Figure 18: Configuration and dimensions for the standard methods: a) ASTM D2344 and b) ASTM D5868

3.3.3. Experimental set-up

The study exposed in this work consist of three phases. Firstly, a simulation model was developed. Then, the experimental tests on the adhesive cure were done. Finally, the mechanical performance of the induction-heated adhesive bonding is assessed by mechanical testing; also, the results of the numerical model were correlated with the experimental ones.

The effects of three process parameters on the induction heating were considered, such as:

- the current, to set the power;
- the maximum temperature at the interface between adherends;

- the holding time at maximum temperature.

Each of these parameters was varied in its range of value, while the others were kept constant. The simulation cycle was designed using the DOE (Design of Experiment), considering the current generator characteristics to be used for the experimental phase, totalling 27 different cases.

In Table 2 are reported the different values of the process parameters imposed.

Because of the not uniformity of heating due to the edge effect that has been reported in previous studies [29], it was decided to vary the Holding time, to homogenise the temperature over the adhesion interface area.

The choice of the three maximum temperature values depends on the Prodas adhesive liquefying temperature which varies between 175 °C and 195 °C.

Table 2: Summary of all simulations performed

Current (A)	Maximum Temperature (°C)	Holding time (s)
10 (I_1)	175 (T_1)	10 (t_1)
	185 (T_2)	20 (t_2)
	195 (T_3)	30 (t_3)
17 (I_2)	175 (T_1)	10 (t_1)
	185 (T_2)	20 (t_2)
	195 (T_3)	30 (t_3)
24 (I_3)	175 (T_1)	10 (t_1)
	185 (T_2)	20 (t_2)
	195 (T_3)	30 (t_3)

The induction heating equipment used is an Egma 30R unit, designed and developed by Felmi (Italy). The generator can vary the frequency by 100-280 kHz, depending on the coil geometry and the current; the power can be tuned to 30 kW, ranging from 20% to 100%.

In this research, during the experimental tests, a "Spiral of Archimedes" shaped induction coil was used, and the same geometry was modelled in the software; Figure 19 shows the geometry of coil used. The material of the coil is electrolytic copper, and the operating frequency was kept constant at 145 kHz.

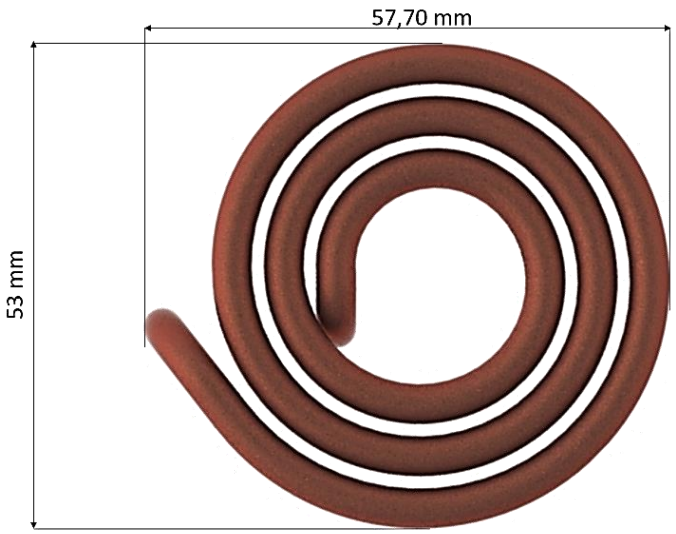

Figure 19: Coil's shape and dimensions

The current generator allows a temperature control in a specific point of the specimen, appropriately chosen. In particular, the control is based on a pyrometer SKS-T14-09. This kind of system has a temperature range between 32 °C and 900 °C. It utilises a silicon cell detector and operates at short wavelengths around 1.0μm where emissivity errors are minimised. It has a fast response time of 5ms. By reading the temperature value, it changes the current of the generator to keep the temperature constant once the imposed maximum temperature value is reached.

The point that experienced the maximum temperature according to the numerical simulation, to avoid adhesive degradation, was chosen. This point is located close to the adhesive area on the lateral side of the specimen as reported in Figure 20.

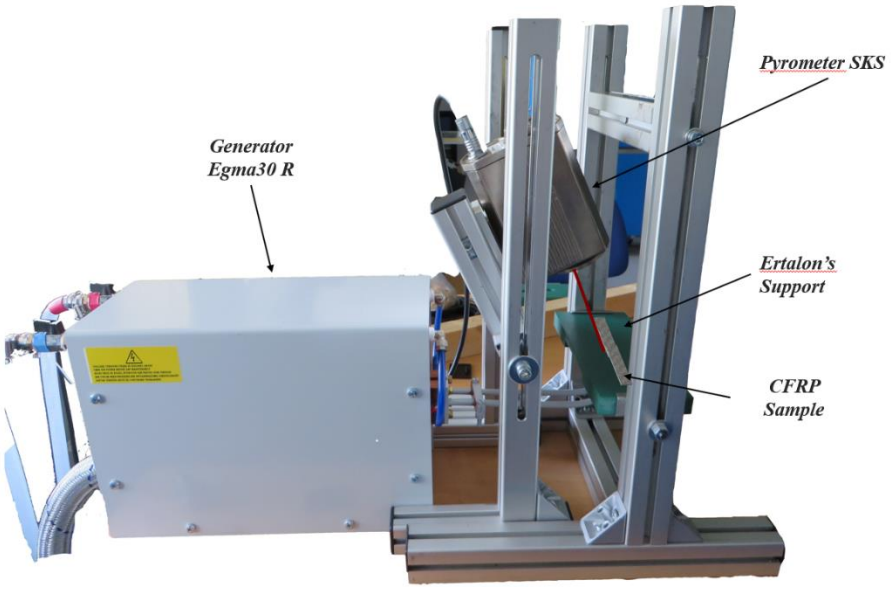

Figure 20: Experimental Set-up

For the correct measure of the temperature it is necessary to know the value of the specimen's material emissivity; for carbon-carbon composites specimens, the emissivity is 0.8 [65]. This value is suitable also for the material used in this work, in fact, it was verified using a thermocouple and calibrating the pyrometer emissivity value on the thermocouple reading.

The specimens were placed on an Ertalon's support, which was also considered in the numerical simulation, with the coil under the support.

As reported above, to measure the mechanical performance of the induction-cured adhesive, mechanical tests were performed, according to ASTM standard D2344 [63] and D5868 [64]. The tests were performed on a universal MTS Criterion Model45 dynamometer with a load cell of 100 kN.

For each series, a minimum of five specimens was tested.

3.4. Results and discussion

All the reported results were obtained from the simulations performed using the method previously described.

By using the Plot Parameters command in Project Manager, it is possible to choose the physical parameter to display, such as the temperature, and it is possible to monitor the evolution of their magnitude by choosing to visualise the value at a precise instant and for a known geometric entity, such as a point, or a line, or an area.

In the present case, it was chosen to extrapolate the temperature trend within the adhesive, as the technological objective is to reach the temperature of liquefying. In Figure 21 the trend of temperature for the case of 10 A current and holding time of 30 sec is reported. The maximum temperature values are 175, 185 and 195 °C, as previously reported.

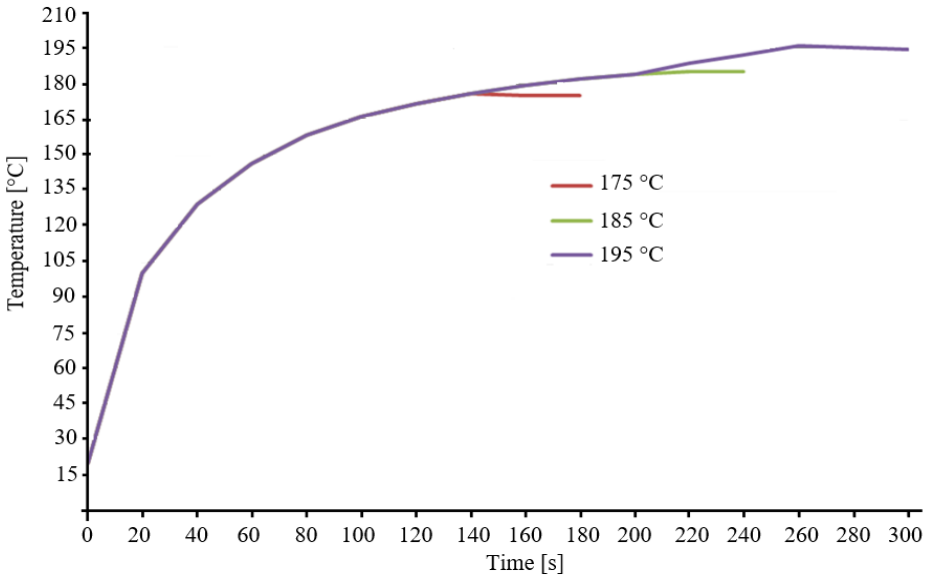

Figure 21: Profile temperature

Figure 22 shows the evolution of the temperature in the adhesive layer. Figure 22(a) shows the temperature distribution just when the maximum temperature was reached, while Figure 22(b) shows the temperature distribution after 30 sec. Figure 22 also shows how the hottest point in the adhesive layer moves from the outer edge inwards, favouring a more uniform temperature distribution.

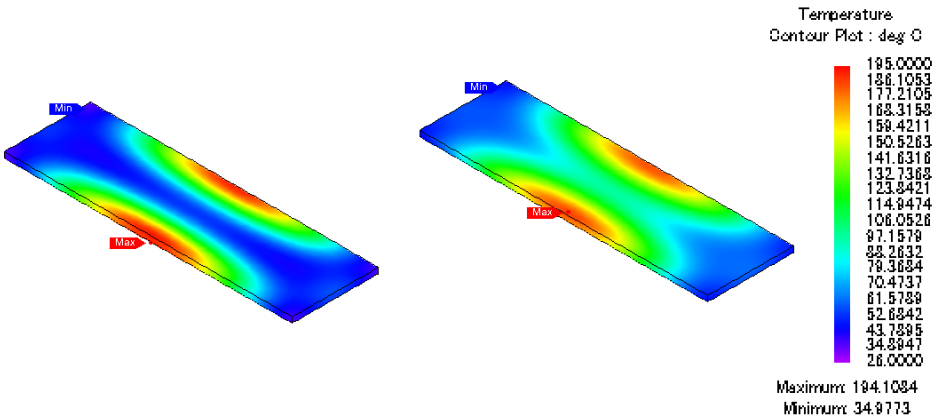

a) b)

Figure 22: Temperature field at holding time at t=0s (a) and t=30s (b).

The simulation allowed to better understand the temperature distribution at the interface between CFRTP specimens and thermoplastic adhesive. Moreover, as is evident from Figure 23, it also considers the heat transfer between the specimen and Ertalon's support.

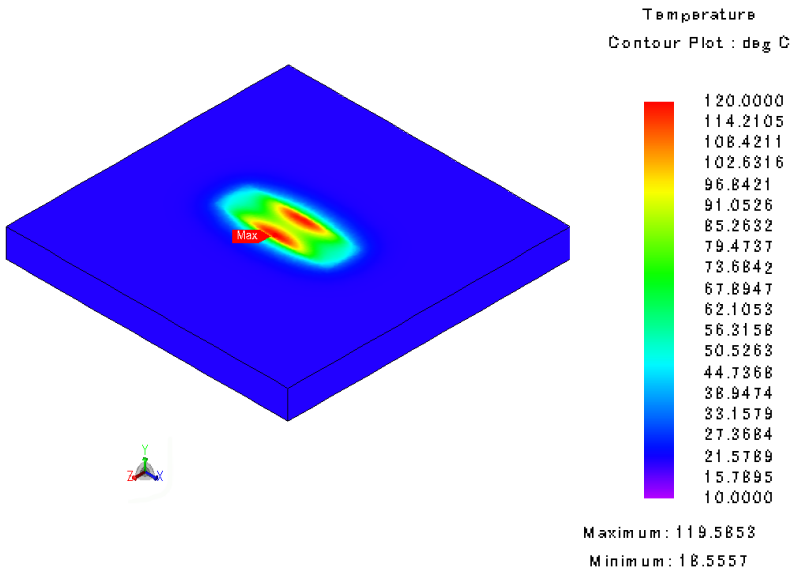

Figure 23: Temperature field of Ertalon's support

3.4.1. Correlation

The numerical model was validated comparing the experimental temperature, measured at the joint interface during the induction bonding process, with the numerical model results.

The feedback, for heating control of the induction bonding, is given by a single point temperature measurement obtained using a pyrometer (SKS), implemented on the current generator as previously reported. As previously stated, it is crucial to control the maximum temperature to avoid the degradation, or even the burning, of the adhesive.

The results of the model were compared with the experimental measurements at the joint interface during the induction bonding process, and, as shown in Figure 24a, they fit the experimental results with outstanding accuracy.

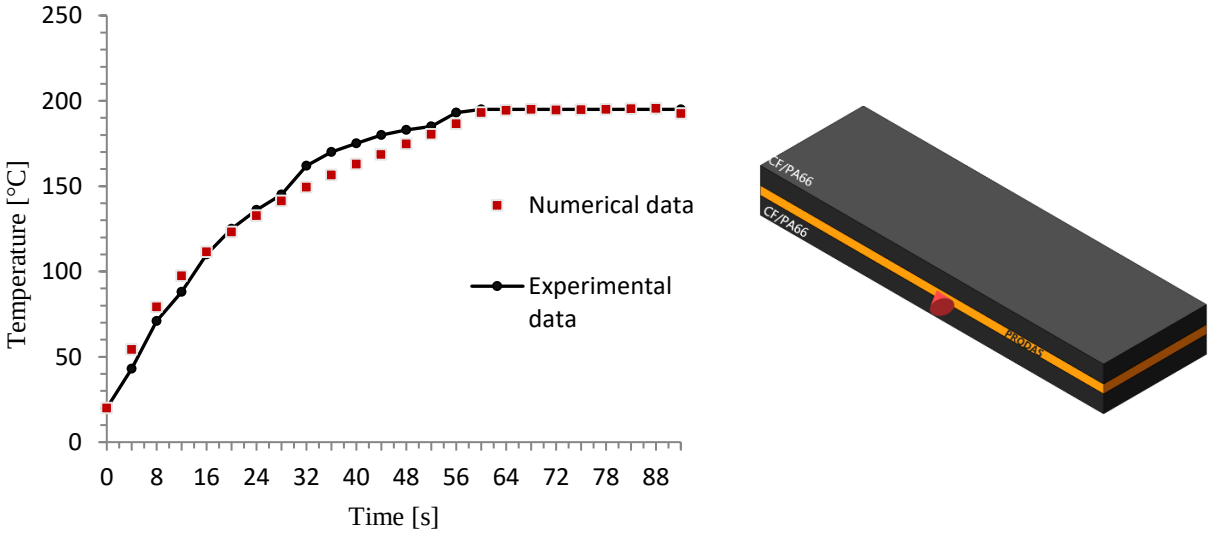

a) b)

Figure 24: a) Comparison of the numerical and experimental temperatures. b) The reported surface is controlled using an optical pyrometer and is the set point adopted for the control of the induction bonding equipment.

3.4.2. Joint Performances

Following the induction bonding tests, the mechanical characterisation was carried out, to verify the effectiveness of the selected parameters.

The tests were performed using a universal MTS Criterion Model45 dynamometer with a load cell of 100 kN.

The standards test used, as described above, are the ASTM D2344 and D5868, the results of these tests are reported in Table 3. The values shown were obtained by averaging over five tests.

Table 3: Results of the mechanical tests according to ASTM D2344 and ASTM D5868 for all the experiments performed

I	T	t	Average D2344 (Mpa)	Average D5868 (Mpa)
I_1	T_1	t_1	16.413	0.451
I_1	T_1	t_2	17.790	0.876
I_1	T_1	t_3	19.928	0.844
I_1	T_2	t_1	20.041	1.156
I_1	T_2	t_2	22.339	1.435
I_1	T_2	t_3	20.079	1.323
I_1	T_3	t_1	20.698	1.198
I_1	T_3	t_2	22.339	1.206
I_1	T_3	t_3	22.107	1.203
I_2	T_1	t_1	20.884	0.740
I_2	T_1	t_2	22.546	1.058
I_2	T_1	t_3	21.767	0.887
I_2	T_2	t_1	19.688	0.892
I_2	T_2	t_2	20.352	1.506
I_2	T_2	t_3	20.698	1.505
I_2	T_3	t_1	21.972	1.471
I_2	T_3	t_2	21.796	1.486
I_2	T_3	t_3	21.610	1.496
I_3	T_1	t_1	21.045	1.029

I_3	T_1	t_2	18.197	0.876
I_3	T_1	t_3	19.780	0.930
I_3	T_2	t_1	20.677	2.086
I_3	T_2	t_2	26.465	1.435
I_3	T_2	t_3	22.359	1.323
I_3	T_3	t_1	19.575	1.743
I_3	T_3	t_2	23.184	1.765
I_3	T_3	t_3	22.858	1.789

The strength of single-lap joints and the interlaminar shear strength was characterised by satisfactory performance comparable with the results of the non-induction cured sample.

The non-induction cured samples were realised by providing the melted adhesive on the overlap zone of one of the adherends, and subsequently coupling the other one adherend. The deposition of the adhesive, PRODAS 1400, was realised using a manual applicator of adhesive hot-melt, set at the nozzle temperature of 185°C. To obtain a constant thickness of adhesive at 1 mm, the joint realised was positioned in a specific tool where a constant pressure acts for 2 minutes, the time during which the adhesive acquire cohesive force.

The maximum values for both standards with the corresponding process parameters are reported in

Table 4; additionally, these values are compared with the reference samples.

Table 4: Maximum values of shear strength for the testing methods ASTM D2344 and ASTM D5868 for induction heated and Reference samples.

I	T	t	Average D2344 (MPa)	Average D5868 (MPa)
I_3	T_2	t_1	20.677	2.086
I_3	T_2	t_2	26.465	1.435
Reference sample			25.675	1.802

It can be noted that for both the test methods the highest values of strength occur for the same process parameter values, except for the holding time. In the case of ASTM D2344, the maximum shear value is reached using a longer holding time than holding time used for the maximum shear value measured with the ASTM D5868; this is explained by the fact that in the case of ASTM D2344, the adhesion area is 480 mm^2, with a rectangular geometry, while in the case of ASTM D5868, the adhesion area is 625 mm^2, with square geometry.

In the case of the rectangular geometry, the heating is more affected by the edge effect than the square one, as highlighted in Figure 25.

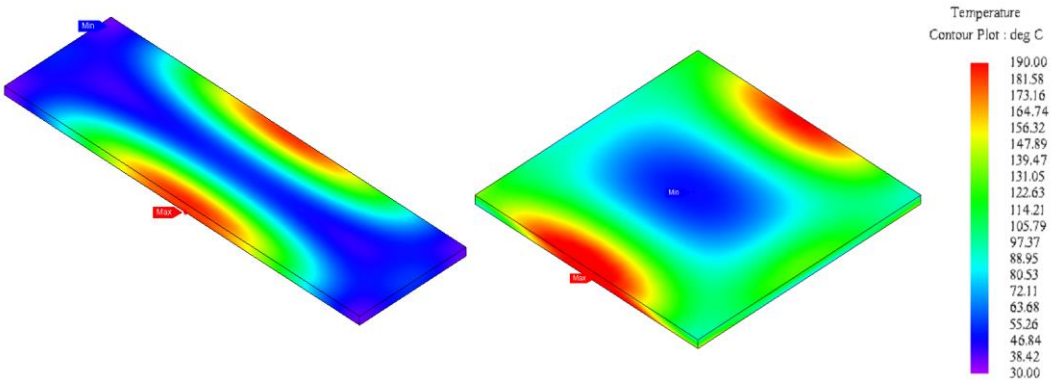

a) b)

Figure 25: Temperature distribution into the adhesive layer: a) D2344 and b) D5868 for the same process parameters: I_3, T_2 and t_2.

Finally, at the end of each test, the fracture surface of the joint has been examined to evaluate the type of failure mode.

Figure 26 shows that the joints realised according to the ASTM D2344, are characterised by a fracture area that does not affect only the adhesive layer, but also the adherends. In the case of the highest shear strength values, reported in Figure 26a, the fracture area affects only the adherends, meaning that the interface adhesive-adherends strength was the highest.

Figure 26b reports the joint realised with a current of 24 A, a maximum temperature of 175 °C and a holding time of 20 s, that is characterised by a shear strength value of 18.2 MPa. Analysing the fracture surface of this sample shows that the value of the shear strength, is lower than in the case of Figure 26a depends on the adhesive fracture surface between adhesive and adherends.

Figure 27 shows that the joints realised according to the ASTM D5868, are characterised by a fracture area that does not affect only the adhesive layer, but also the adhesive-adherends interface. In the case of the highest shear strength values of the joint, the fracture area affects only the adhesive, meaning that the fracture was cohesive, or mostly cohesive 88% (Figure 27a). In Figure 27b the picture of the sample realised with 24 A, with a maximum temperature of 175 °C and a holding time of 20 s is shown. This sample is characterised by a shear strength value of 0.88 MPa that, as highlighted by Figure 27b; it is affected mainly by an adhesive fracture surface, 70% adhesive.

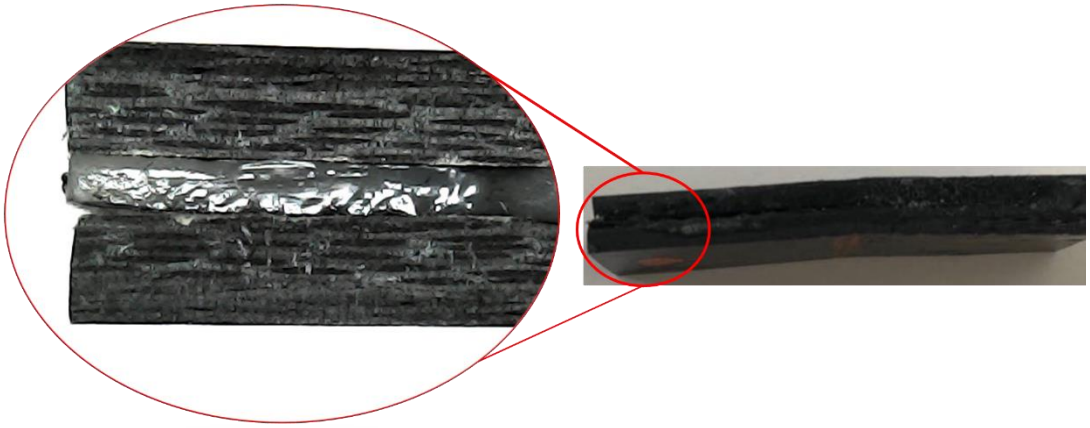

a)

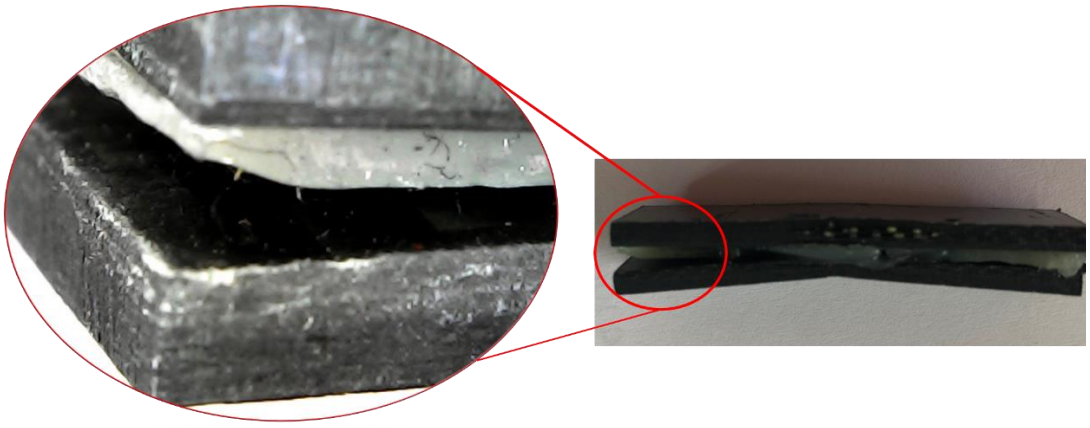

b)

Figure 26: Example of the fracture surface of a tested specimen realised according to D2344: a) adherends failure and b) failure at the adhesive-adherends interface

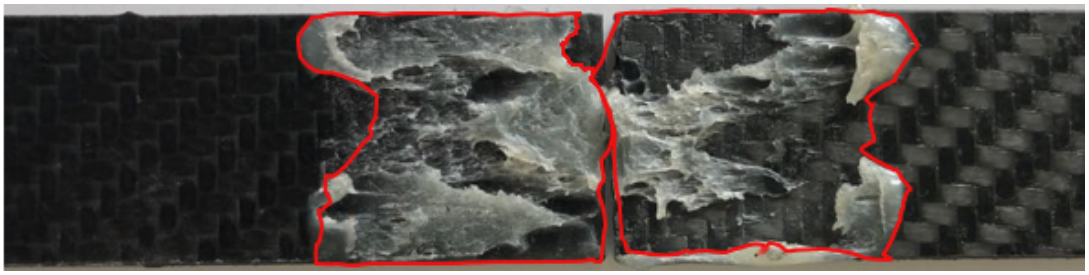

a)

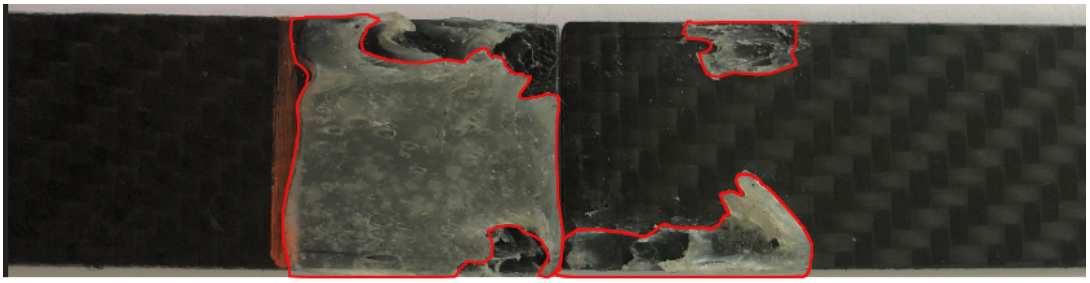

b)

Figure 27: Example of the fracture surface of a tested specimen realised according to D5868: a) cohesive failure, about 88% and b) adhesive failure, about 70%

3.4.3. Analysis of Variance

After the mechanical test, the shear strength results were evaluated by Analysis of Variance (ANOVA). Firstly, a bar graph is reported, which considers all the average values of the shear stress obtained. Figure 28 and Figure 29 show the trend of the strength stress as a function of the process parameters, such as Holding time, Temperature and Current, for the two different ASTM standard methods adopted. In particular, it is evident how in case of ASTM D2344, Figure 28, the average value is less influenced by the process parameters adopted than the D4858 case, Figure 29. In fact, in this case increasing the holding time, the temperature and the current, along with the horizontal axis, the shear strength increases.

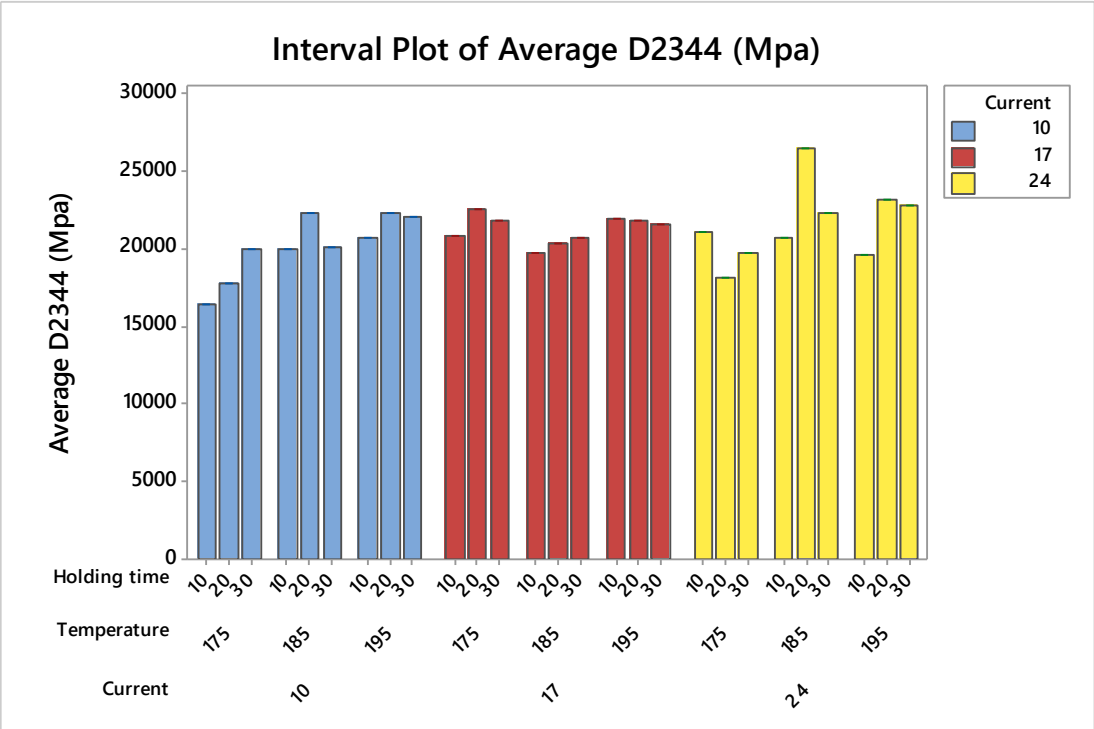

Figure 28: Interval Plot of Average D2344

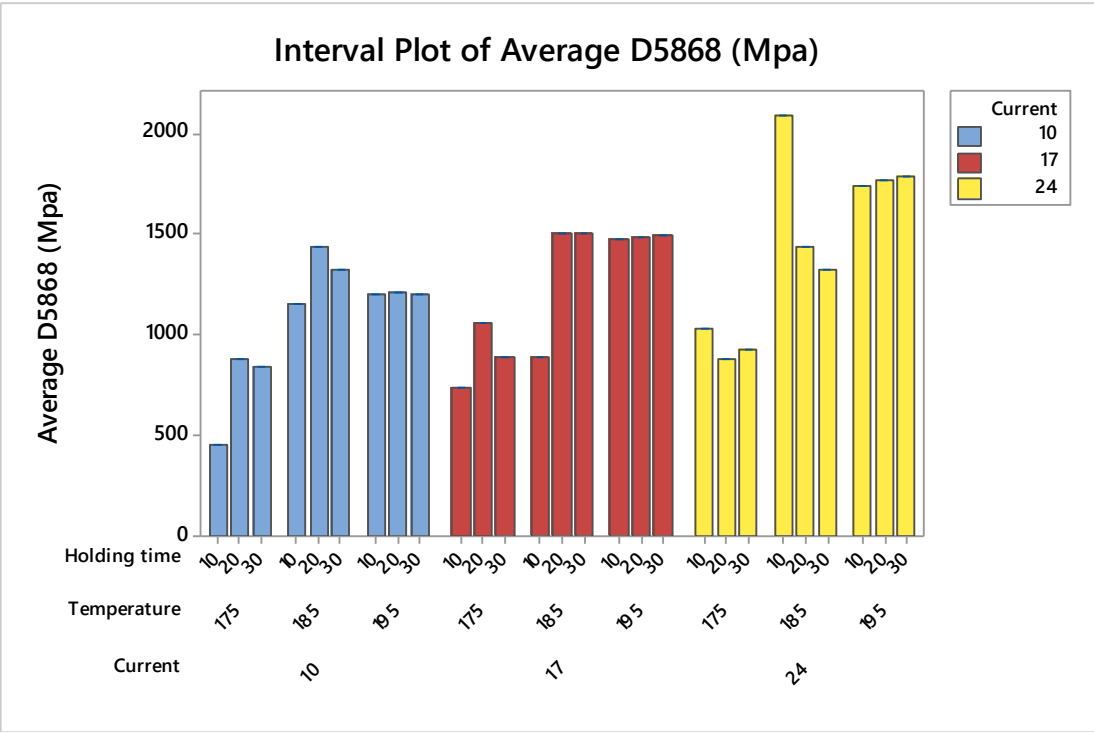

Figure 29: Interval Plot of Average D5868

The Main Effects Plot provides for each factor the trend of the response or the influence of the factor on the response and the relative interaction between them. A line joins all the average values of the factors: when the line is horizontal (parallel to the X-axis) then there is no main effect, each level of the variable affects the response in the same way, and the response average is the same for all levels. When the line is not horizontal (parallel to the X-axis) then there is the main effect, and different levels of the categorical variable affect the response differently. The higher the difference in the vertical position of the points plotted (the more the line is not parallel to the X-axis), the higher the scope of the main effect. For better understanding, dashed lines have been drawn that combine extreme values and give the idea of the resulting slope.

The graph reported in the Figure 30: Main Effects Plot for D2344 results shows how, in the case of the D2344 standard, the three factors identified, such as the current, the temperature and the residence time have a strong influence on the mechanical strength of the joint. This also applies to the D5868 standard, even if in this case the effect of holding time concerning the other process parameters is less incident, Figure 31.

In both cases both the current and the temperature show an increasing linear trend; it is possible to see how increasing both the current value and the maximum temperature reached by the adhesive, the strength assumes increasing values, that is, re-enters in these cases of positive influence.

Whereas, in the case of holding time, there is a parabolic trend with a downward concavity; however, in the presence of a positive influence, from 10 to 20 seconds the value of the average load increases, but vice versa from 20 to 30 decreases. For this reason, having chosen the interval 10 s- 20 s - 30s has allowed envying the holding time value for which the maximum value for the shear stress is obtained. Choose two levels instead of three and therefore only the 10s-30s interval would have allowed identifying the same the positive influence of the holding time on the task but would not allow identifying the maximum value, losing analytical information.

Additionally, in the case of the ASTM D5868 standard, it is possible to see how the effect of holding on joint resistance is relatively less influential than the case

of ASTM D2344. The variation of effort is less than in the case of temperature, so time has less effect on the response parameter. This effect depends on the different configuration of the joint linked to the applied normative. In fact, as already explained above, in the case of D5868 the heating area is more extensive and with a square geometry, consequently it is less affected by the edge effect, thus making the effect of holding time less effective; in fact, in the case of D2344, the effect of holding time is more significant.

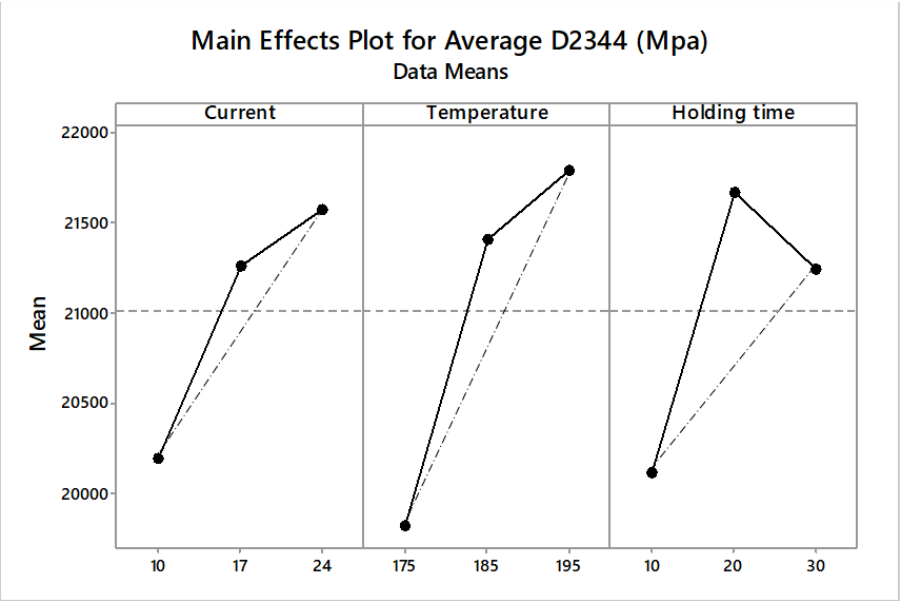

Figure 30: Main Effects Plot for D2344 results

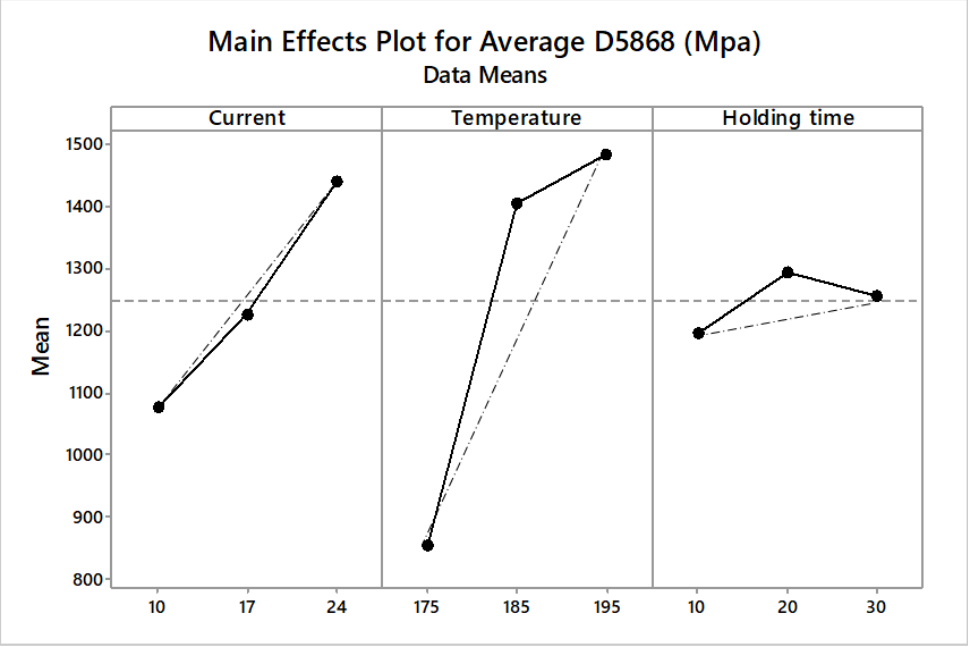

Figure 31: Main Effects Plot for D5868 results

3.5. Conclusions

This part of the work investigates the curing behaviour and mechanical performance of electromagnetic induction-heated adhesive bonded joints of CFRTP composites, as a possible alternative to traditional manual processes. The heat for liquefying the thermoplastic adhesive layer was generated in the adherends thank the presence of carbon fibre fabric.

It was used the PRODAS 1400 thermoplastic adhesive as it is widely used in the automotive, industrial field.

The results of numerical and experimental activities could be summarised as follows:

- A numerical model of induction heating has been proposed varying the process parameters such as current, maximum temperature and holding time.
- The temperature trend of the maximum temperature point provided by the numerical model is in excellent agreement with the experimental results.
- The holding time at a maximum temperature of the selected point is the key to obtain a more uniform temperature field, that leads to the improvement of the joint mechanical strength.
- Curing the adhesive layer by the induction heating, results in a slight increase in strength for both different configuration of join studied, compared to the standard manual method.
- Induction heating could be a good alternative for curing hot-melt adhesive used for realising bonded joint of CFRTP, widely used in the automotive industry. The main advantage is the possibility of easy automation and the real-time control of temperature, instead of the traditional methods for which it is difficult to implement a correct temperature control of the adhesive.

Effect of Current Frequency

4.1. Introduction

Adhesive bonding requires extensive surface preparation and high cure times of adhesives, as demonstrated by Fotsing et al. [66], who claim in their study that the density of surface porosities affects the bonding quality.

Among other advantages, such as strength to impact and environmental stress, deformation capacity, TPCs allow the possibility of performing welded joints of the parts.

Fusion bonding, also known as welding, allows to join two or more parts by fusing their contact interfaces; this technique overcomes all problems related to the techniques mentioned above.

This joining technique is characterised by local melting and reconsolidation of two or more parts at a joint interface[67].

Over the years, various welding techniques for thermoplastics matrix composite materials have been proposed and tested, such as resistance, ultrasonic, and electromagnetic induction welding, that are reviewed by Stokes [68] and Ageorges et al.[9]

For instance, Yousefpour et al. [69] focused their attention to studying the different fusion-bonding methods for thermoplastic composite components and described the various welding techniques, the effects of processing parameters on weld performance and quality, the advantages/disadvantages of each method, and the applications.

Amongst welding processes, induction welding is one of the joining methods being most suitable for thermoplastic composites [29, 40]. It offers advantages such as rapid heating of the laminate to its melting temperature within seconds, heat input directly to the laminate, and free contact localised heating.

Induction heating provides excellent flexibility and is suited for long and thin structures [40]. Additionally, it could be easily automated with industrial robots.

Over the years, various welding techniques for thermoplastics matrix composite materials have been proposed and tested, such as resistance, ultrasonic, and

electromagnetic induction welding, that are reviewed by Stokes [68] and Ageorges et al. [9]

For instance, Yousefpour et al. [69] focused their attention to reviewing the different fusion-bonding methods for thermoplastic composite components and described the various welding techniques, the effects of processing parameters on weld performance and quality, the advantages/disadvantages of each technique, and the applications.

Shi et al. [70] have developed a process model, coupling electrical and heat transfer phenomena, to simulate continuous resistance welding of the thermoplastic composite; in particular, they considered glass fabric reinforced Polyphenylene sulphide, using a stainless-steel mesh as the heating element.

Among the different technologies of welding, induction welding is that the composites reinforced with carbon fibre have allowed obtaining joints with high mechanical features included.

Electromagnetic induction heating is based on induced eddy currents that appear when a ferromagnetic or conductive material is placed close to an alternating magnetic field, operating in the kilohertz to megahertz frequency range, generated by a current circulating in a coil. Usually, neat polymers cannot be heated by electromagnetic induction because they are neither electrically conductive nor electromagnetic. So, it is necessary to apply susceptors, such as particles, metallic or carbon fibre fabric.

By Ahmed et al. [29], the term “susceptorless” induction heating was defined; in this case, the workpiece already consists of a type of material, like carbon fibre fabric reinforcement, which enables induction heating to occur.

In carbon fibre reinforced materials, the fundamental conditions for the generation of eddy currents are the formation of closed electrical loops as demonstrated in the works of Miller et al.[26] and then later by Fink et al.[34].

To obtain the electrical loops in the composite is primary to use fibres in woven form; Rudolf, et al.[52] performed a parametric study of continuous induction welding process with a different matrix, such as polyphenylene sulphide (PPS) and polyamide 6.6 (PA66) and also investigated the effects of the different fabrics showing that the heating is more efficient compared to unidirectional laminates.

As reported by Bayerl et al. [33], three mechanisms co-occur for volumetric heating in conductive fibre fabrics: heating by Joule losses along the fibres, dielectric heating at fibre junctions [27] and heating by contact resistance at junctions [15].

An essential factor to obtain a reasonable value of adhesion between two carbon fibre reinforced laminates is the process temperature of matrices, as demonstrated by Villegas and Rubio [51], which presented a procedure to prevent thermal degradation of the resin during high-temperature welding successfully. The laminates must be heated above the melting temperature T_m, for semi-crystalline matrices, and the glass transition temperature T_g, for amorphous one; on the other hand, the maximum temperature must be lower than the degradation temperature of the matrix.

By the above, induction heating of fibre-reinforced composites represents a very complicated Multiphysics process, which is characterised by the electromagnetic and heat transfer physics.

The main parameters that characterise induction heating of TPCs are coil geometry, the applied electrical power, and the coil current; but also, the frequency and the coupling distance play a key role.

The coil geometry is one of the principal factors affecting the heating performance and should be designed to fit the heating requirement; in fact, a possible unwanted effect is the “edge effect” resulting from a coil’s proximity to an edge of the workpiece.

As reported by Miller et al. [26], when the coil is larger than the workpiece, the currents are unable to follow the shape of coil, and in order to create closed-loop paths, the eddy currents are forced to move along the edge of the laminate; this causes a non-uniform heating, because higher current densities produce higher temperatures.

Although keeping constant, the current I, a higher frequency results in more power in the workpiece and faster heating of composites, as stated by Rudolf et al. [52]; Moser [37] with his work has highlighted that high frequencies limit the penetration depth of the electromagnetic field. This phenomenon is typical for metals and is called “skin effect”.

Until now the attention of researchers has been dedicated to study and model the process and the role of parameters such as heating time, pressure and temperature and never the current frequency.

The frequency of the current flowing in the coil is a fundamental parameter, whereas it is from this that depend on the characteristics of the alternating magnetic field that is generated, and consequently the eddy currents that are induced in the material.

The frequency of the current, also, influences the heat penetration depth: for the metal the higher the frequency, the lower is the heat penetration depth.

In the occurrence of metal alloys, the heating depth of penetration can be obtained by Maxwell's equations, the formula of which is as follows:

$$\delta = \sqrt{\left(\rho/(\pi * \mu * f)\right)} \tag{22}$$

where ρ is the resistivity of the material [Ωm], μ is the magnetic permeability [H/m] and f is the frequency [Hz].

It can then note that the depth of penetration depends on the one hand by the characteristics of the material to be heated and on the other hand is influenced by the current frequency.

For this reason, it was decided to study originally the influence of the frequency keeping almost constant the power.

Therefore, given the complexity of the phenomenon, a three-dimensional finite element model of the induction heating of Polyphenylene Sulfide (PPS) laminates reinforced with carbon fibres, has been developed with the use of a Multiphysics software, COMSOL. The model can predict the temperature during the induction heating, and the Multiphysics problem has been solved by coupling electromagnetic and heat transfer equations. The simulations were carried out changing the current and the frequency to study the influence of the process parameters.

After the simulations, experiments were carried out to verify the numerical model validity and assess the role of current frequency in heat distribution.

4.2. Three-Dimensional Finite Element Model

Due to the complexity of induction heating, a process simulation is a powerful tool for process development. In this Chapter, three-dimensional finite element models of static induction heating are developed and validated.

Finite element simulations, using COMSOL Multiphysics software, were carried out-coupling electromagnetic and temperature equations for the prediction of temperature distribution.

The model used consists of a Magnetic fields physics analyses and a Heat Transfer in solids physics analyses, with Multiphysics coupling features.

The software divides the physical phenomenon into two analyses: the analysis of the losses by Joule effect and the thermal analysis. In the first one, the magnetic field generated in the specimen is studied to understand the phenomenon caused by the induced current. In the second one, thermal analysis, the generation and diffusion of heat produced inside of the specimens, is studied.

Static heating conditions were simulated, considering the coil in a fixed position.

The solved equations in 3D are:

$$(i\omega\sigma - \omega^2 \varepsilon_0 \varepsilon_r) \begin{pmatrix} A_x \\ A_y \\ A_z \end{pmatrix} + \begin{pmatrix} \frac{\partial H_z}{\partial y} - \frac{\partial H_y}{\partial z} \\ \frac{\partial H_x}{\partial z} - \frac{\partial H_z}{\partial x} \\ \frac{\partial H_y}{\partial x} - \frac{\partial H_x}{\partial y} \end{pmatrix} = \begin{pmatrix} J_{e_x} \\ J_{e_y} \\ J_{e_z} \end{pmatrix} \tag{23}$$

$$\begin{pmatrix} B_x \\ B_y \\ B_z \end{pmatrix} = \begin{pmatrix} \frac{\partial A_z}{\partial y} - \frac{\partial A_y}{\partial z} \\ \frac{\partial A_x}{\partial z} - \frac{\partial A_z}{\partial x} \\ \frac{\partial A_y}{\partial x} - \frac{\partial A_x}{\partial y} \end{pmatrix} \tag{24}$$

Where H is the intensity of magnetic field, B the magnetic flux density, J_e the external electric current density, A the magnetic vector potential, ε_0 the permittivity of free space, $\boldsymbol{\varepsilon}_r$ the relative permittivity and σ the electric conductivity of carbon fibres.

Due to the architecture of the reinforcement of the material under inspection, sufficient electrical contact between the roving's is assumed, and consequently, fibre heating is the dominant heating mechanism. Therefore, resistivity is determined by the electrical properties of the fibres.

These equations must be coupled with the constitutive equations of the electric and magnetic field:

$$D = \varepsilon_0 \varepsilon_r E \tag{25}$$

$$B = \mu_0 \mu_r H \tag{26}$$

where E represents the intensity of the electric field, D the electric displacement field, μ_0 the magnetic permeability of free space and μ_r the relative permeability.

The energy balance was given by:

$$\rho C_p \frac{\partial T}{\partial t} = \frac{\partial}{\partial x}\left(K_x\left(\frac{\partial T}{\partial x}\right)\right) + \frac{\partial}{\partial y}\left(K_y\left(\frac{\partial T}{\partial y}\right)\right) + \frac{\partial}{\partial y}\left(K_z\left(\frac{\partial T}{\partial z}\right)\right) + Q_e \tag{27}$$

where T is the temperature, ρ the density of the composite, Cp the specific heat, K the thermal conductivities along the three Cartesian axes and Q_e the heat generation.

The FE solution of induction heating, defined by the equations reported above, was carried out using the "the magnetic fields" and "heat transfer in solids" modules of COMSOL Multiphysics 5.2 software.

A study in the frequency domain was done with the COMSOL "Magnetic Fields" module, to simulate the heat generation produced by the alternating magnetic field, due to the alternate current, which flows in the coil.

Some simplifications have been made in order to reduce the complexity of this phenomenon, basing on a literature review:

- Latent heat: some studies have reported that the effect of the latent heat due to crystal melting has not affected the time to melt of some composites [39]. For this reason, in this model crystallisation kinetics are not considered.
- Heating mechanism: as reported in paragraph 2.1.3, the principal heating mechanism is fibre heating. So, the junction heating was not considered. However, this induces inaccuracies for the model, also confirmed by the experimental results.

- Homogenised material model: woven composite materials consist of many elements. Thus, it is not possible to take the real geometry into account and create a model on the micro-scale. So, a homogenization technique was used [53]. In this work, the laminates are represented as an anisotropic material with homogenized material properties.
- Temperature-related material properties: constant values are used for the electrical conductivity of the carbon fibre reinforcement; also, the density of the materials is assumed to be constant, such as thermal conductivity; this is supported by the fact that thermal conductivity of the PPS matrix matches the other semi-crystalline thermoplastic materials and is almost independent to temperature changes.

4.2.1. Material Properties

The physical properties of all the material used in the model are reported in Table 5. The specific heat, Cp, the density, ρ, the electrical and thermal conductivity of the composite were obtained from the material data sheet. The anisotropy of the electrical and thermal conductivity was considered by determining the in-plane values (x, y) and the out of planes values (z). For the magnetic permeability is considered a value of μ_r=1. In general, carbon fibre reinforced composites with woven reinforcement can be treated as an anisotropic homogeneous material concerning electromagnetic properties, having no electrical conductivity in the thickness direction.

The composite density, ρ, specific heat, Cp, and thermal conductivities in-plane directions (x and y-axes) and out plane direction, z-axis, were obtained from the properties of fibres (T300 carbon fibres technical data sheet) and the matrix. The thermal properties were obtained using the rule of mixture for C_p, ρ and longitudinal thermal conductivities while the inverse rule of mixture for transversal thermal conductivity was used. The thermal properties adopted for the solution of the energy balance are also reported in Table 5. The heat generation term, Q_e, couples the two equations. The energy balance is solved only in the composite part and support.

Additionally, electrical properties for the induction coil (copper) and surrounding air are needed, Table 6. For numerical stability reasons, the air is attributed a low electrical conductivity.

Table 5: Input parameters of the FE model

Parameter		Value
ε_0	Electrical permittivity of free space	$8.8541 * 10^{-12}$ F/m
ε_r	Relative electrical permittivity of the composite	80
μ_0	Magnetic permeability of free space	$4\pi * 10^{-7}$ H/m
μ_r	Relative magnetic permeability of the composite	1
σ	Electric conductivity of carbon fibres	2000 1/(m)
Cp	Composite specific heat	710 J/ (kgK)
$k_x = k_y$	Thermal conductivity (in the composite plane)	1.4W/(mK)
k_z	Thermal conductivity (through the thickness)	0.25W/(mK)

Table 6: Electrical Properties of Copper and air

Parameter	Unit	Air	Copper
Electrical conductivity	S/m	10	$5.99 * 10^7$
Relative permeability	H/m	1	1
Relative permittivity	F/m	1	1

4.2.2. Boundary Conditions

The initial conditions are of uniform temperature (room temperature); a convective heat flux was set as a boundary condition for all the domains, to consider the heat transfer by convection with the surrounding air.

Only for the domains in contact, a continuity condition was set. So, the surface of the CF/PPS laminates was subjected to natural convection, h_c=5W/m^2, considering “still air” [71].

The model was solved in the frequency-transient domain; this study was used to compute temperature changes over time together with the electromagnetic field distribution in the frequency domain.
It is wanted to emphasise the effect of frequency on the temperature inside of the material analysed; indeed, the simulations were carried out by combining two frequencies with five current values reported in Table 7.

Table 7: Summary of the values of the frequencies and current imposed

Frequency (kHz)	Current (A)
130	
150	10, 15, 20, 25, 30
200	

4.2.3. Geometry and Mesh

The modelled geometry consists of a CF/PPS laminates (40x40 mm2) of 2.7 mm thickness. The circular coil, as previously described, was located at 2 mm from the top of the surface of the laminate. The 3D simulations were performed in a control volume with a radius of 200 mm and a height of 150 mm including the air surrounding the composite part, as shown in Figure 32: Control Volume of air.

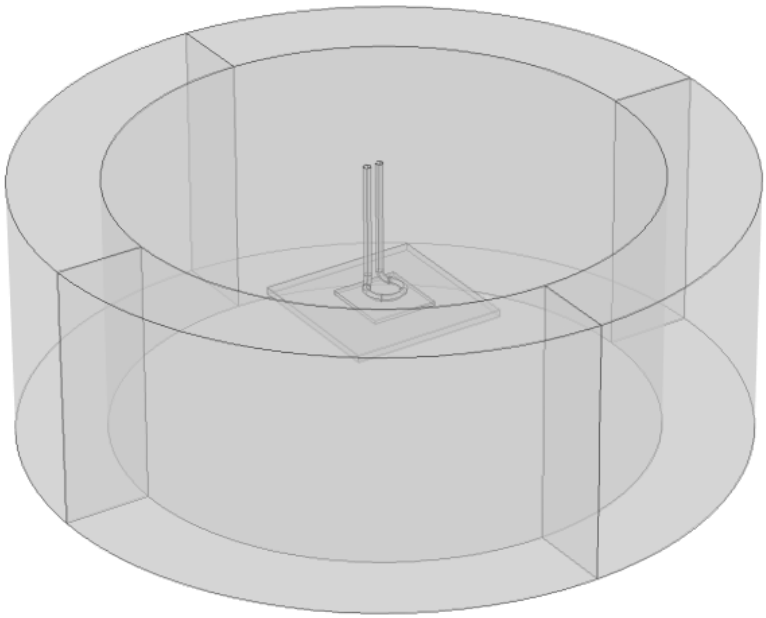

Figure 32: Control Volume of air

The outer faces of the air domain represent a magnetic insulation boundary, i. e. no magnetic flux over these boundaries is possible.

For the thermal model, the outer faces of the composite sheet are attributed both a convective cooling and a surface-to-ambient radiation boundary condition.

Figure 33 shows the modelled geometry (a) and the mesh realised (b); an unstructured mesh was performed using tetrahedral elements (80818), prismatic (4180), triangular (8549), and quadrilateral (645). The elements are four nodes characterised by three DOFs for magnetic potential and four DOFs for temperature field.

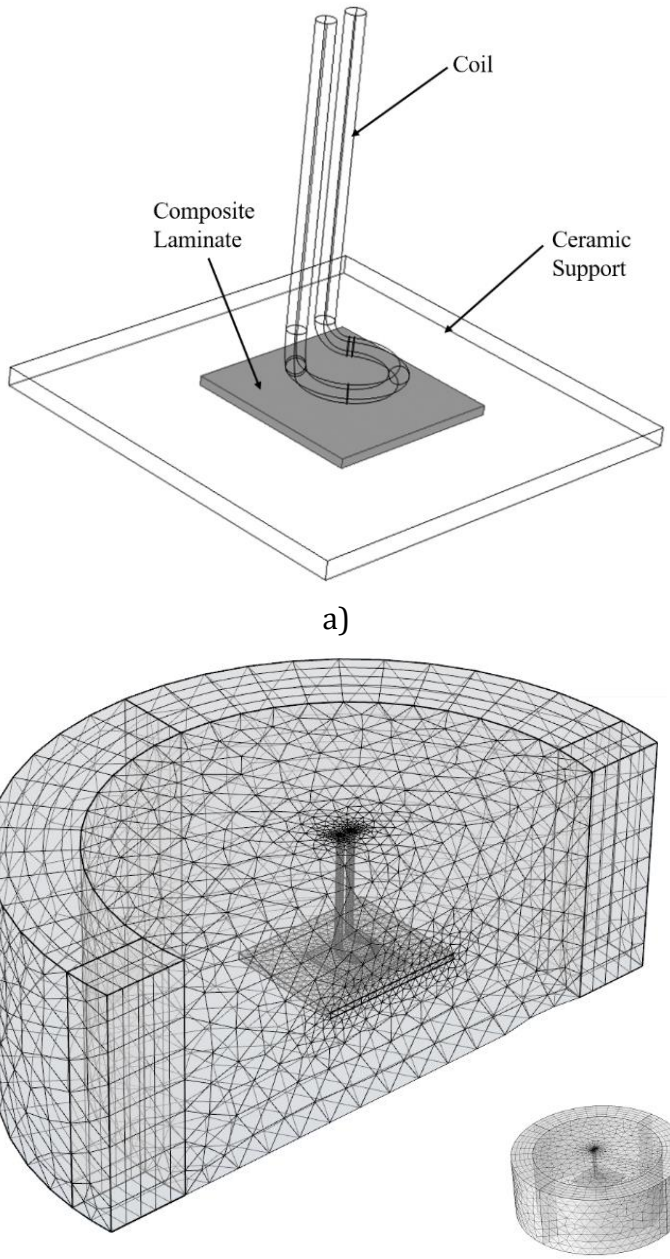

Figure 33: (a) Geometry of the FE model, with the composite laminate, ceramic support and coil and mesh generated (b)

4.3. Induction Heating Experiments

4.3.1. Materials

TenCate Advanced Composites (TenCate Cetex) provided the material used in this work. It consisted of Polyphenylene sulfide (PPS) semicrystalline matrix and a T300 Carbon fabric, with a volume fraction of 50%; a thickness of 2.7 mm characterises CF/PPS laminate.

4.3.2. Experimental Setup

The experimental tests were carried out with the Egma 30R generator designed and developed by Felmi (Italy). The generator is entirely static, i.e. there are no motors or other moving devices, and the magnetic field is generated by an electronic circuit called inverter.

The inverter supplies the coil, generating the magnetic field necessary to obtain the heating of a piece when it is placed near the electromagnetic field.

The equipment consists of two parts: the cabinet where the power supply and control circuits are located, and the heating head where the power section is located and to which the inductor is connected. The Egma 30R is also equipped with a water-cooling system, due to the powers involved and the consequent losses. The refrigeration unit is in the cabinet, in this way the flow and the temperature of the water are constant during the working.

Through the control panel of the generator, it is possible to select the process parameters and to read the value imposed.

The maximum power is 30 kW and can be controlled by percentage power, which ranges from 20% to 100%.

Figure 34: Egma 30R generator panel control

Static heating experiments were performed to assess the heating behaviour of the preconsolidated laminates. For this purpose, specimens of 40 mm x 40 mm x 2.7 mm were placed on a ceramic support.

The frequency range can vary from 130 to 280 kHz by changing the coil geometry. From preliminary bibliographic studies, the importance of the shape of the coil used, to prevent the occurrence of edge effects has been highlighted [26]. The shape of the coils adopted was chosen after a study on this effect [72]; the shape and dimensions of the coil were designed and developed to obtain a uniform temperature distribution on the surface. The final shapes chosen were shown in Figure 35.

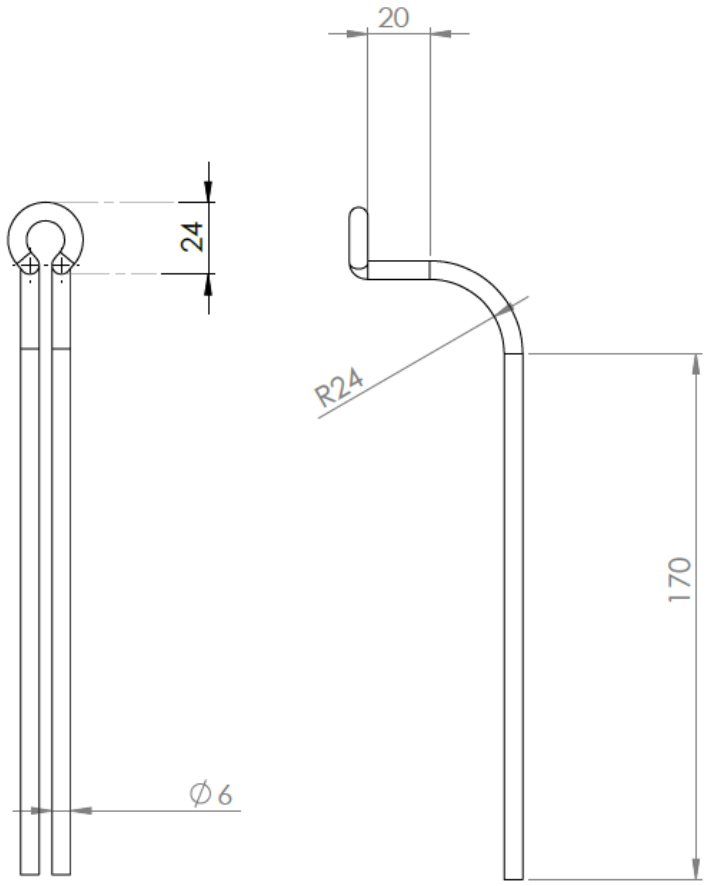

Figure 35: Geometry of the coil used

The coil geometry consists of a horizontal part that is oriented parallel to the laminates and a part that is coupled to the heating head of the generator. The second part of the coil features does not contribute to the heating, but with its dimensions affect the final value of the frequency.

The Horizontal part has an external diameter of 24 mm, while the diameter of the copper tube used is 4 mm with 2 mm of thickness.

The coil was not in contact with the composite laminate, but it is at a fixed distance of 2 mm from the specimen's surface.

During the experiments, an IR camera Optris PI450 with a temperature range -20 °C to 900 °C, a spectral range of 7.5 to 13 μm and a frame rate up to 80 Hz, was used.

The images obtained from the camera have been analysed with a specific software; for the correct measure of the temperature it is necessary to know the value of the specimen material's emissivity; for carbon-carbon composites

specimens, the emissivity is 0.8 [65]. This value was verified using a thermocouple and calibrating the emissivity value on the thermocouple reading. Static heating experiments were performed to assess the heating behaviour of the pre-consolidated laminates. For this purpose, specimens of 40 mm x 40 mm x 2.7 mm was used. Moreover, the composite laminates were placed on a ceramic support. This support is necessary and was chosen in ceramic material for better dissipation of the heat during the experiment and between one trial and another. The set-up is shown in Figure 36 and is characterised by a heating unit including the "circular" coil, the ceramic support, and the temperature acquisition system.

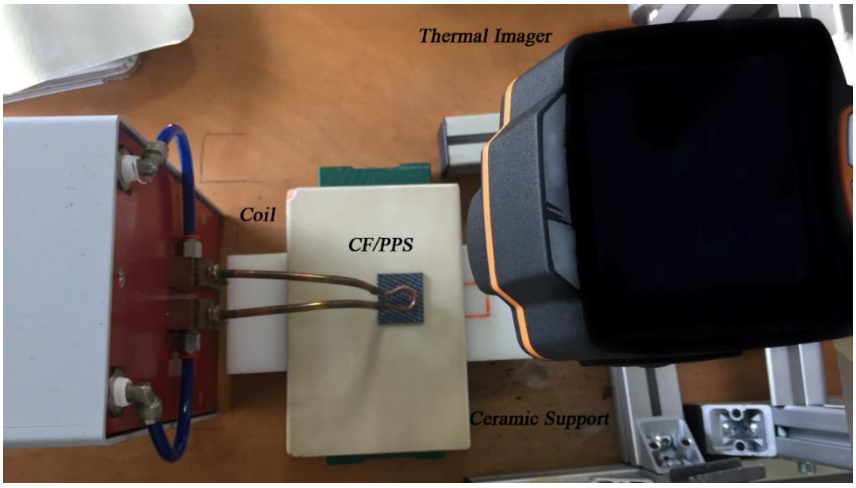

Figure 36: Experimental set-up for induction heating of CF/PPS

As mentioned above, to highlight the effect of the frequency between the different parameters that characterise this heating process, induction heating experiments with three different value of the frequency and four different current settings were performed, see table for each combination were executed three experiments using a new specimen for each test.

The generator controls the current frequency by an automatic coupling system called "auto-tuning system" depending on the geometry characteristics of coil used, as highlighted in the following.

The high-frequency alternate current in the coil produced a time-variable magnetic field of the same frequency in near surroundings, which then induced eddy currents in the composite laminate to be heated.

As the generator used does not allow varying the frequency by a panel control, the way to obtain this was by changing the geometry and the size of the coil.
The frequency at which the generator oscillates is that of resonance between the inductance of the connected coil and the capacitance of the capacitor placed inside the generator.
The formula to apply is:

$$f = \frac{1}{2\pi\sqrt{LC}} \tag{28}$$

Where **L** is the inductance and C is the capacitance.
The value of the inductance depends on the geometrical features of the coil such as length **l**, the section **A** of the spire, the number of turns **N** (span density n =N/l); moreover, by keeping the geometry constant, the way to change the frequency, is varying the total length of the coil.
According to what has been said, to obtain a 200 kHz frequency, the coil has a length of 200 mm, as shown in Figure 35.
Conversely, to obtain a frequency of 130 kHz and 150 kHz has used the coil shown in Figure 37, with the same geometry of the coil at 200 kHz, but with a total length of 500 mm.

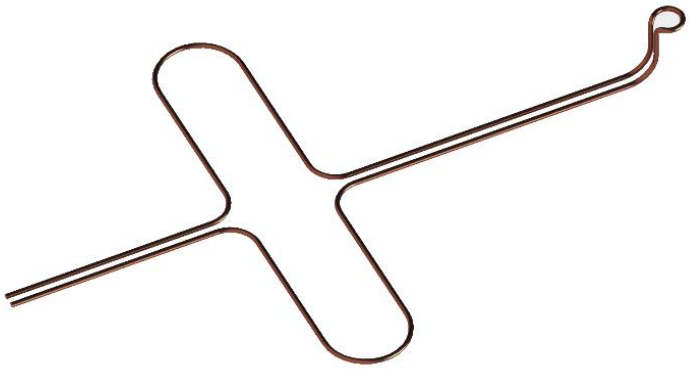

a)

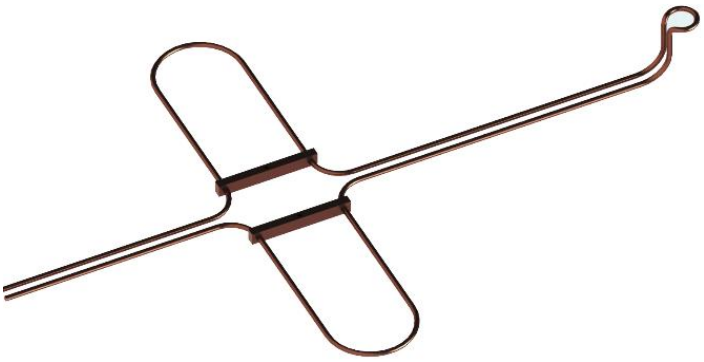

b)

Figure 37: Geometry of the Coil, realised to obtain the frequency of 130 kHz (a) and 150 kHz (b)

The possibilities to pass from 130 kHz to 150kHz is given by the copper shunts inserted, that short-circuit the two wings, reducing the total length of the coil and allow to change the final frequency.

The actual frequency set, varying the coils, was verified by the machine display used for the experimental tests. The display shows the operating parameters of the machine, such as coil current, voltage, and frequency.

4.4. Results and Discussion

In all experiments a significant in-plane temperature gradient is noticeable. An area of higher temperature, which represents the global current loop of the approximate size of the induction coil, is surrounded by colder areas at the outer diameter and a cold spot in the centre of the specimen's surface,

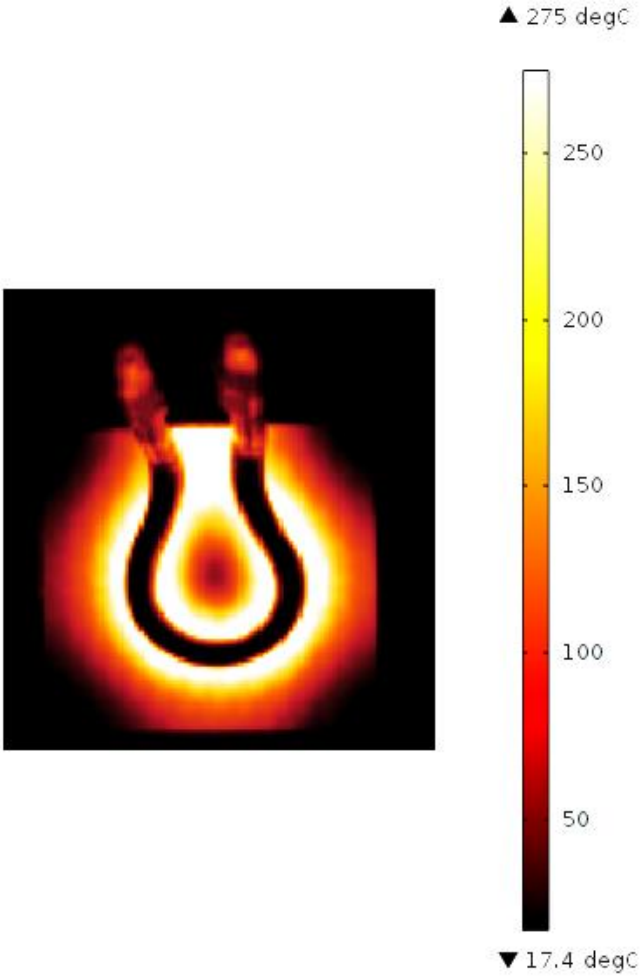

Figure 38: Heating patterns of the surface of CF/PPS laminate

Due to the global current loop, the surface temperature patterns are characterised by a significantly uneven distribution throughout the heating cycle. The peak temperature is always located around the global current loop whereas the centre and the outer areas show considerably lower temperatures. Because of the low thermal diffusivity of polymers, no compensation by heat transfer occurs.

For validation of the induction heating model the parameters used for experimental characterisation, Table 7, were used as input parameters.

The time-dependent simulations provided the evolution of the temperature field during the induction process. As an example, the simulated temperature maps of the laminate composite for the case of a current of 15 A and 200 kHz of frequency is reported in Figure 39 (a); also, in Figure 39 (b), the image obtained with the camera during the experimental tests is reported.

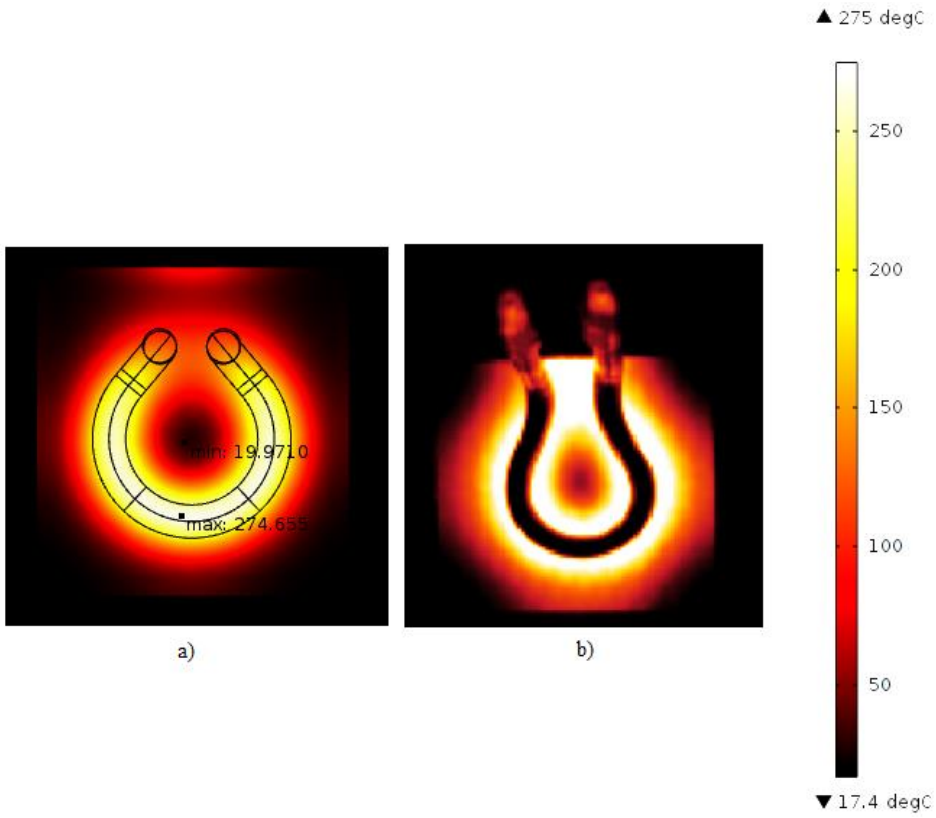

Figure 39: Correlation between simulated temperature maps (a) and thermal camera image (b) at the heated surface coil current 20 A and frequency 200 kHz.

The simulation results are like the images obtained from the thermographic camera, except for minimal differences due to the apparent difference between CAD design and actual coil used for the experiments.

The time variation of the temperature, in the maximum temperature point, individuated analysing the IR camera images captured during the heating experiments, is reported in Figure 40, and is compared with the numerical results.

The results obtained from the developed model were in excellent agreement with the temperature detected during experimental tests.

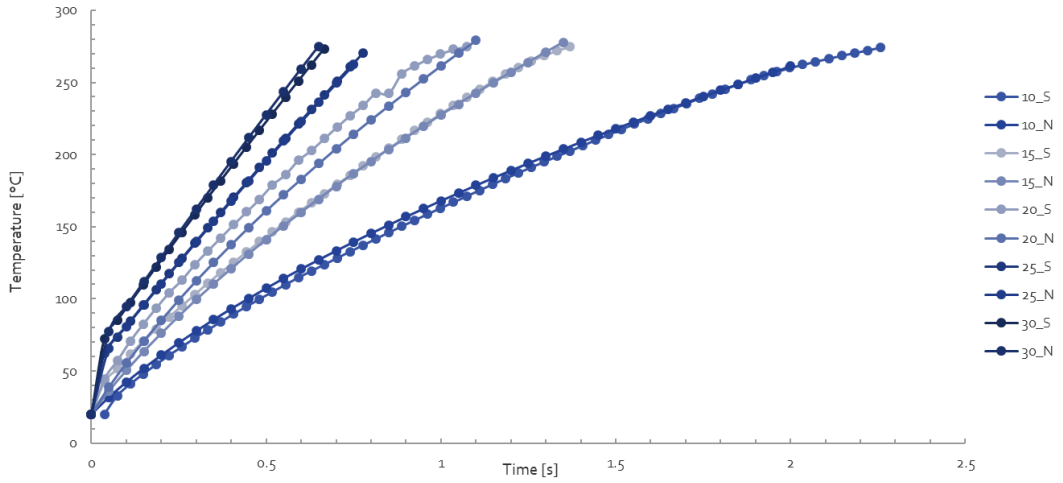

Figure 40: Evolution of temperature for the CF/PPS during heating at 200 kHz and values of current from 10 to 30 A: comparison between simulated, N, and experimentally, E, measured values.

4.4.1. Influence of frequency

A significant result that could be extrapolated by the numerical model is the graph reported in Figure 41. It is possible to obtain the iso-power curve, applying the equation (1) and (2), reported in paragraph 2.1.1.

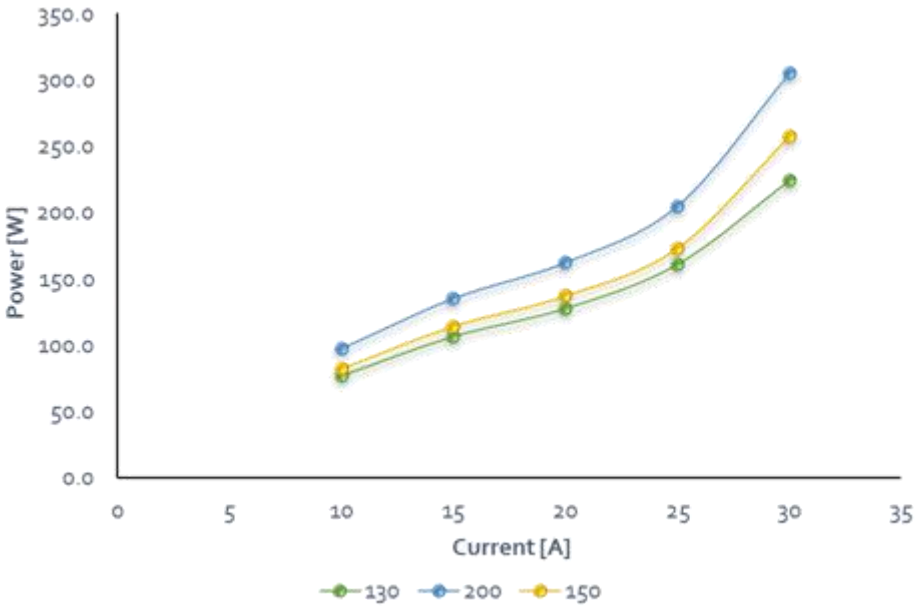

Figure 41: Iso-power curve obtained by the numerical model

Through these curves, the value of the current and the frequency that allows an iso-power induction heating was chosen.

The current and frequency values adopted to evaluate the variation in the depth of heat penetration in the iso-power regime, are shown in Table 8. Three iso-power regimes were adopted, 97 W, 135 W and 200W.

Table 8: Values of the frequency and the current for induction heating in the iso-power regime

Power [W]	Frequency [kHz]	Current [A]
97	130	15
	150	13
	200	10
135	130	22
	150	20
	200	15
162	130	27
	150	25
	200	20

The influence of frequency on the depth of penetration of the heat in the material thickness was evaluated using an NDE ultrasound system. After the heating tests, the specimens were inspected by using a US Multi2000 Pocket 16 x 64 system by M2M; NDE tests were performed with a Probe, 5 MHz, 64 Elements.

The choice of a low-frequency probe (f =5 MHz) is related to a consistent decrease of the signal attenuation and a more efficient measurement [73]. The single Probe used was the DS 6 HB 2-7 produced by KARL DEUTSCH, with a 6-mm diameter.

The apparatus operates in the form of reflection: the probe is used both as an emitter and as a receiver of the ultrasonic waves; for this reason, during the acquisition, the pulse Echo technique was adopted.

The depth of heating was evaluated assuming the consideration that the resin in amorphous state absorbs more energy of the ultrasonic waves than in the crystalline or semi-crystalline state.

Short-duration ultrasound pulses are transmitted into the region to be studied, and echo signals resulting from scattering and reflection, are detected and displayed.

The depth of a reflective structure is influenced by the delay between pulse transmission and echo reception; so, using an unheated specimen, in the semi-crystalline state, the real thickness plate is obtained (Figure 42), and the acquisition system is calibrated.

In the figures of the US tests, the vertical axis is labelled the Amplitude, and the horizontal axis is labelled the thicknesses.

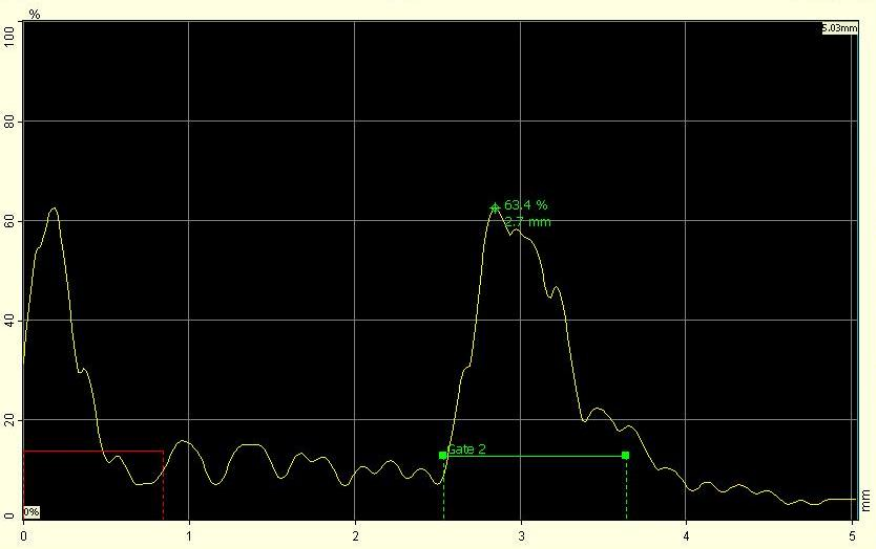

Figure 42: A-scan of an unheated specimen

A-scans inspection was carried out in two points: on edge and at the centre of the specimen. As can be seen from both the simulations and the images of the thermal camera, the heating is not uniform. (Figure 43)

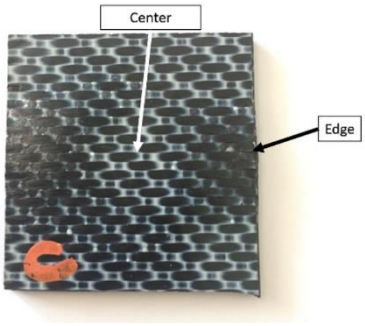

Figure 43: Image of the measurement point for the NDI tests.

As a result of this inspections, it can be noticed how the echo reception, of the heated sample, shows reduced amplitude respect the unheated sample; this is due to the absorption generated by the loss of crystallinity in the resin phase following the heating and cooling effect. The cooling of our specimens, characterised by small dimensions, was conducted in air, resulting in a rapid temperature fall and amorphous phase formation in the resin [74].

So, it is possible to detect within the thickness of the specimen, how deeply the heat has penetrated to alter the structure of the resin. For this reason, the results of the inspections of the sample at a different frequency, but as previously stated, with the same power were analysed.

In Figure 44, the samples heated at the iso-power level of 97 kW are compared. Figure 44a shows the echo reception of the specimen heated at 130 kHz and 15A; its amplitude is higher than the echo of the sample heated at 150 kHz and 13 A (Figure 44b), that is higher than the sample heated at 200 kHz and 10 A (Figure 44c). Consequently; it is possible to assert that higher the frequency higher the depth of heat penetration.

The mentioned above behaviour occurs in all the three cases analysed, as can be seen in Figure 45 where the response of the NDE test is compared for the samples heated at the iso-power level of 135 kW, and in Figure 46 at the iso-power level of 162 kW.

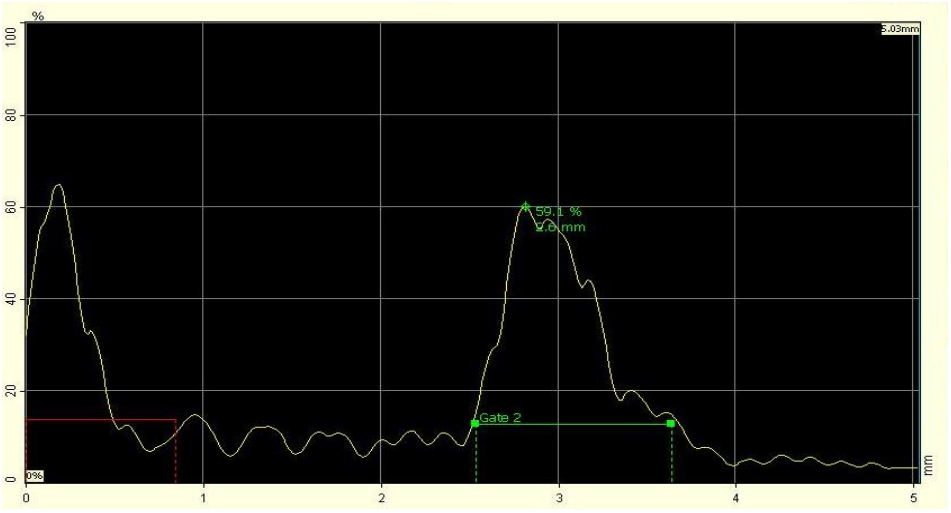

a)

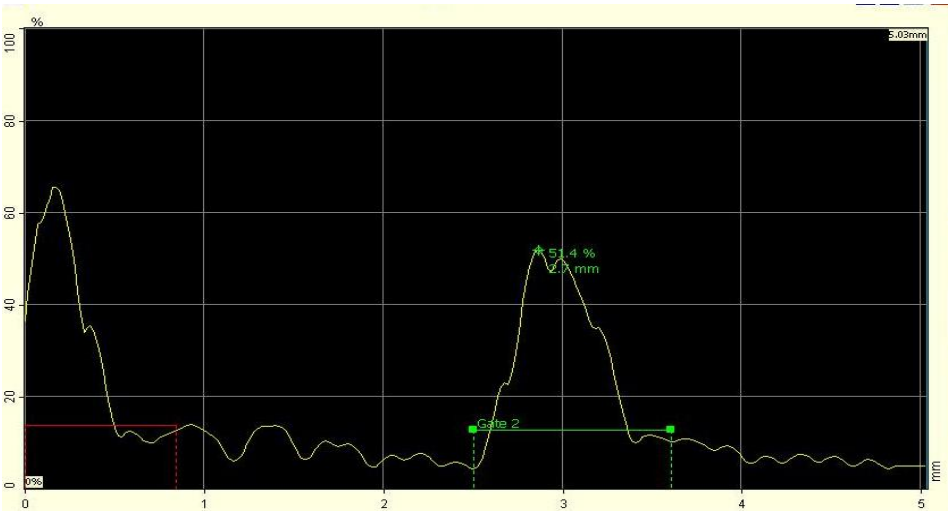

b)

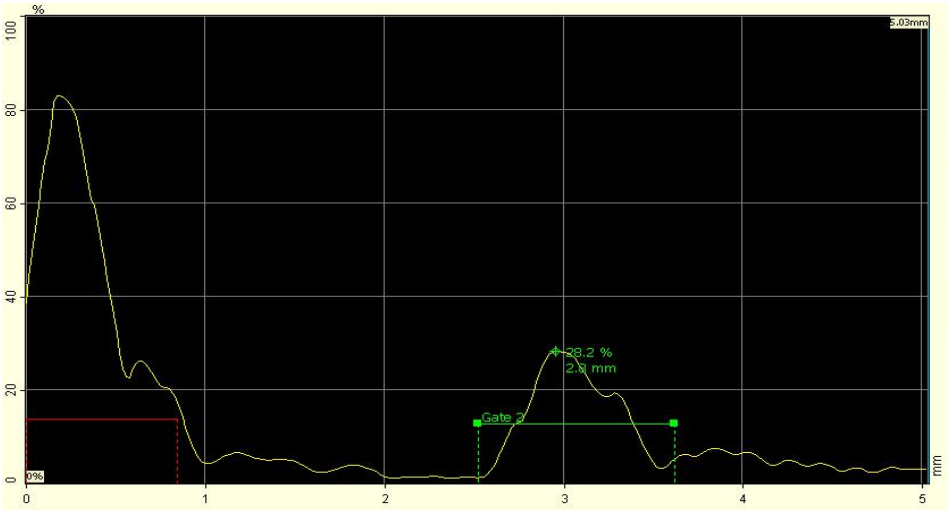

c)

Figure 44: A scan of samples heated at iso-power of 97 kW with 130 kHz and 15 (a), 150 kHz and 13 A (b) and 200 kHz and 10 A (c).

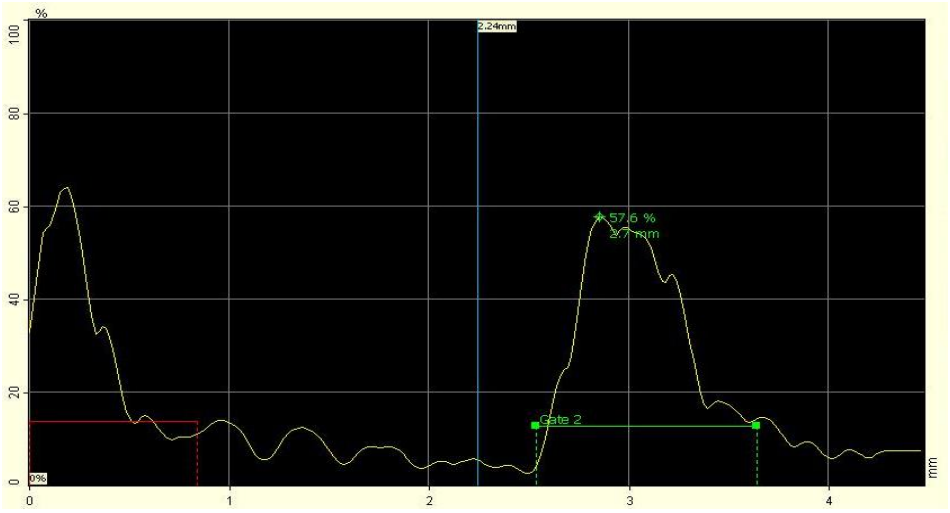

a)

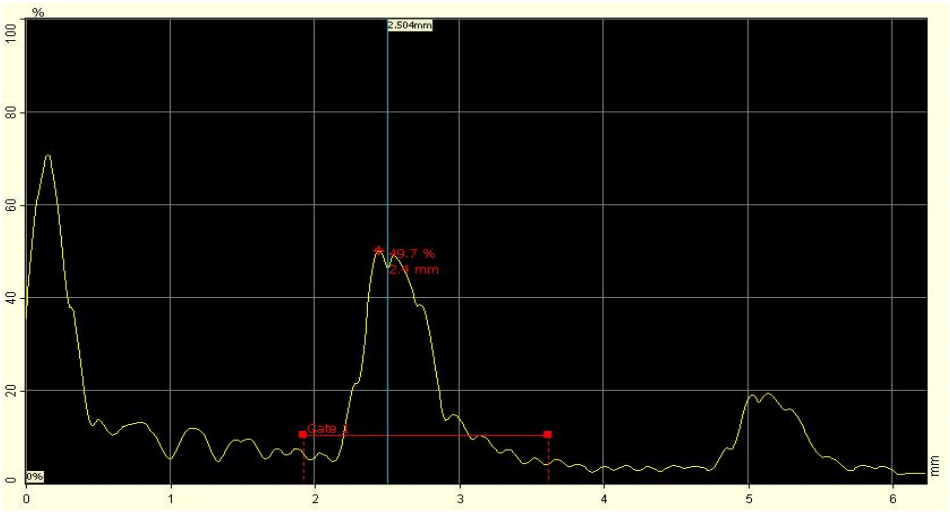

b)

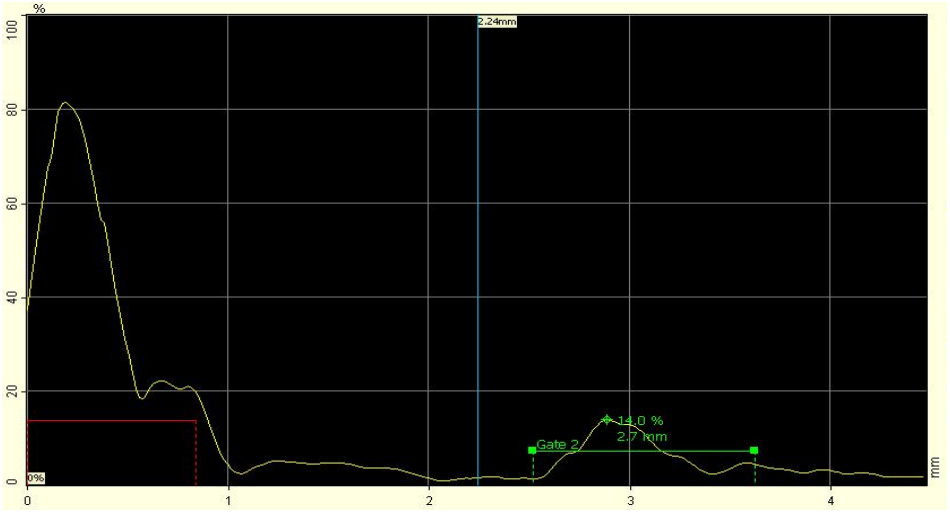

c)

Figure 45: A scan of samples heated at iso-power of 135 kW with 130 kHz and 22 (a), 150 kHz and 20 A (b) and 200 kHz and 15 A (c).

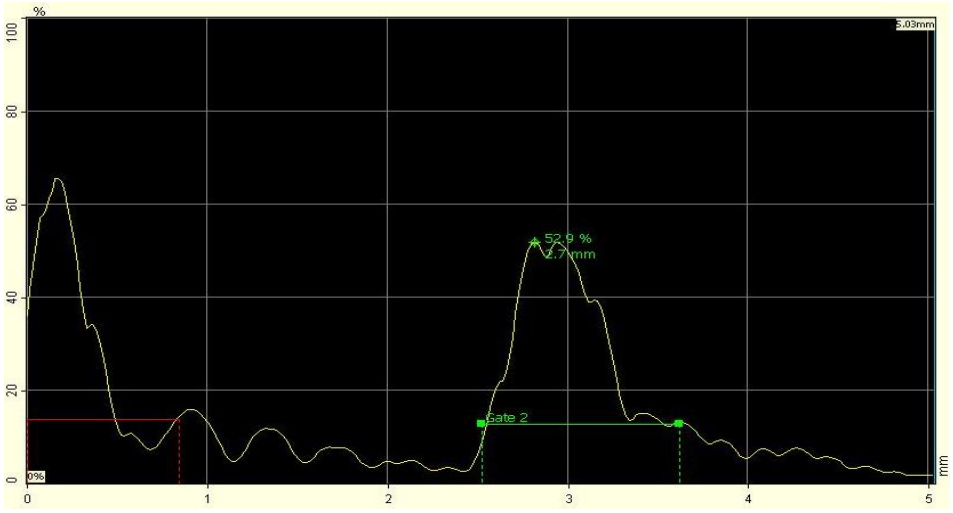

a)

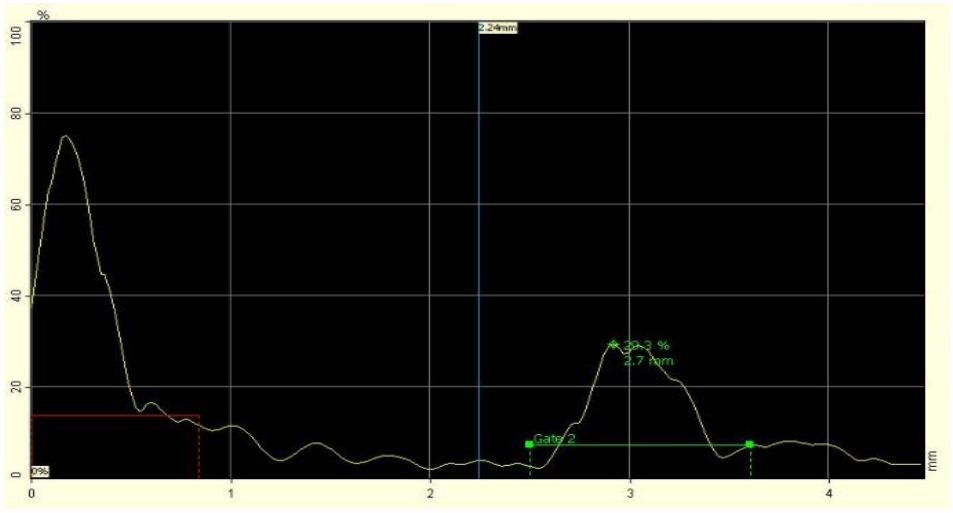

b)

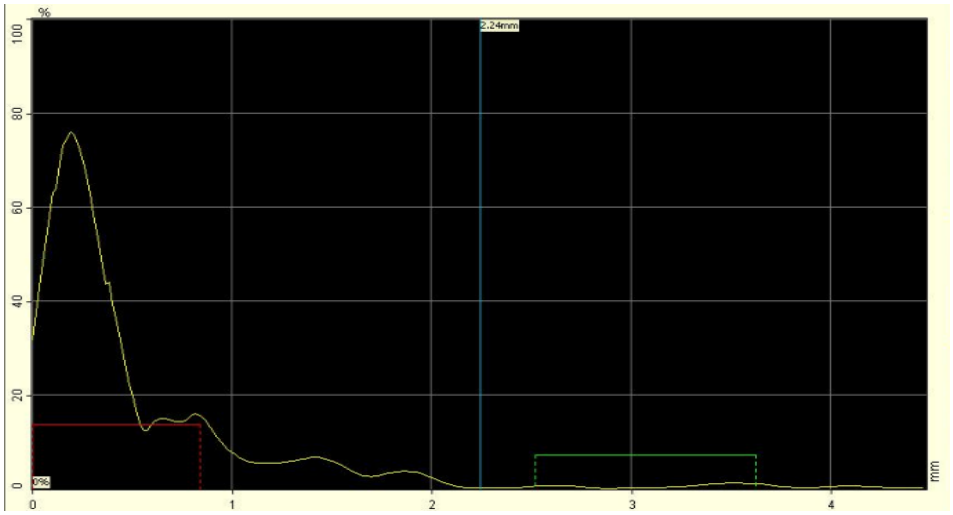

c)

Figure 46: A scan of samples heated at iso-power of 162 kW with 130 kHz and 27 (a), 150 kHz and 25 A (b) and 200 kHz and 20 A (c).

The time-temperature diagram reported below highlights the different heating between the two specimens at the same power but with different values of current and frequency.

In

Figure 47, the temperature trend for both numerical (N) study and the experimental (E) specimen heated at 150 kHz and 20 A and the ones heated at 200 kHz and 15 A are compared. In

Figure 48, the temperature trend for both numerical (N) study and the experimental (E) specimen heated at 150 kHz and 25 A and the ones heated at 200 kHz and 20 A are compared.

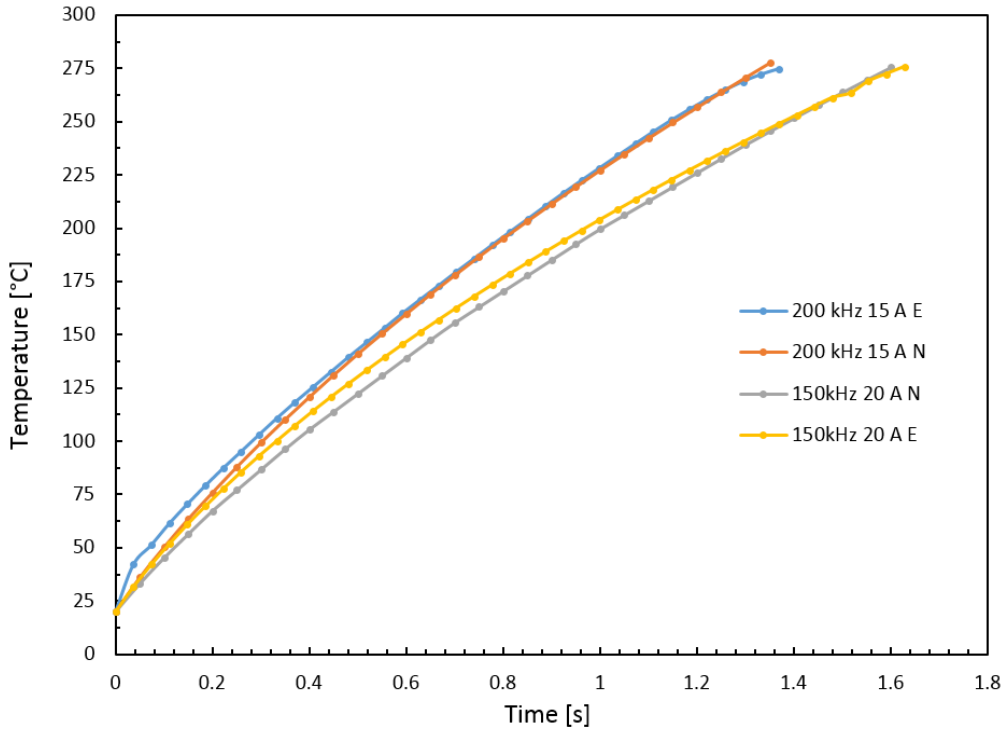

Figure 47: Temperature-Time Diagram for the samples heated at 150 kHz 20 A and 200 kHz 15A

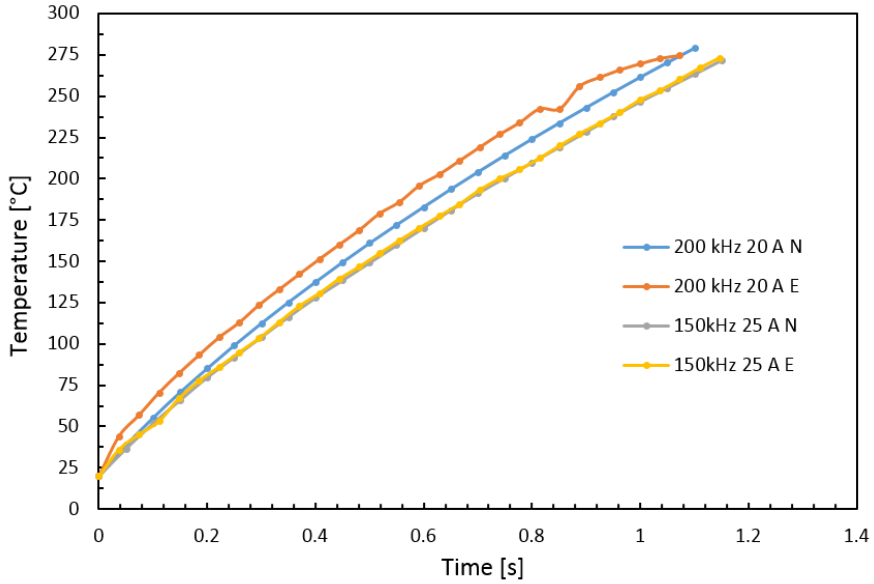

Figure 48: Temperature-Time Diagram for the samples heated at 150 kHz 25 A and 200 kHz 20 A.

In the three cases, it is possible to notice that even if the power is the same, the higher frequency samples are more efficiently heated, as was also demonstrated by the NDE tests.

This phenomenon is explainable according to the study of Fink et al. [34], where is demonstrated how the heating of cross-ply carbon fibre composites does not depend only on joule losses, but also on dielectric losses in the polymer. They have demonstrated that the presence of polymer, of thickness *h,* between two crossing layers of filaments, can be treated as a capacitor.

They have also considered that the heat generation can be written as:

$$W(x,y)_{\Delta A} = \omega \cdot tan\delta \cdot C(x,y)_{\Delta A} \cdot V(x,y)^2 \tag{29}$$

where $tan\delta$ is the imaginary part of the complex dielectric constant for the polymer; C is the capacitance at the point (x,y) and V the potential difference that exists between the plates of the capacitor (Figure 49).

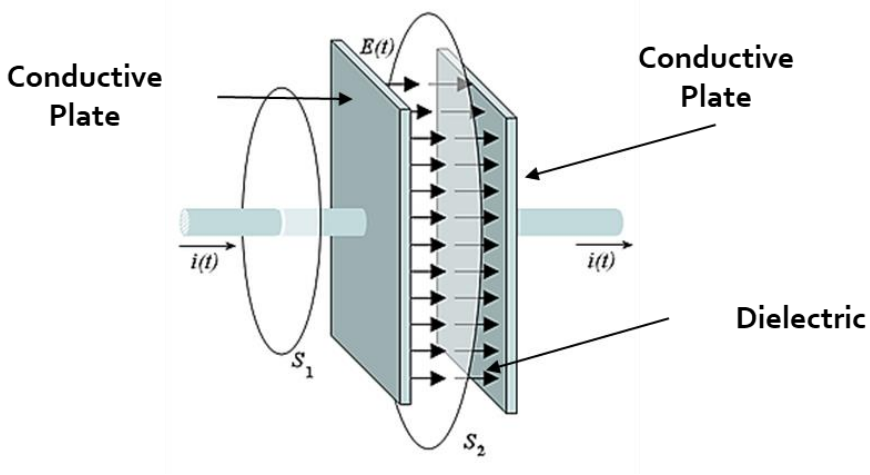

Figure 49: Capacitor scheme of the laminate

Considering the composite laminate as a sequence of parallel plate capacitive interacting through the thickness, and according to Eq. (29), increasing the frequency increases also the heat generation due to the dielectric losses.

4.5. Conclusions

The susceptorless induction heating process of high-performance thermoplastic polymer composites was analysed in this study focusing the attention on the effect of the current frequency.

In the experimental part, induction heating of continuously reinforced CF/PPS laminates with a circular coil was characterised.

The temperature field was analysed using a thermal camera, and it is highly localised and anisotropic in-plane.

The upper side of a laminate near the induction coil is subject to significantly higher temperature compared to the lower side which will form the bonding line in an overlap joint the temperature gradients between the surface facing the inductor and the opposite side depending on the processing parameters such as frequency and generator power.

A three-dimensional fully coupled electromagnetic/thermal finite element model of static induction heating using the commercial FEM code Comsol Multiphysics was developed. The accuracy of the model is right.

The most significant, original and very interesting result is that the current frequency plays a different role in composites than in metal alloys case. The NDE US tests allow noticing how, at the same power level, the higher the current frequency, the higher the heat penetration in the material thickness.

At higher frequency, the magnetic field penetrates more deeply, and consequently, the distribution of heat within the specimen is more uniform and, keeping constant the power as previously defined, the composite tends to heat up faster. On the contrary, the lower the current frequency, the lower the heat penetration. As previously highlighted, this is due to the composite laminate could be considered as a sequence of parallel plate capacitive interacting through the thickness.

However, considering that the parameters were not optimised, further improvements in weld quality can be expected. The developed induction heating technique opens the possibility of continuous induction welding without thermally induced damage and eliminates the need for sophisticated tooling.

Possible applications include the manufacturing of complex aerospace components or automotive parts.

Future works and perspective

The results obtained from the induction heating experiments have highlighted how one of the most critical process parameters is the frequency.

To better understand this phenomenon, a new study has been prepared, developing a new experimental campaign.

In this campaign, different process parameters will be analysed, such as:

- Coupling distance between coil and laminate composite;
- Current Frequency;
- Dimension of the coil, number of spires and their distance;
- Current.

Basing on the results obtained by the previous work, a new improved shape of the coil was designed, reported in Figure 50.

This shape showed a distribution of temperature more uniform on the specimen surface, while the spire on the sides allows varying the frequency.

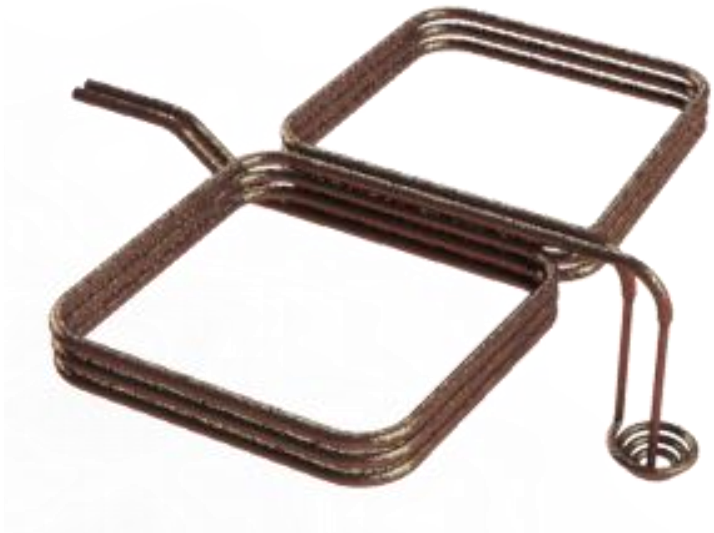

Figure 50: New coil designed for the next experimental campaign.

For this new shape, the numerical model was developed, basing on what state in paragraph 4.2.

The geometry was realised with the aim of a CAD software and then imported in COMSOL environment, as shown in Figure 51.

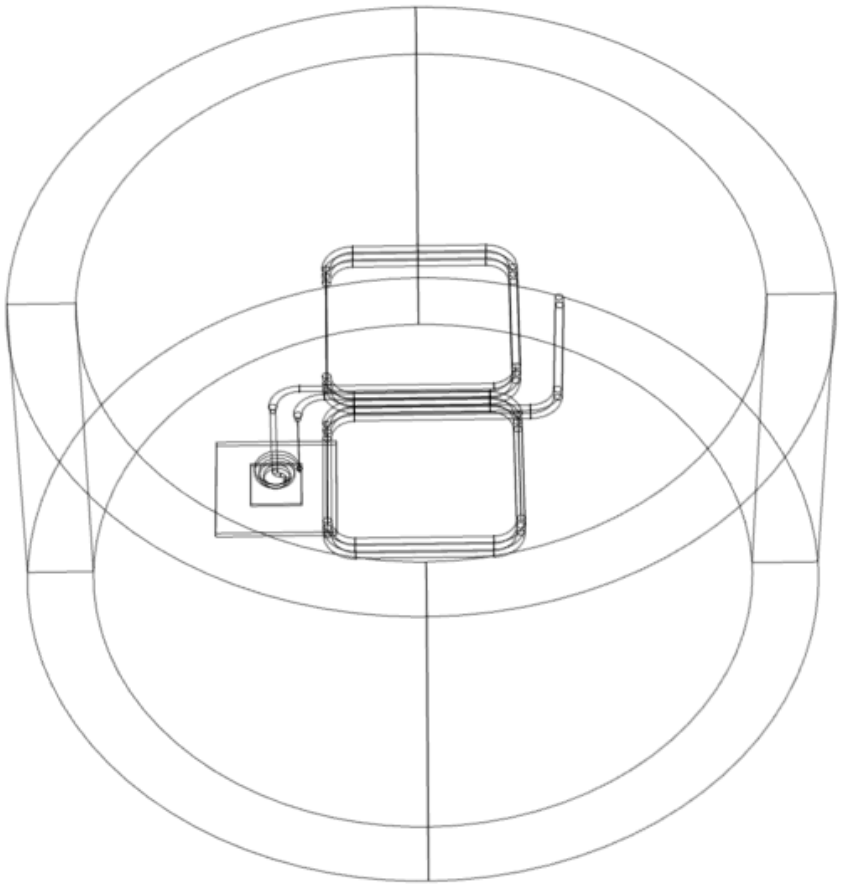

Figure 51: 3D Model of the conic shape coil

In Figure 52 the mesh realised for this new model is reported.

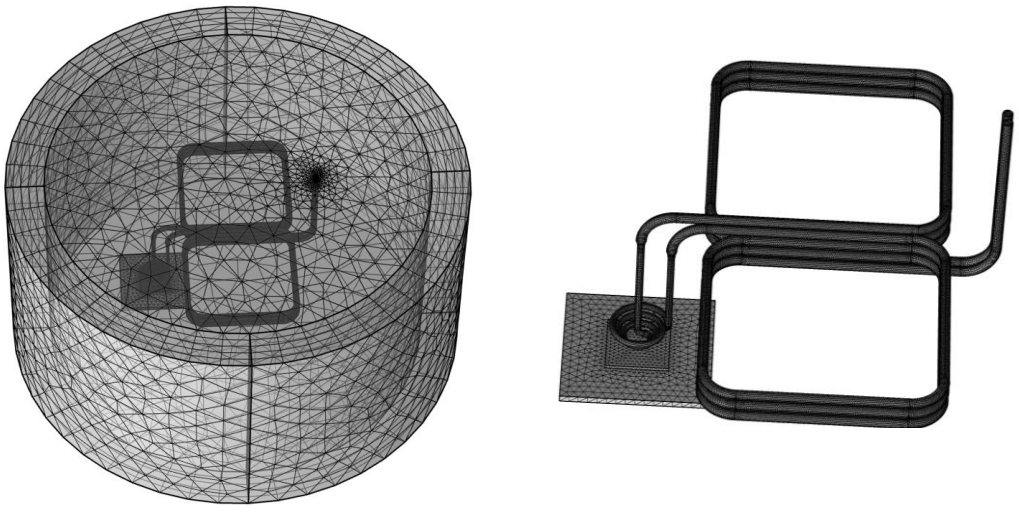

a) b)

Figure 52: Mesh realised for the conic coil simulation

The results of the simulation isreported in Figure 53, additionally a simulation was carried designed the coil without the conic spiral to understand if the new spires affect the electromagnetic field. The geometry is reported in Figure 54.

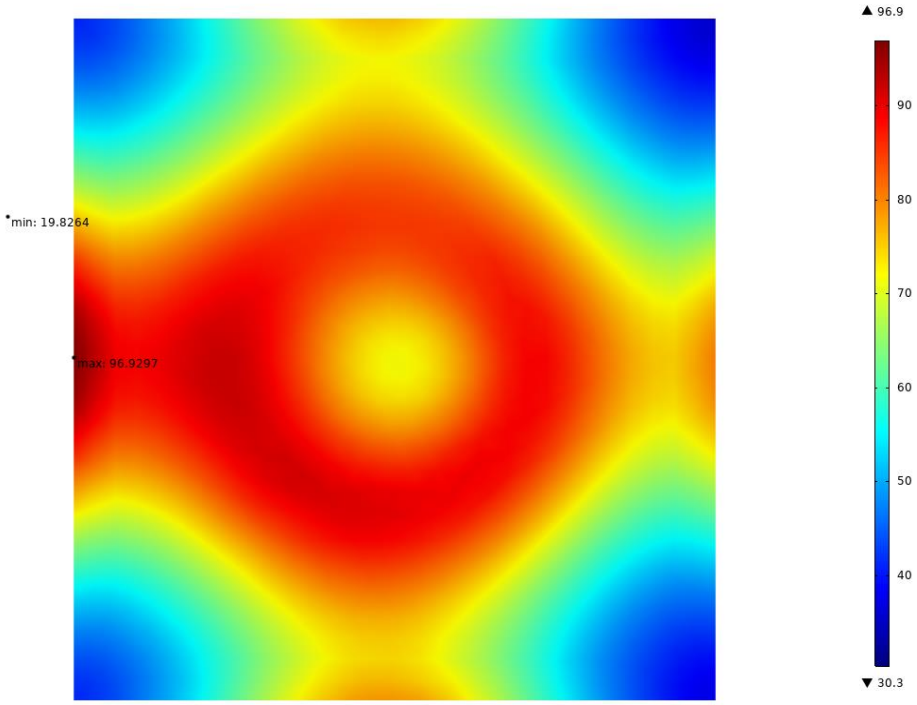

Figure 53: Temperature distribution of the conic coil

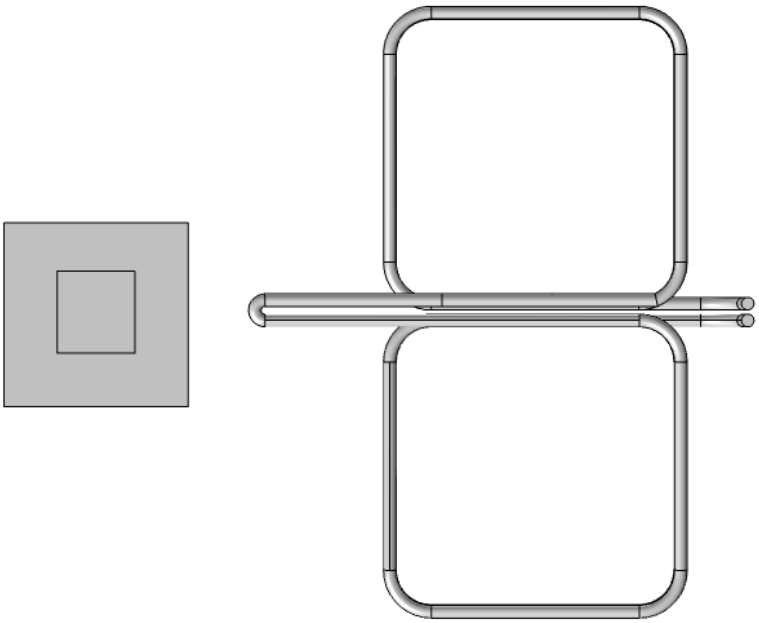

Figure 54: Geometry of the coil with only the spires

As shown in Figure 55, the spire realised to vary the frequency doesn't affect the heat distribution. Considering an initial temperature of 20°C, the increase is only 0.2 °C.

Concluding the new shape of the coil, confirm a more uniform distribution of the temperature respect the circular coil one, as highlighted in Figure 56.

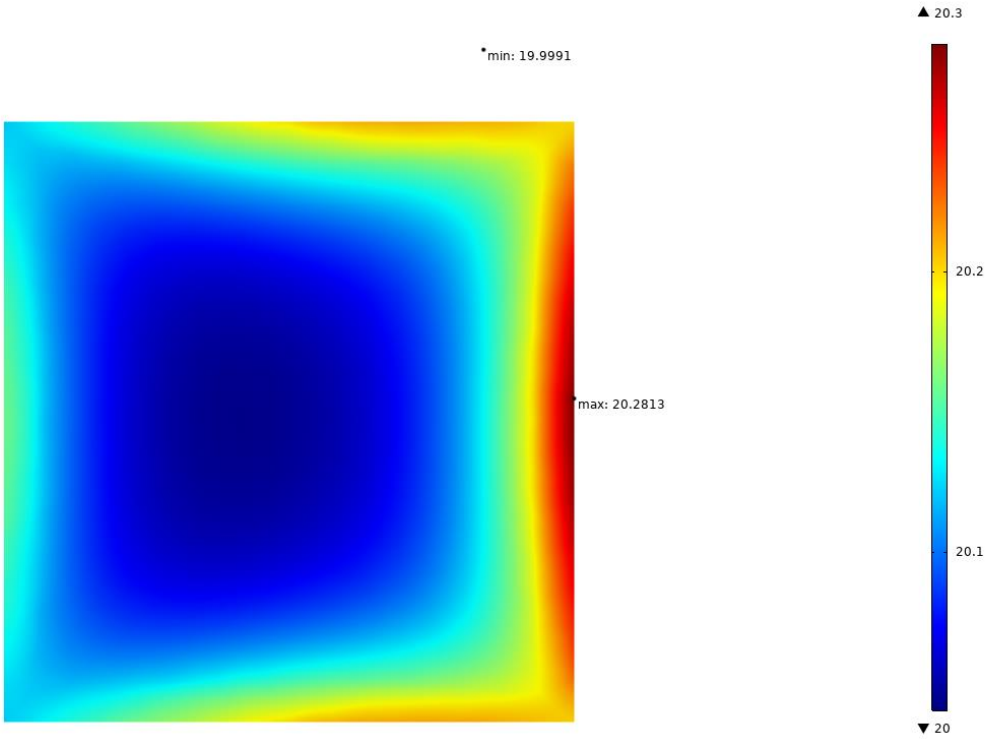

Figure 55: Temperature Distribution of the coil with the only spires.

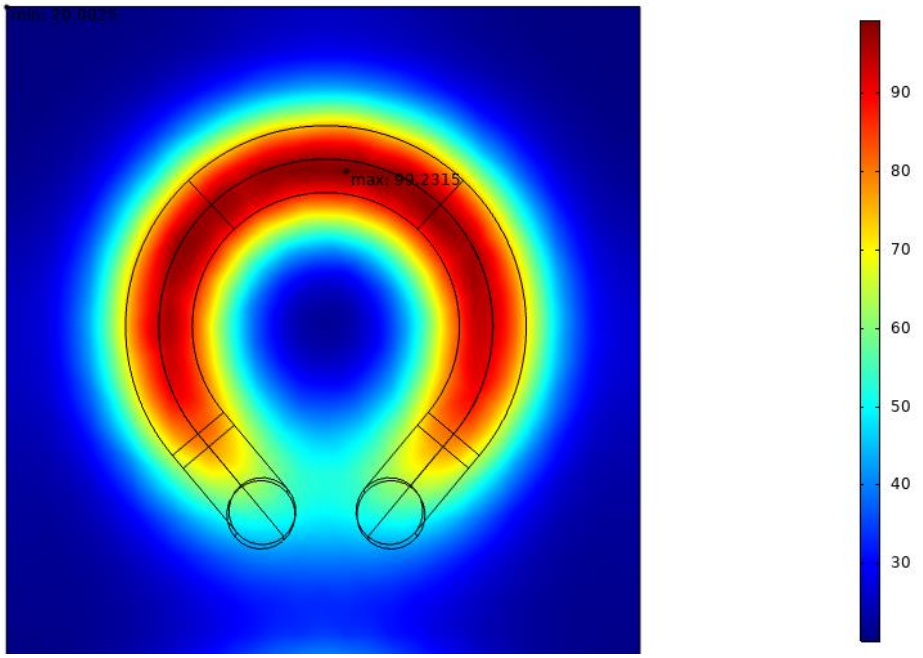

a)

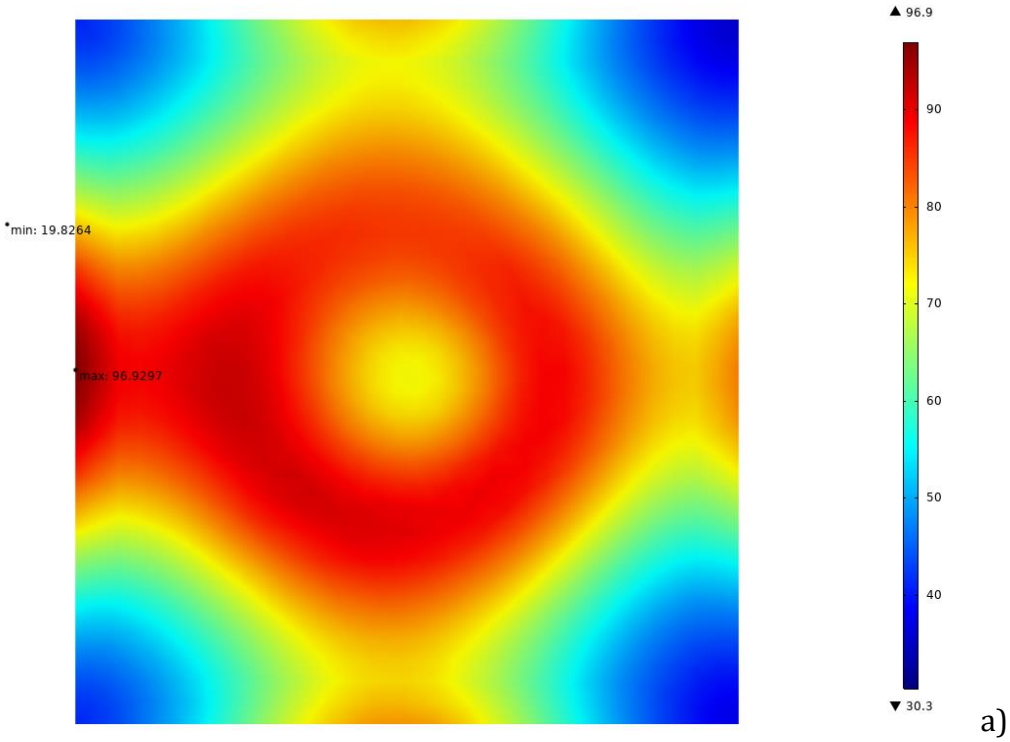

a)

b)

Figure 56: Heating distribution generated by the circular coil (a) and the new conical coil realised (b).

Conclusion

The present thesis work is occupied by the study of the bonding technology of thermoplastic matrix composites, using electromagnetic induction heating.

In the first part of this work, the electromagnetic induction-cured thermoplastic adhesive was investigated, as a possible alternative to traditional manual processes. Firstly, the introduction of this type of application has been reported, after that a numerical model has been developed, varying the process parameters such as current, maximum temperature and holding time. The choice of the process parameters has the objective to optimise the temperature distribution at the bonding interface. As stated by the bibliographic research and confirmed by the numerical model, one of the first limits of this application is the non-uniform distribution of the temperature. Subsequently, an experimental test was performed applying the process parameters used in the numerical phase. The first result was the excellent agreement between the temperature trend provided by the numerical model and the one obtained by the experimental results. Finally, the joint realised were tested following two different standard methods: ASTM D5868 and ASTM D2344.

The mechanical tests have highlighted two different and important results: first of all, the temperature control has allowed obtaining a more uniform temperature distribution, that leads to the improvement of the mechanical strength of the joints; additionally, curing the adhesive layer by the induction heating, results in a slight increase in strength for both different configuration of joint studied, compared to the standard manual method.

Finally, Induction heating could be a good alternative for curing hot-melt adhesive used for realising bonded joint of CFRTP.

The second part of this work focused on the use of electromagnetic induction heating for fusion bonding of thermoplastic matrix composites. The bibliographic research done has highlighted that there is a deep lack of knowledge on the effect of important process parameters as the current frequency. The previous works studied, focused only on the effect of the frequency on the heating rate, not considering the effect of this parameter on the depth penetration of the heating.

In the case of metal alloys, the skin effect occurs so higher frequency lower heat penetration depth.

This part of the work aimed to understand if this phenomenon also occurs in the thermoplastic composites. For this reason, a new campaign of simulation was performed using different software respect the previous one, as COMSOL Multiphysics. The choice of this new software is linked to its more programmability, that is fundamental also for future study.

These new simulations were divided into two different phases. In the first phase, for each value of frequency chosen, the current was varied, and the trend of the power was obtained. Basing on these curves, an iso-power level was chosen, and for each of the three different values of the current frequency, the relative value of the current was chosen. After that, experimental tests were performed, applying the value of the current and frequency current chosen. It is important to note, that the generator used the experimental heating tests, not allowed to change the frequency electronically, so the dimensions of the coil were varied to change its resonance frequency.

After the experimental tests, NDE US tests we performed; these tests have allowed noticing how at the same power level, the higher the current frequency, the higher the heat penetration in the material thickness. At higher frequency, the magnetic field penetrates more deeply, and consequently, the distribution of heat within the specimen is more uniform. On the contrary, the lower the current frequency, the lower the heat penetration.

So, the original and very interesting result is that the current frequency plays a different role in composites than in metal alloys case; this is due to the composite laminate could be considered as a sequence of parallel plate capacitive interacting through the thickness. With this study, the incipit for experimentation was marked off the induction welding of thermoplastics, which will constitute the continuation of the research work.

References

1. Harper CA (2002) Handbook of plastics, elastomers, and composites. McGraw-Hill
2. Bersee HE., Beukers A (2002) Diaphragm forming of continuous fibre reinforced thermoplastics: influence of temperature, pressure and forming velocity on the forming of Upilex-R® diaphragms. Compos Part A Appl Sci Manuf 33:949–958. https://doi.org/10.1016/S1359-835X(02)00037-4
3. Hou M, Ye L, Mai YW (1999) An Experimental Study of Resistance Welding of Carbon Fibre Fabric Reinforced Polyetherimide (CF Fabric/PEI) Composite Material. Appl Compos Mater 6:35–49. https://doi.org/10.1023/A:1008879402267
4. Modeling P (2002) Process Modeling and Optimization of Resistance Welding for Thermoplastic composites. J Compos Mater. https://doi.org/10.1106/002199802023507
5. DON R, Bastien L, Jakobsen T, Gillespie J (1990) Fusion bonding of thermoplastic composites by resistance heating. SAMPE J
6. Ageorges C, Ye L (2001) Resistance Welding of Metal/Thermoplastic Composite Joints. J Thermoplast Compos Mater 14:449–475. https://doi.org/10.1106/PN74-QXKH-7XBE-XKF5
7. Ageorges C, Ye L (2002) Fusion Bonding of Polymer Composites. Springer London, London
8. Srinivasan T, Palanikumar K, Rajagopal K, Latha B (2017) Optimization of delamination factor in drilling GFR–polypropylene composites. Mater Manuf Process 32:226–233. https://doi.org/10.1080/10426914.2016.1151038
9. Ageorges C, Ye L, Hou M (2001) Advances in fusion bonding techniques for joining thermoplastic matrix composites: a review. Compos Part A Appl Sci Manuf 32:839–857. https://doi.org/10.1016/S1359-835X(00)00166-4
10. Rudnev V (2003) Handbook of induction heating. Marcel Dekker
11. Beuken CL, Kegel K (1974) Elektrow�rme : Theorie und Praxis. Girardet, Essen

12. Maxwell JC (1865) A Dynamical Theory of the Electromagnetic Field. Philos Trans R Soc London 155:459–512
13. Haimbaugh RE (2001) Practical induction heat treating. ASM International
14. Border, J.; Salas R (1989) Induction Heated Joining of Thermoplastic Composites without Metal Susceptors. 34th Int SAMPE Symp May 8-11:
15. Yarlagadda S, Kim HJ, Gillespie JW, et al (2002) A Study on the Induction Heating of Conductive Fiber Reinforced Composites. J Compos Mater 36:401–421. https://doi.org/10.1177/0021998302036004171
16. Rudolf R, Mitschang P, Neitzel M (2000) Induction heating of continuous carbon-fibre-reinforced thermoplastics. Compos Part A Appl Sci Manuf 31:1191–1202. https://doi.org/10.1016/S1359-835X(00)00094-4
17. Mamunya YP, Muzychenko Y V., Pissis P, et al (2002) Percolation phenomena in polymers containing dispersed iron. Polym Eng Sci 42:90–100. https://doi.org/10.1002/pen.10930
18. Duke CB (1987) Metal-filled polymers—properties and applications, Swapan K. Bhattacharya, Ed., Marcel Dekker, New York, 1986, 360 pp. Price: $74.00. J Polym Sci Part C Polym Lett 25:263–263. https://doi.org/10.1002/pol.1987.140250605
19. Henini M (2002) Principles of Electronic Materials and Devices (Second Edition)
20. Donnet J-B (2017) Carbon Black : Science and Technology, Second Edition
21. Demain A, Issi J-P (1993) The Effect of Fiber Concentration on the Thermal Conductivity of a Polycarbonate/Pitch-Based Carbon Fiber Composite. J Compos Mater 27:668–683. https://doi.org/10.1177/002199839302700702
22. SUWANWATANA W, YARLAGADDA S, GILLESPIEJR J (2006) Hysteresis heating based induction bonding of thermoplastic composites. Compos Sci Technol 66:1713–1723. https://doi.org/10.1016/j.compscitech.2005.11.009
23. Suwanwatana W, Yarlagadda S, Gillespie JW (2006) Influence of particle size on hysteresis heating behavior of nickel particulate polymer films. Compos Sci Technol 66:2825–2836.

https://doi.org/10.1016/j.compscitech.2006.02.033

24. Nichols RJ, Lamarca DP, Agosto B (2006) Performance of susceptor materials in high frequency magnetic fields. Annu Tech Conf - ANTEC, Conf Proc 4:2211–2215
25. Haimbaugh RE (2015) Practical induction heat treating. ASM International
26. A.K. Miller, C. Chang, A. Payne, M. Gur, E. Menzel AP (1990) The nature of induction heating in graphite–fiber, polymer–matrix composite materials. SAMPE J 26:37–54
27. Fink BK, McCullough RL, Gillespie JW (2004) A local theory of heating in cross-ply carbon fiber thermoplastic composites by magnetic induction. Polym Eng Sci 32:357–369. https://doi.org/10.1002/pen.760320509
28. Severijns C, de Freitas ST, Poulis JA (2017) Susceptor-assisted induction curing behaviour of a two component epoxy paste adhesive for aerospace applications. Int J Adhes Adhes 75:155–164. https://doi.org/10.1016/j.ijadhadh.2017.03.005
29. Ahmed TJ, Stavrov D, Bersee HEN, Beukers A (2006) Induction welding of thermoplastic composites—an overview. Compos Part A Appl Sci Manuf 37:1638–1651. https://doi.org/10.1016/J.COMPOSITESA.2005.10.009
30. A.K. Miller, C. Chang, A. Payne, M. Gur, E. Menzel AP (1990) The Nature of Induction Heating in Graphite-Fiber, Polymer-Matrix Composite Materials. SAMPE J 26:37–54
31. Mitschang P, Rudolf R, Neitzel M (2002) Continuous Induction Welding Process, Modelling and Realisation. J Thermoplast Compos Mater 15:127–153. https://doi.org/10.1177/0892705702015002451
32. Fink BK, McCullough RL, Gillespie JW (1996) Experimental verification of models for induction heating of continuous-carbon-fiber composites. Polym Compos 17:198–209. https://doi.org/10.1002/pc.10605
33. Bayerl T, Duhovic M, Mitschang P, Bhattacharyya D (2014) The heating of polymer composites by electromagnetic induction – A review. Compos Part A Appl Sci Manuf 57:27–40. https://doi.org/10.1016/j.compositesa.2013.10.024
34. Fink BK, McCullough RL, Gillespie JW (1995) A model to predict the

through-thickness distribution of heat generation in cross-ply carbon-fiber composites subjected to alternating magnetic fields. Compos Sci Technol 55:119–130. https://doi.org/10.1016/0266-3538(95)80024-7

35. Zinn S, Semiatin SL, Institute EPR, Laboratories BMIC (1988) Elements of induction heating: design, control, and applications. ASM International
36. Zinn S, Semiatin SL (1988) Coil Design and Fabrication: Basic Design and Modifications. Heat Treat 32–41
37. Moser L (2012) Experimental analysis and modeling of susceptorless induction welding of high performance thermoplastic polymer composites. Inst. für Verbundwerkstoffe
38. Grewell, D. A.; Benatar, A.; Park JB (2003) Plastics and Composites Welding Handbook. munich: Hanser
39. Ageorges C, Lin Y, Mai Y-W, Meng H (1998) Characteristics of Resistance Welding of Lap Shear Coupons. Part I: Heat Transfer. Compos Part A Appl Sci Manuf 29:899–909
40. Benatar A, Gutowski TG (1986) Method for fusion bonding thermoplastic composites. SAMPE Q; (United States) 18:1:
41. Tateishi N, North TH, Woodhams RT (1992) Ultrasonic welding using tie-layer materials. part I: Analysis of process operation. Polym Eng Sci 32:600–611. https://doi.org/10.1002/pen.760320906
42. Pires I, Quintino L, Durodola JF, Beevers A (2003) Performance of bi-adhesive bonded aluminium lap joints. Int J Adhes Adhes 23:215–223. https://doi.org/10.1016/S0143-7496(03)00024-1
43. M. Silverman E, A. Griese R (1989) Joining Methods for Graphite/Peek Thermoplastic Composites
44. Hodges T, R. Tyeryar J, Berry M (1985) Bonding and nondestructive evaluation of graphite/PEEK composite and titanium adherends with thermoplastic adhesives
45. Davies J, Simpson P (1979) Induction heating handbook. McGraw-Hill Companies
46. Atkinson JR, Ward IM (1989) The joining of biaxially oriented polyethylene pipes. Polym Eng Sci 29:1638–1641.

https://doi.org/10.1002/pen.760292303

47. Dubé M, Hubert P, Gallet JN, et al (2012) Metal mesh heating element size effect in resistance welding of thermoplastic composites. J Compos Mater 46:911–919. https://doi.org/10.1177/0021998311412986
48. Arias, M. and Ziegmann G (1996) The Impulse Resistance Welding: A new Technique for Joining Advanced Thermoplastic Composite Parts. 41st Int SAMPE Symp Exhib 41(2):1361–1371
49. Wise RJ, Froment ID (2001) Microwave welding of thermoplastics. J Mater Sci 36:5935–5954. https://doi.org/10.1023/A:1012993113748
50. Fernandez Villegas I, Vizcaino Rubio P (2015) On avoiding thermal degradation during welding of high-performance thermoplastic composites to thermoset composites. Compos Part A Appl Sci Manuf 77:172–180. https://doi.org/10.1016/J.COMPOSITESA.2015.07.002
51. Fernandez Villegas I, Vizcaino Rubio P (2015) On avoiding thermal degradation during welding of high-performance thermoplastic composites to thermoset composites. Compos Part A Appl Sci Manuf 77:172–180. https://doi.org/10.1016/j.compositesa.2015.07.002
52. Rudolf R, Mitschang P, Neitzel M (2000) Induction heating of continuous carbon-fibre-reinforced thermoplastics. Compos Part A Appl Sci Manuf 31:1191–1202. https://doi.org/10.1016/S1359-835X(00)00094-4
53. Bensaid S, Trichet D, Fouladgar J (2005) 3-D Simulation of induction heating of anisotropic composite materials. IEEE Trans Magn 41:1568–1571. https://doi.org/10.1109/TMAG.2005.845047
54. Sánchez Cebrián A, Zogg M, Ermanni P (2013) Methodology for optimization of the curing cycle of paste adhesives. Int J Adhes Adhes 40:112–119. https://doi.org/https://doi.org/10.1016/j.ijadhadh.2012.09.002
55. Gouin O'Shaughnessey P, Dubé M, Fernandez Villegas I (2016) Modeling and experimental investigation of induction welding of thermoplastic composites and comparison with other welding processes. J Compos Mater. https://doi.org/10.1177/0021998315614991
56. Chadegani A, Batra RC (2011) Analysis of adhesive-bonded single-lap joint

with an interfacial crack and a void. Int J Adhes Adhes 31:455–465. https://doi.org/10.1016/J.IJADHADH.2011.02.006

57. Luo Q, Tong L (2009) Analytical solutions for nonlinear analysis of composite single-lap adhesive joints. Int J Adhes Adhes 29:144–154. https://doi.org/10.1016/J.IJADHADH.2008.01.007
58. da Silva LFM, das Neves PJC, Adams RD, Spelt JK (2009) Analytical models of adhesively bonded joints—Part I: Literature survey. Int J Adhes Adhes 29:319–330. https://doi.org/10.1016/J.IJADHADH.2008.06.005
59. de Castro J, Keller T (2008) Ductile double-lap joints from brittle GFRP laminates and ductile adhesives, Part I: Experimental investigation. Compos Part B Eng 39:271–281. https://doi.org/10.1016/J.COMPOSITESB.2007.02.015
60. Reis PNB, Ferreira JAM, Antunes F (2011) Effect of adherend's rigidity on the shear strength of single lap adhesive joints. Int J Adhes Adhes 31:193–201. https://doi.org/10.1016/J.IJADHADH.2010.12.003
61. Pahr DH, Rammerstorfer FG, Rosenkranz P, et al (2002) A study of short-beam-shear and double-lap-shear specimens of glass fabric/epoxy composites. Compos Part B Eng 33:125–132. https://doi.org/10.1016/S1359-8368(01)00063-4
62. Kranjc M, Zupanic A, Miklavcic D, Jarm T (2010) Numerical analysis and thermographic investigation of induction heating. Int J Heat Mass Transf 53:3585–3591. https://doi.org/10.1016/J.IJHEATMASSTRANSFER.2010.04.030
63. Precision WS (2011) Standard Test Method for Short-Beam Strength of Polymer Matrix Composite Materials. Annu B ASTM Stand 00:1–8. https://doi.org/10.1520/D2344
64. Specimen J, Results T (2005) ASTM D5868 Standard Test Method for Lap Shear Adhesion for Fiber Reinforced Plastic (FRP). Reproduction 01:4–5. https://doi.org/10.1520/D5868-01R14.2
65. Li X, Strieder W (2009) Emissivity of high-temperature fiber composites. Ind Eng Chem Res 48:2236–2244. https://doi.org/10.1021/ie8008583
66. Fotsing ER, Miron F, Eury Y, et al (2012) Bonding analysis of carbon/epoxy

composites with viscoelastic acrylic adhesive. Compos Part B Eng 43:2087–2093. https://doi.org/10.1016/j.compositesb.2012.03.009

67. Schwartz MM (1994) Joining of composite-matrix materials. ASM International
68. Stokes V (1989) Joining methods for plastics and plastic composites: an overview. Polym Eng Sci
69. Yousefpour A, Hojjati M, Immarigeon J-P (2004) Fusion Bonding/Welding of Thermoplastic Composites. J Thermoplast Compos Mater 17:303–341. https://doi.org/10.1177/0892705704045187
70. Shi H, Villegas IF, Octeau M-A, et al (2015) Continuous resistance welding of thermoplastic composites: Modelling of heat generation and heat transfer. Compos Part A Appl Sci Manuf 70:16–26. https://doi.org/10.1016/j.compositesa.2014.12.007
71. Kreith F, Manglik RM, Bohn MS (2012) Principles of heat transfer. Cengage learning
72. Palmieri B, Nele L, Galise F (2018) Numerical modeling and experimental validation of thermoplastic composites induction welding. In: AIP Conference Proceedings. p 050013
73. Scarponi C, Valente M (2006) An application of a new ultrasonic technique to jute composite laminates subjected to low-velocity impact. Int J Mater Prod Technol 26:6. https://doi.org/10.1504/IJMPT.2006.008977
74. Spruiell JE, Janke CJ, Case SW, Reifnider KL (2004) A review of the measurement and development of crystallinity and its relation to properties in neat PPS and its fiber reinforced composites